A Robust Wide Area Measurement Based Controller for Networks with Embedded HVDC Links

By

PRASHANT AGNIHOTRI

A Thesis submitted to the Faculty of Graduate Studies of
The University of Manitoba
in partial fulfillment of the requirements of the degree of

Doctor of Philosophy

Department of Electrical and Computer Engineering
University of Manitoba
Winnipeg, Manitoba

Abstract

The advent of Wide-Area measurement Systems has spurred interest in the use of non-local feedback signals for power swing damping control.

Although damping can be improved through generator excitation systems, dc links and other grid connected power electronic converters, the full potential of wide-area measurements can be realized by coordinating the strategies used for multiple controllable devices in a grid. These strategies also need to be robust to partial or complete loss of communication, changes in operating points, topology and equipment outages, improve damping of all the controllable swing modes, and have adequate stability margins to avoid destabilization of untargeted modes.

This thesis investigates a control strategy for multi-infeed and multi-terminal (also referred to as multiple embedded dc links in this thesis) dc links using local frequency difference signals as well as the frequency difference signals obtained from other dc links. This strategy combines the advantages of the local frequency difference signal with the additional degrees of freedom provided by the use of non-local frequency difference signals, to achieve targeted and enhanced swing mode damping for the poorly damped modes. Since the strategy uses only a limited set of non-local signals, the signals may be directly communicated to the dc links without having to be centrally collated with other system-wide measurements.

The key aspect of the proposed strategy is the use of a *symmetric positive definite (spd) gain matrix*. This results in enhanced damping for all controllable swing modes. Furthermore, loss of communication between the dc links does not destroy the symmetric positive definiteness and the gain elements can be tuned to selectively enhance damping of poorly damped modes.

Eigenvalue sensitivity analysis and case studies on a 3 machine 9 bus and 16 machine 68 bus system with multiple HVDC links are presented to demonstrate the key attributes and the effectiveness of this strategy.

Acknowledgements

Although, the words are not enough to express my deep sense of gratitude towards everyone who has contributed to my Ph.D., I am trying to express my feelings in a few words.

I would like to thank God, the almighty, for giving me the opportunity and strength to do my research in the prestigious institute, University of Manitoba.

I convey my sincere thanks to my supervisor Prof. A. M. Gole for giving me an opportunity to work with him. His comments and suggestions were extremely helpful in preparing the research papers and the final version of this thesis.

I cannot express in words for the support I received from Prof. A. M. Kulkarni during my research. I always got a positive and fruitful reply from him whenever I approached him with a difficulty. I am extremely grateful for his incredible and timely guidance throughout this research work. I have learned lots of new concepts related to power system dynamics and control from him.

I am sincerely thankful to IIT Bombay especially the International Relations Department for their support in all the academic and technical matters during my periods of stay at IIT Bombay.

I am grateful to MITACS for approving my research grant and providing me the opportunity to apply my research finding at Manitoba Hydro. I would also like to thank Brian Archer and M. A. Weekes for their permission to work at Manitoba Hydro in the System Planning Department.

I am especially thankful to my Research Progress Committee members, Dr. A. Rajapakse, and Dr. Norman Richards for their valuable feedback and constructive suggestions.

Support provided by the office staff, especially, Traci Hofer, and Amy Dario of the Department of Electrical and Computer Engineering at University of Manitoba, is highly appreciated. I am grateful to the Department of Electrical and Computer Engineering, University of Manitoba for providing an excellent working environment during my stay. Support provided by the Faculty of Graduate Studies deserves a special mention.

I owe a great deal to my lab-mates at IIT Bombay and University of Manitoba who were partners in highly fruitful days. These people always kept me in good spirits. My special thanks to Mukesh, Kunal, Pranav, Kalyan, Vedanta, and Rajesh.

Last but not the least, my parents, my inlaws, wife Tejaswini, and my son Arjun have been my pillars of strength during this entire tenure. It was their patience and sacrifice due to which I was able to concentrate on the research work. Their love and care have been the major driving forces of this work.

Prashant Agnihotri

Contents

List of Figures

List of Tables

NOMENCLATURE

ac	:	alternating Current
dc	:	direct Current
MVA	:	megavolt ampere
PMU	:	phasor Measurement Unit
WAMS	:	wide Area Measurement System
IGBT	:	insulated-gate bipolar transistor
HVDC	:	high-voltage direct-current
FACTS	:	flexible ac transmission systems
LCC	:	line commutated converter
VSC	:	voltage source converter
MMC	:	multi modular converter
SCR	:	short circuit ratio
ESCR	:	effective short circuit ratio
PWM	:	pulse width modulation
SPWM	:	sinusoidal pulse width modulation
SPD	:	symmetric positive definite

List of Symbols

δ	:	Generator rotor angle
ω	:	Generator rotor speed
ω_B	:	Machine base speed
ϕ	:	Bus voltage phase angle
ζ	:	Line current phase angle
ϕ_d	:	Voltage phase angular difference between the buses to which a two terminal dc link is connected
H	:	Generator inertia constant
I	:	Line current magnitude
I_R	:	Shunt injected reactive current
P_e	:	Power injected by generators
P_{sh}	:	Shunt injected real power
P_{ser}	:	Series injected real power
P_{dc}	:	Two terminal dc link power flow
V	:	Bus voltage magnitude
V_R	:	Series injected reactive voltage (voltage in quadrature with current)

Chapter 1

Introduction

1.1 Background

Power system networks are continuously subjected to faults and disturbances. These disturbances could be small or severe in nature and trigger electromechanical oscillations. The movement of the electro-mechanical variables (frequency and phase angles) after a disturbance is the superposition of the relative motion (swing modes) and the common mode [1]. Relative motion is generally oscillatory for small disturbances (swing modes) and the damping of the swings is generally a major concern. Large disturbance stability of relative motion is also a concern [2]. While angular stability is associated with the dependence of power flow on the relative rotor positions, Centre of Inertia (COI) or frequency stability is dependent on the cumulative load-generation balance within a synchronous grid [3].

In an ac system followed by a disturbance, machines tends to remain in synchronism by providing two components of the restoring torques known as synchronizing and damping torques. Where the synchronizing torque prevents any instability due to angular drift in the machine's rotor angle, the damping torque is critical to damp oscillatory behavior. Another important component which plays a major role in the

dynamic behavior of the machines during transients is the inertia of the system. A high inertia ensures the inherent capability of the system to avoid any deviation from the synchronous frequency during disturbances. The equations of motion in per unit describe the behavior of the synchronous machines during such disturbances [1] as described below.

$$\frac{d}{dt}\begin{bmatrix}\Delta\omega_r\\ \Delta\delta\end{bmatrix}=\begin{bmatrix}\frac{-K_D}{2H} & \frac{-K_s}{2H}\\ \omega_0 & 0\end{bmatrix}\begin{bmatrix}\Delta\omega_r\\ \Delta\delta\end{bmatrix}+\begin{bmatrix}\frac{1}{2H}\\ 0\end{bmatrix}\Delta T_m \tag{1.1}$$

Where,

K_S=synchronizing torque coefficient in pu torque/rad

K_D=damping torque coefficient in pu torque/pu speed deviation

H=inertia constant in MW.s/MVA

$\Delta\omega_r$=speed deviation in pu=$\frac{(\omega_r-\omega_0)}{\omega_0}$

$\Delta\delta$=rotor angle deviation in elec. rad

ω_0=rated speed in electrical rad/sec

1.2 Nature of Electromechanical Oscillations

As discussed earlier, during disturbances there is a relative motion between the rotors of the machines, these oscillations can be classified as intra plant, local plant, inter area, control, and torsional oscillations [4]-[5].

- **Intra-Plant oscillations:** When the machines in the same generating power station oscillate against each other it gives rise to intra-plant oscillations. Oscillation frequencies are generally in the range of 2-3 Hz.
- **Local Plant oscillations:** When one machine in a plant oscillates against other machines, the oscillation are termed as local plant mode. These are in

the range of 1-2 Hz.

- **Inter-area oscillations:** Inter area modes are triggered when a group of machines in one area starts swinging against a group of machines in another area. These are generally of frequencies in the range 1 Hz or less.

- **Control oscillations:** These are mainly associated with the poorly tuned controller of the exciters, governors, power system stabilizers (PSS), HVDC, and FACTS devices etc. The frequency range can vary.

- **Torsional oscillations:** These are associated with the turbine generator shaft system. These modes are generally excited due to the line compensation and modes are less than the natural frequency in the range of 10-46 Hz. This phenomenon is also known as Sub Synchronous Resonance (SSR).

The damper windings in the rotor are mainly effective to damp the oscillations in the local machines but offers less contribution to the damping of the inter area modes. As far as the intra-area and local plant modes are concerned, PSS are generally used to modulate the voltage reference of the AVR to damp these oscillations. Traditionally PSS design was based on the feedback parameters measured locally in an area and therefore mainly utilized to damp local modes. But now with the advent of the Wide Area Measurement Systems (WAMS), system wide information is available and therefore signals rich in modal observability can be synthesized to obtain feedback signal for the PSS design which can control the damping of the critical modes [6]-[7]. Despite these developments, many references have report on the limited capability of PSS to damp inter-area oscillations [5]-[8].

The deployment of High Voltage DC Transmission (HVDC) and Flexible AC Transmission System (FACTS) devices combined with the wide area measurement system have ushered in new possibilities in the design of robust and effective controls for improving angular stability. HVDC allows for precise control of power flow

between connected ac networks, without requiring them to be synchronous. Series FACTS devices such as Thyristor Controlled Switched Capacitor (TCSC), and Static Synchronous Series Capacitor (SSSC) injects voltage in the system can also effectively control power flow on the line by modulating its impedance. Shunt FACTS devices such as STATic COMpensator (STATCOM) injects the current into the system and thus by controlling the reactive power supply and thereby the voltage at the connected buses, the real power transfer capability of the system can be increased. FACTS devices like Thyristor Controlled Series Compensator (TCSC) and Static Synchronous Series Compensator (SSSC) which are series connected devices, and Static VAR Compensator (SVC) and Static Synchronous Compensator (STATCOM), which are shunt connected devices, have been deployed in many large power grids. HVDC links (both Line Commutated Converter(LCC) and Voltage Sourced Converter(VSC) based) are also embedded in many synchronous grids to transfer bulk power over large distances. The fast response provided by the power electronic converters can be used to improve angular stability. However, inter-area swing mode controllability depends on their location in the grid and the quantity which is controlled e.g., shunt/series real or reactive power[9].

1.3 Local or WAMS based remote feedback signals for controller design

Consider a system shown in Fig. 1.1. Here a damping controller for DC links between buses 8-9 and 4-6 based on the local feedback signals (frequency difference between buses 8-9 and 4-6 respectively) are an obvious choice for damping controllers, as communication reliability will not be a concern. However, local signals may have some constraints: a local feedback signal may contain, in addition to the critical modes of interest, several other non-critical modes. Therefore, control effort may be unnecessarily expended due to the presence of these non-critical modes. Moreover,

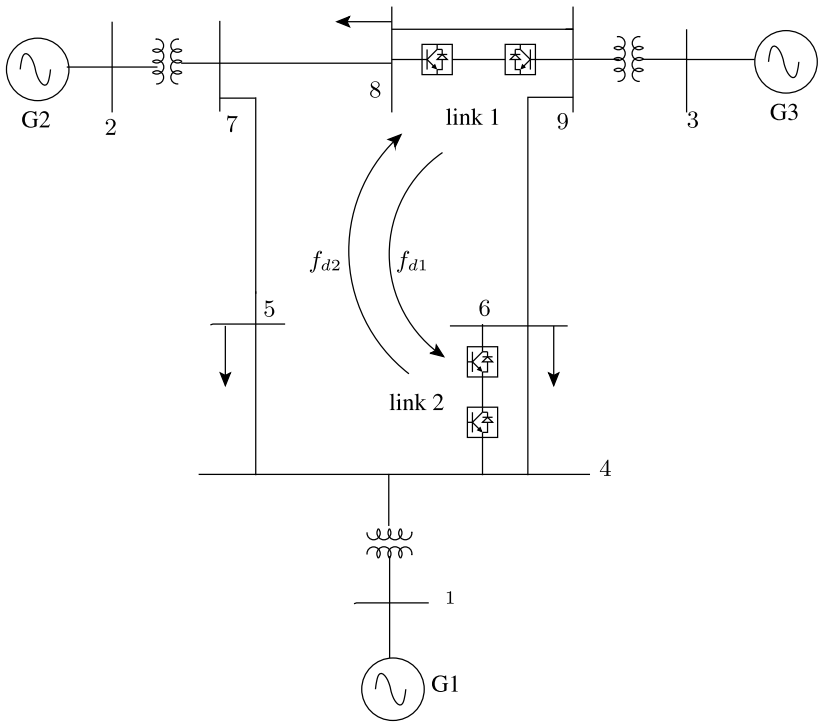

Figure 1.1: Multi-infeed with two dc links, exchanging frequency difference signals

controller design has to be constrained so as to prevent possible destabilization of these modes. Therefore, it is worthwhile to consider a wide choice of candidate feedback signals including global signals available from WAMS [10]-[12].

WAMS involve the use of time synchronized measurements obtained using Phasor Measurement Units deployed at several locations in a network[13]. High accuracy system-wide relative angular information is made available by this technology, which can be made available to stabilizing controllers. These remote measurements can be used for the synthesis of signals with good observability properties (i.e., only the modes of interest are dominantly observable in them). However, if a controller is designed with remote measurements, it should be robust to a partial or complete loss of remote signals and communication latencies. The control strategy should also work well for different operating conditions including major changes in the network.

1.4 High Voltage DC Current Transmission (HVDC)

HVDC technology offers various advantages over ac transmission such as smaller right of way, increased and controllable power flow for the same insulation level compared to ac lines, ability to connect asynchronous systems, no requirement of series power compensation, phase angles between ac systems interconnected through dc link can be arbitrary, no skin effect, and lesser fault current levels.

There are also certain disadvantages of the HVDC such as, high cost of the converter, tapping of DC power is difficult, high reactive power demand at the converter ends, requirement of filters at the converter ends due to increased harmonics in the system, and difficult to operate in DC grids. Based on the high cost of converter and filter requirements but cheaper insulation level for HVDC, several references have reported a break over distance of 600 km beyond which the overall cost for the HVDC system is cheaper than the ac system. Thus, HVDC system are gaining popularity for the long distance power transmission. Line Commutated Converter (LCC), and Voltage Source Converter (VSC) are the two widely used HVDC techniques [14]-[15].

1.4.1 HVDC with Line Commutated Converter (LCC)

The basic building block for the LCC is thyristor. A thyristor conducts when a gate pulse is provided and a positive voltage is applied between anode and the cathode terminals. A thyristor cannot be turned off by removing the gate pulse, it turns off when the current goes below the holding current. The commutation of the current from one thyristor to another depends on the firing sequence, source inductance, and the line voltage applied across the thyristor. Thyristors are triggered in a cyclic order by providing appropriate firing pulses to the gate terminal of the thyristors to obtain a DC voltage at the output. This DC voltage can be controlled by the firing angle of the gate pulses. In the LCC converter, the direction of the current cannot be reversed

whereas the voltage polarity at the converters can be reversed[1].

There are some limitations in the conventional HVDC transmission such as: the terminating ac networks must provide the commutation voltage, require reactive power at the converter which must vary with loading (i.e. switched filter banks), difficulty in operating into weak ac systems (Short Circuit ratios under 2), generates Ac and Dc side Harmonics. They also have difficulty in operating into "weak" ac systems. The strength of the ac system is quantified by the short circuit ratio (SCR), which is the ratio of short circuit MVA to the dc power. When the ac filters and shunt capacitors as shown in the figure are considered, the SCR is replaced by "Effective Short Circuit Ratio" (ESCR) defined by[16]-[17].

$$ESCR = \frac{SCMVA - Q}{P_{dc}} \tag{1.2}$$

Where,

SCMVA=Short Circuit MVA

Q=Reactive power generated by the filters and shunt capacitors

P_{dc}=DC power

1.4.2 HVDC with Voltage Source Converter (VSC)

In the VSC converter, an IGBT with an antiparallel diode is used as the switching device. The IGBT can be turned on by providing a gate pulse. Additionally, unlike the thyristor of the LCC, the IGBT turns off on removal of the gate pulse. The switching pulses can be produced by Pulse Width Modulation (PWM) technique such as Sinusoidal PWM, Space Vector Modulation, or Harmonic Elimination. Compared to the conventional LCC based HVDC, VSC HVDC systems are less affected by the system strength[18]. They are suitable for use in dc grid as shown in the Fig 1.2 as power direction can be changed by current reversal, no filter requirements due to

less harmonics, and provides independent real and reactive power control. However, VSC technology poses problems such as high switching losses and have higher cost compared to LCC HVDC.

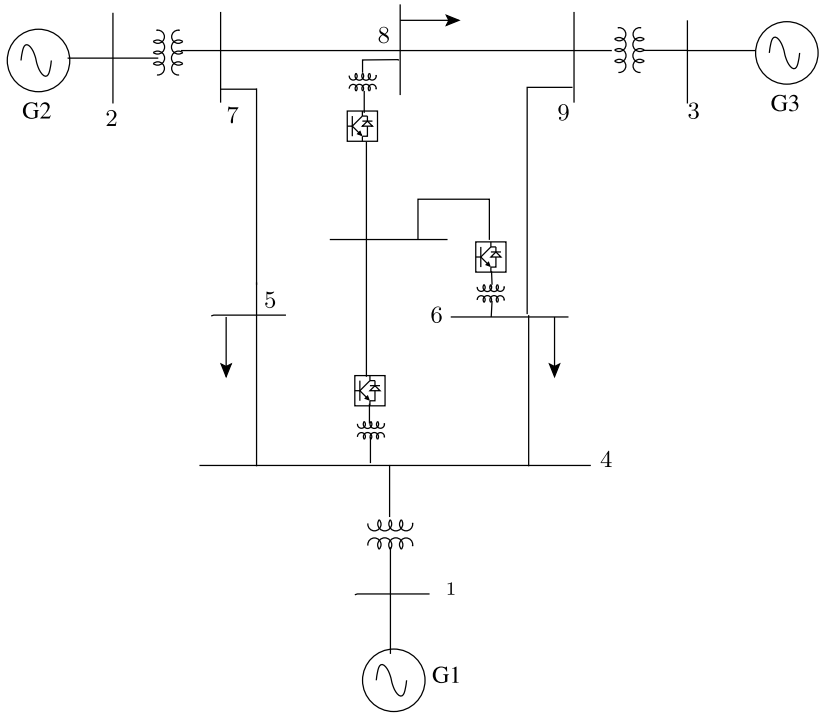

Figure 1.2: Multi-terminal dc link

In order to improve the harmonic spectrum of the voltage waveform in VSC, the switching frequency has to be high. However, with the increase in the voltage level it may not be possible to operate the switches at a high frequency due to switching losses, EMI, and increased stress on the switches. But as discussed earlier decreasing the switching frequency will deteriorate the harmonic spectrum of the output waveform[19].

1.4.3 HVDC with Multi-Modular (MMC) Voltage Sourced Converter

Multi-Modular Converter (MMC) is new technique that is essentially becoming the de-facto option for large VSC-HVDC systems.

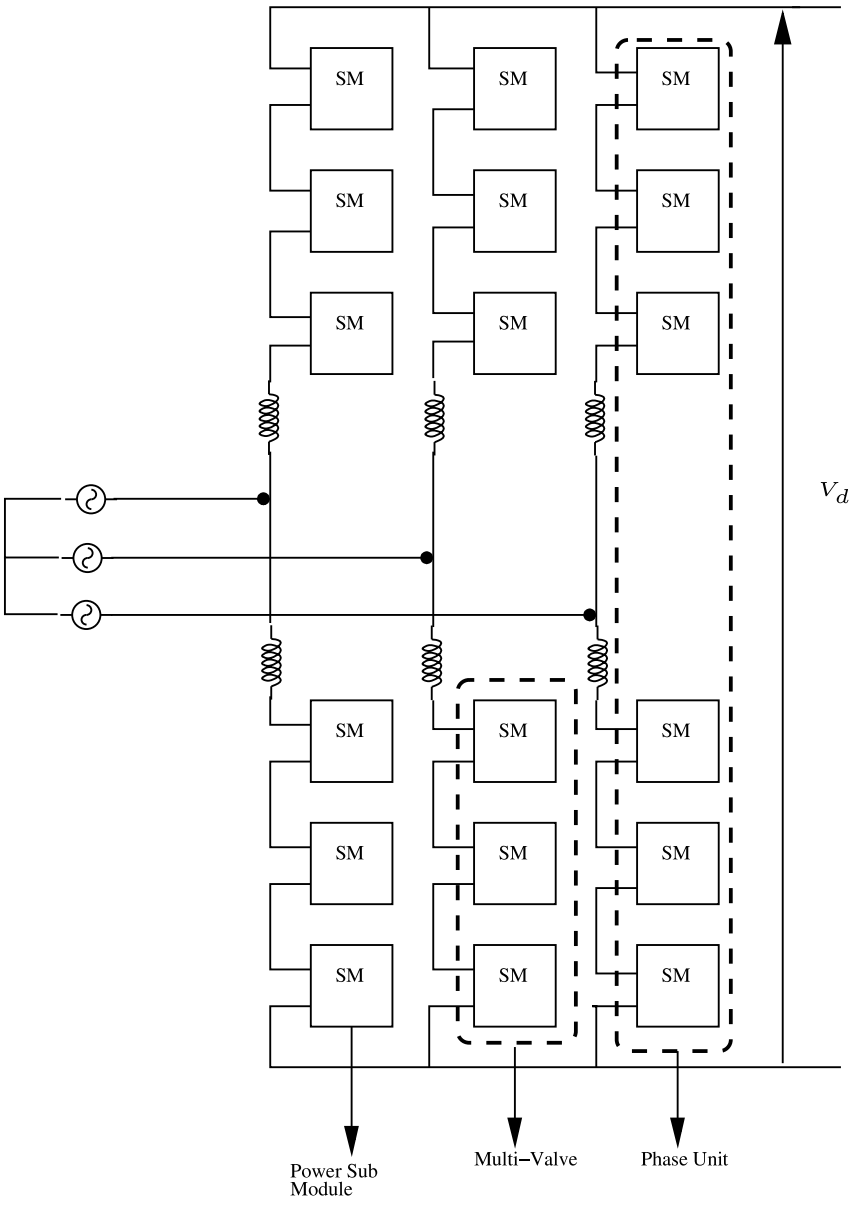

Figure 1.3: Multi-Modular Converter

As shown in the Fig.1.3 in the MMC, multiple sub-modules can be cascaded together. Each sub-module as shown in Fig.1.4 produces either a zero voltage when switch T_2 is closed or V_c voltage when the switch T_1 is closed. These sub-modules can be switched to produce a nearly sinusoidal voltage as shown in Fig.1.5 which results in better harmonic spectrum (hence no harmonic filters are required) where each sub-module acts as a controllable voltage source. A reference waveform is quantized

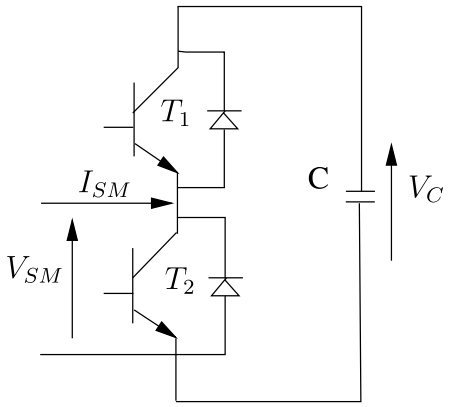

Figure 1.4: MMC Building Block

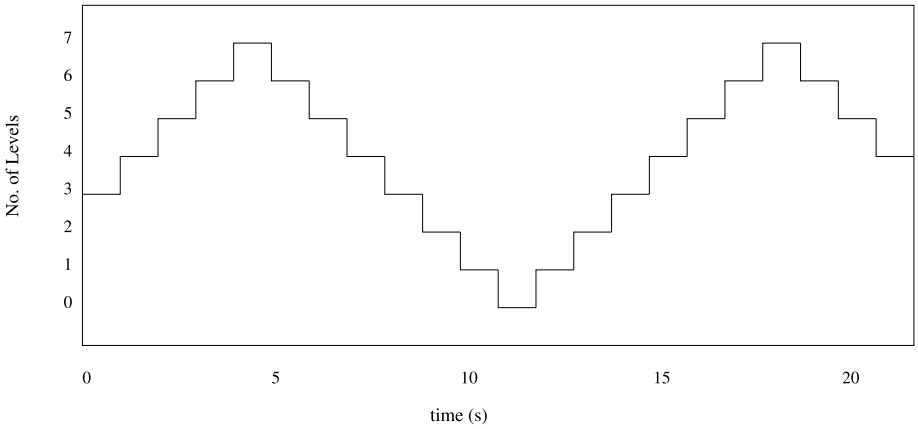

Figure 1.5: Level Order

to determine switching instants for the sub-modules, special algorithms for capacitor voltage balancing and ensuring sharing of module duty, and higher level controls identical to other VSC topologies (i.e. decoupled id/iq control etc.)[20]-[21].

1.5 DC links embedded in ac systems

Many schemes exist in which HVDC links are embedded into the synchronous grid for bulk and controlled power transmission. Multi-infeed and multi-terminal HVDC systems are examples of such systems as shown in Fig. 1.1 and 1.2. Where, multi-infeed systems either share a common ac bus or connected to the buses that are electrically close [22], multi terminal comprise of system where more than two converter

terminate at the same bus.

During faults, if some of the ac lines trip then the remaining ac lines have to share the burden of the tripped lines. Despite the capability of the DC links to transmit additional power (on top of the steady state power) for transient periods, if the DC link operates in constant power then it may result in the overloading of the adjacent ac lines. This may even result in the loss of synchronism between the two ac networks which the dc line connects. An example of such blackout was in Pacific DC intertie in the year 1996[23]. This problem can be addressed if the power flow in a dc line is allowed dynamically to take up the slack. A margin is generally kept to allow for increased power flow in the dc link under transient conditions. Stability controls will typically modulate or boost power in order to improve stability. Their action is usually transitory and does not affect steady state power flow. In some dc links, a run-up feature is provided wherein power flow is automatically increased when a parallel ac line trips. The fast response provided by the power electronic converters can be used to improve angular stability.

In a synchronous network with parallel AC-DC scheme, a derivative of the ac line power or frequency difference between the converters can be measured to modulate the power flow through the DC link. Such change in the DC power flow will result in the increase in the damping of the swing modes. For instance in pacific intertie, a derivative of power flow through the parallel ac line is obtained. This signal is passed through appropriate filters and lead lag block to finally supplement the current order at the dc link which has resulted in significant damping of the inter area modes.

1.6 Example of HVDC schemes that uses damping control

We will now summarize some of the existing asynchronous schemes in North-America such as Square Butte HVDC, Nelson River Bipole in Manitoba, CU HVDC scheme, Eel River Back to Back scheme which uses supplementary control to modulate the

power through DC link to damp the oscillations in the ac systems.

- Square Butte HVDC scheme transmits 500 MW coal generated power from North Dakota to Duluth, Minnesota. The bipolar dc system is rated at ± 250 kV and 1000 A dc. Low frequency swings were observed in the sending end North Dakota system. Since the receiving end is a strong system, sending end frequency deviation are measured and used as a feedback signal which modulate the dc power by ± 100 MW to damp any oscillations at the sending end [24].

- Eel River scheme interconnects Hydro Quebec and New Burnswick Power in the eastern Canada through two back to back HVDC converters each rated at 160 MW. Local frequencies at both the ends are measured to control the tie-line power so that their is no communication requirement [25].

- CU HVDC scheme has rectifier unit in North Dakota and inverter in Minneapolis, Minnesota to transmit 1000 MW power. Damping power controller (DPC) in the system modulates the dc line power in response to the change in the deviation of rectifier end frequency with its output limited to ± 300 MW [26].

- In the Nelson River Bipole, power is produced at Limestone, Long Spruce, and Kettle generating stations in the North and is collected at the Henday and Radisson Converter station as DC. This power flows to southern Manitoba through a corridor of 900 km via Bipole I & II HVDC links (at 450 and 500 kV respectively). In the south, Dorsey converter stations convert this DC power to AC and feed into the provincial grid for distribution to customers [27]-[29].

1.7 Literature Review

- Due to the fast acting power electronic converter, the capability of HVDC link embedded in an ac system to respond quickly for the variable power demand

and thus to improve the stability of the ac-dc system was first recognized in 1964 [30]. It was reported that by using feedback signals such as the frequency deviations of the ac system to modulate the dc power can significantly improve the damping of the low frequency oscillations. [31]- [32].

- During the disturbances, generators electric power is less than the mechanical power which results in the acceleration/deceleration of the rotors. This phenomenon is known as first swing instability and their is a high probability that the machines may go out of step if the angular drift is high. As discussed earlier, following a disturbance, machines provide synchronizing torque which is mainly useful to address the first swing instability as this torque is proportional to the angular drift. However, since the turbine action is generally slow compared to the fast acting HVDC control, short term overload capability of the DC link ***may be*** utilized to give a burst of energy in the initial fault duration to decelerate the generators. Such optimal bang-bang control is discussed in [33].

- The problem of negatively damped low frequency oscillations in a realistic ac-dc system was first brought into focus in Pacific AC Intertie in the year 1968 to 1971 shortly after the energization of the AC line between Pacific Northwest and Southwest. The installation of PSS mitigated these oscillations temporarily when these oscillations resurfaced in the year 1974. This posed a restriction on the amount of the hydro power being transmitted to the southwest. However, due to $\pm$400 kV DC line embedded into the system, the studies showed that modulation of the current order for the link proportional to the rate of change of ac power was very effective to improve the damping [34].

- Fig. 1.6 shows the DC power modulation control to damp the swing modes in the Pacific DC intertie. The system receives ac power as the input which is

passed through a notch filters to mitigate the impact of the modulation on the local swing mode frequency followed by differentiator and compensator blocks for signal conditioning. The parameters of the compensator can be selected to provide the best damping at a selected frequency of choice. However, with changing network conditions or loadings, the most critical frequency to be damped may change, and the controller may not work satisfactorily. Hence, there is a need to develop a robust controller, as is the subject of this thesis.

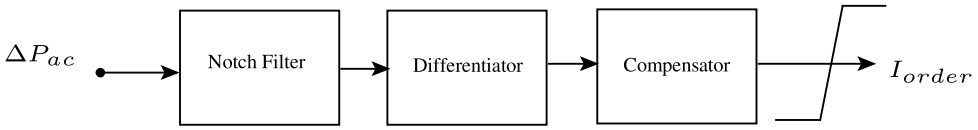

Figure 1.6: Pacific DC Intertie block diagram of the dc modulation system

- Several asynchronous links connecting the two synchronous regions also employed the dc power modulation technique to improve the stability of the ac systems [35]. Local frequency at the converter station was an obvious choice as the feedback signal to modulate dc power.

- The techniques to compute the eigenvalues for the large power system network were also developed which could determine the controller action on the system stability and detailed modal analysis of the system [1], [5].

- Since the real and reactive power are coupled in the LCC, only real power modulation to damp the oscillations may result in the uncoordinated reactive power modulation which may decrease the effectiveness of the method especially in the weak ac system. A more rigorous explanation of the real and reactive power modulation of HVDC link to improve the damping of the slow oscillations was carried out by [36]. The analysis showed that active power modulation is efficient when applied at a short mass-scaled electrical distance from one of the swinging machines, and reactive power modulation is most efficient when there

exists a well-defined power flow direction and the modulation is made at a point close to the electrical midpoint between the swinging machines. It was shown that the intuitively appealing feedback signals frequency and derivative of the voltage are appropriate for active and reactive power modulation, respectively. Detailed analysis on a test system was performed to show the effect of the control on the eigenvalues of the system[37].

- Generally for the control design, classical control theory using frequency domain methods has been traditionally employed where the objective of the controller is to provide adequate damping for the dominant modes which lie in a narrow band while taking care that it does not undamp the other modes. The optimization of the controller performance is usually done by trial and error. Modern techniques using optimal control and pole placement techniques are more attractive. For such techniques a detailed mathematical model of the system is provided which can determine the response of the system. The Kalman filter is used to generate the estimates which in turn are fed to the regulator to generate the modulation signal [38], [15].

- A strategy based on "collocated" sensor-actuator pairs, which was proposed for the damping of space structures [39] also generated interest [40] due to its inherent robustness. The strategy introduces damping in the system by mimicking the effect of viscous friction. Similar strategies for the damping of swings in a power system using certain local measurements and FACTS/HVDC devices (the actuators) have been described in [41][42].

- One of the common problem faced while designing the damping controllers using local feedback signals was the lack of observability of the swing modes and the presence of non critical modes. Research has been carried out to develop the use of wide area measurement signals for the controller design in the power system.

For generator tripping and reactive power compensation switching to improve transient stability and voltage support, Bonneville Power Administration (BPA) has developed and demonstrated a Wide-Area Stability and Voltage Control System termed WACS [43]. Hydro-Qubec plans to add new control loops to the present SCs and SVCs regulators and to take advantage of extended wide-area measurements to provide supplementary damping of the main 0.6 Hz inter-area mode, and the idea has been validated in through simulations [44]-[46]. The TEPCO in Japan and EDF in France are also planning to carry out the project about monitoring of out-of-step and separation control system based on PMU [47]-[48]. In China, WADC was implemented on the Gao-Zhao HVDC supplementary control in the China southern power grid.

- Since WAMS involves transmission of signals over long distances the time delay involved cannot be ignored. This time delay can effect the damping and may also lead to instability [49]. Two kinds of solutions have been adopted to address this issue, one is to design based on Lyapunov Stability criterion to keep the system stable under time delay. Under this Linear Matrix Inequality (LMI) method is used where Pade approximation by a rational polynomial is used to remove the delay. Second method was to predict the delay by Smith Predictor and compensate for the delay [50]-[52].

- Some literature have also discussed the concept of "Synthetic Inertia" in the wind turbine systems which is essentially extracting the stored energy from the accelerating or decelerating turbine during disturbances that can momentarily increase the total inertia of the system and thus reducing the frequency deviation [53]-[57].

1.8 Gaps in the existing research

- Although state of the art techniques have discussed on introducing damping effect through the dc links, none of the references have explicitly mentioned how to mimic important properties of the ac line through dc such as synchronizing torque which is essential to prevent loss of synchronism due to the first swing instability.

- In case the WAMS signals are used for the controller design and the remote signals are lost then ideally the controller should revert back to the local feedback signals. However, if the feedback signal is synthesized from the remote and local signals using complex methods then it becomes difficult to predict the system behavior during loss of communication.

- Control of power flow through the DC links bring changes to the jacobian matrix of the system. Such change may bring positive or negative changes to the eigen values of the jacobian matrix. While several references have tried to ensure that for their control design to damp critical modes does not accidentally destabilize the non critical modes, this problem becomes complex as the system size increases. A niche method has to be developed for controlled injection of the dc power at the ac buses which **always** brings positive damping effect to all the eigenvalues of the jacobian matrix.

- In a multi-machine system with multiple HVDC links embedded into the ac system, various swing modes can be present out of which some modes may be well damped while others with a low damping. Coordination of power flow between the dc links can bring extra degrees of freedom to achieve selective modal damping, but no such strategy has been explored.

- In the asynchronous DC links, which connects two synchronous systems the em-

phasis has been given to the damping of the frequency swings in the individual synchronous systems. However, the overall centre of inertia motion of the rotors of synchronous machines is also a concern.

- The concept of synthetic inertia has not been explored in the synchronous AC systems with embedded DC links. This could prove to be an important concept to improve the stability of the HVDC system connected to a weak AC system.

1.9 Objectives of the thesis

- Since the behavior of a system of AC transmission lines is quite well understood, the guiding principle in this thesis is to make a dc line mimic beneficial aspects of ac transmission lines, particularly their contribution to synchronizing torque. This may be achieved by designing an appropriate phase angle and voltage dependence of real and reactive power injected by a dc link. On the other hand, problems in ac line characteristics like the non-linear power-phase angle relationship can be avoided. The overall concept is to make a dc line like a super ac line, with flexible control parameters, much like the FACTS concept.

- The objective is to extend the above concept by making power flows in multiple dc links or multi-terminal dc links mutually coupled to each other by exchanging measurements local to the dc links. This strategy gives us additional degrees of freedom in the form of the parameters $\mathcal{M}$ and $\mathcal{R}_m$. These may be used to selectively increase the leverage on a particular swing mode.

- Another objective is to develop a robust control strategy using local and remote signals which always brings positive synchronizing and damping effect to the critical and non-critical modes and which should gracefully degrade to the local signal during the loss of communication. In order to achieve this a control gain matrix which modulates the power flow through the DC links by measuring

feedback signals are designed to be symmetric positive definite in nature. This brings two advantages, firstly when a jacobian matrix of the system is perturbed by a symmetric positive definite matrix it always results in a positive synchronizing and damping effect and secondly if the communication through a link is lost the change in gain matrix corresponds to making the subsequent rows and column elements to zero. This will still preserve the positive definiteness of the matrix and ensure positive synchronizing/damping effect.

- The thesis also examines strategies like emulation of synthetic inertia using signals like the local $\frac{df}{dt}$ to reduce frequency transient deviation. Both Line Commutated Converter (LCC) based dc links and Voltage Source Converter (VSC) based dc links are considered.

1.10 Organization of the Thesis

The thesis is organized into six chapters. This section gives a brief account of the content presented in each chapter.

Chapter 2 describes the static power flow approach through the dc links which will result in a controlled injection of power at the ac terminals. If the power through the DC links is made proportional to the phase angle difference and voltage across the converter bus then it will mimic an ac line and will result in a modified jacobian matrix of the ac network. Since the real and reactive power are coupled in the LCC network its power control will be different from the VSC. Strategies to control this power through LCC and VSC such that it brings non negative change in the eigenvalues of jacobian matrix is discussed such that it will always result in increase of synchronizing effect. A 4 machine case study is presented to show the proof of concept in order to understand the DC power control on the system stability.

In Chapter 3 we have introduced a simple circuit analogy which helps us to understand the control strategy to improve the angular stability by introducing both

synchronizing and damping effect with controllable DC link. An extension of the control strategy to multiple HVDC links embedded in the ac system and the impact of using local and remote signals for the control design has been presented. A formal state space approach has been used to quantify the results.

In chapter 4 we have shown various case studies which shows the implementation of the proposed control strategy. 3 machine and 16 machine systems with multiple VSC HVDC links are described to illustrate the degrees of freedom which can be utilized to put more leverage on the damping of the selective modes. Small signal analysis of the ac-dc system is carried out to show the eigenvalue movement for the proposed control strategy.

Since in the earlier chapters we have discussed the utility of the dc power flow control to improve the system stability in the synchronous grids, we can also extend this strategy in the asynchronous system in Chapter 5. Appropriate feedback signals can be chosen for the emulation of system inertia and load-frequency dependence in order to improve frequency stability. A test system is simulated in MATLAB/SIMULINK based transient stability program with the implementation of proposed controller.

The main conclusions of this thesis are summarized in Chapter 6.

Chapter 2

Embedded DC line as a "Super AC" Line

This chapter discusses how a dc line can be controlled with a simple algorithm that makes its behavior similar to that of an ac line. This avoids any sophisticated tuned higher level controls and imparts the synchronizing torque transfer characteristics to the dc line.

- This property can be implemented by modulating the power order signal to the dc controller in proportion to the phase angle difference between the sending and receiving end.
- How the real and reactive power flow control through a VSC and LCC link will result in the change in the jacobian matrix of the ac network such that the synchronizing effect increases?
- How the control strategy can be extended to multiple HVDC links embedded in an ac system?
- A four machine case study with the LCC HVDC link is used to show the proof

of concept.

2.1 A Static Power Flow Approach To Show Essential Relationship between the Real and Reactive Power Injections to the Phase Angular Difference and Bus Voltage

It is instructive to examine the following relationship which holds true for an ac network, for small deviations in real and reactive power injections.

$$\begin{bmatrix} \Delta P_{sh} \\ \Delta Q_{sh} \end{bmatrix} = A \begin{bmatrix} \Delta \phi \\ \Delta V \end{bmatrix} \tag{2.1}$$

P_{sh} and Q_{sh} denote the incremental vector of injected real and reactive powers respectively, while $\Delta\phi$ and ΔV denotes the vector of bus voltage phase angles and magnitudes. For a lossless ac network with transmission lines, generators and interconnected transformers, and passive compensation, the Jacobian matrix A is symmetric [42].

The addition of dc links results in a controlled injection of power at the ac terminals. If the dc link power is made a function of phase angular differences and voltage (like an ac line), the link manifests the behavior of an ac line. This will result in a modified A matrix. Strategies to control dc link power which cause a non-negative change in all eigenvalues of A are preferable [58].

Addition of an ac line in an existing ac network results in semi positive definite change in A. This will increase the magnitude of the frequency of the eigenvalues, i.e. strengthen the system. It is to be noted that if a symmetric matrix (A) is perturbed by adding to it a symmetric positive semi-definite (having positive or zero eigenvalues), or a symmetric positive definite matrix (having positive eigenvalues), then this results in a non-negative change in all the eigenvalues of A [59]. Motivated by this, we consider phase angle and voltage magnitude dependent power flow strategies for dc links, which cause symmetric positive definite (or semi-definite) perturbations of the

A matrix.

2.1.1 Single VSC based dc link emulating an AC line

With VSC based systems it is possible to control real and reactive power independently. The simplest possibility is to make the dc link emulate ac line equations with two *controllable* parameters of reactance x and susceptance B. The strategy could be augmented to include the steady offsets which are controllable by a system operator. For a single VSC based dc link connected between buses r and i - see Fig. 2.1, the real power flow and the reactive power *drawn* from the buses should be controlled as shown in the equations below. The losses in the dc link are neglected.

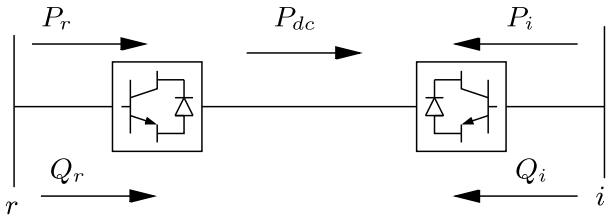

Figure 2.1: VSC based DC link

$$P_{dc} = P_{dc_o} + \frac{V_r V_i \sin(\phi_r - \phi_i)}{x}, \tag{2.2}$$

$$Q_r = Q_{r_o} + \frac{V_r^2}{x} - \frac{V_r V_i \cos(\phi_r - \phi_i)}{x} - V_r^2 B \tag{2.3}$$

$$Q_i = Q_{i_o} + \frac{V_i^2}{x} - \frac{V_r V_i \cos(\phi_i - \phi_r)}{x} - V_i^2 B \tag{2.4}$$

P_{dc_o}, Q_{r_o} and Q_{i_o} could be adjusted by an operator during actual system operation.

This is a simple, predictable strategy which can be analyzed quite easily using existing system analysis tools. To simplify it even further, the sinusoidal relationship can be replaced with a linear one as shown in equations (2.2)-(2.4). The change in angle still creates an increase in power which would tend to provide a synchronizing torque. It does not seem necessary, however, to mimic the non-linear (sinusoidal)

phase angular dependence of power flow (see Fig. 2.2 (a)) which is also the cause of transient instability in ac networks following large disturbances. Therefore, the following linear characteristics are proposed (see Fig. 2.2 (b)).

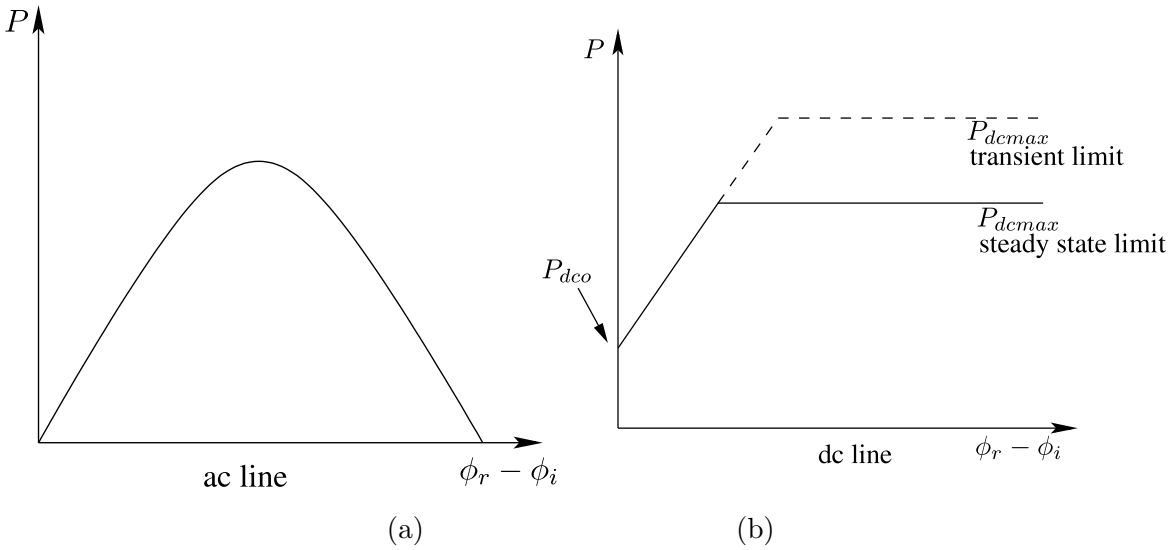

Figure 2.2: Power Angle dependence in (a) ac line (b) dc line with linear phase angle dependence

$$\begin{bmatrix} \Delta P_r \\ \Delta P_i \\ \Delta Q_r \\ \Delta Q_i \end{bmatrix} = \begin{bmatrix} k_p & -k_p & 0 & 0 \\ -k_p & k_p & 0 & 0 \\ 0 & 0 & k_r V_{ro} & 0 \\ 0 & 0 & 0 & k_i V_{io} \end{bmatrix} \begin{bmatrix} \Delta\phi_r \\ \Delta\phi_i \\ \frac{\Delta V_r}{V_{ro}} \\ \frac{\Delta V_i}{V_{io}} \end{bmatrix} \tag{2.5}$$

The constants k_p, k_r and k_i are controller parameters that can be appropriately selected. ϕ^*, V_r^* and V_i^* can be adjusted along with P_{dc_o}, Q_{r_o} and Q_{i_o} to modify the steady state power flow as desired.

The matrix A in equation (2.1) is augmented due to the voltage and angle dependent terms of the real and reactive power injected by the dc link. The parameters k_p, k_r and k_i should be selected to be positive numbers as then the augmentation itself is symmetric and positive semi-definite. This causes a non-negative change in all the eigenvalues of the matrix A, as discussed in the previous section.

This strategy also ensures that in case parallel AC paths are weakened due to an ac line outage, then the dc link in the same corridor will automatically run-up and share the burden with the remaining ac lines.

2.1.2 Power Flow control in a single LCC HVDC link

Unlike a VSC based link, the reactive power drawn by a LCC link is a non-linear function of power flow in DC link and rectifier and inverter AC side voltage magnitudes. Independent control of reactive power is not feasible. Therefore in this case, the choice of power flow characteristics has to be different.

The change in reactive power drawn at the two terminals r and i, as a function of the deviation in real power and bus voltages is given by the following equation.

$$\begin{bmatrix} \Delta Q_r \\ \Delta Q_i \end{bmatrix} = \begin{bmatrix} g_r \\ g_i \end{bmatrix} \Delta P_{dc} + H \begin{bmatrix} \frac{\Delta V_r}{V_{ro}} \\ \frac{\Delta V_i}{V_{io}} \end{bmatrix} \tag{2.6}$$

Both the coefficient matrices are *operating point dependent*, and are derived in the Appendix A. V_{ro} and V_{io} are the quiescent values of bus voltages.

Consider following power flow characteristic

$$P_{dc} = P_{dc_o} + \Delta P_{dc},$$

where,

$$\Delta P_{dc} = k_p \left[(\phi_r - \phi_i - \phi^*) + g_r \frac{(V_r - V_r^*)}{V_{ro}} + g_i \frac{(V_i - V_i^*)}{V_{io}} \right] \tag{2.7}$$

Therefore,

$$\begin{bmatrix} \Delta P_r \\ \Delta P_i \\ \Delta Q_r \\ \Delta Q_i \end{bmatrix} = \begin{bmatrix} k_p & -k_p & k_p g_r & k_p g_i \\ -k_p & k_p & -k_p g_r & -k_p g_i \\ k_p g_r & -k_p g_r & k_p g_r^2 & k_p g_r g_i \\ k_p g_i & -k_p g_i & k_p g_r g_i & k_p g_i^2 \end{bmatrix} \begin{bmatrix} \Delta\phi_r \\ \Delta\phi_i \\ \frac{\Delta V_r}{V_{ro}} \\ \frac{\Delta V_i}{V_{io}} \end{bmatrix} + \begin{bmatrix} [0] & [0] \\ [0] & [H] \end{bmatrix} \begin{bmatrix} \Delta\phi_r \\ \Delta\phi_i \\ \frac{\Delta V_r}{V_{ro}} \\ \frac{\Delta V_i}{V_{io}} \end{bmatrix} \tag{2.8}$$

$$= k_p \sigma \sigma^T \begin{bmatrix} \Delta\phi \\ \frac{\Delta V}{V} \end{bmatrix} + k_H \begin{bmatrix} \Delta\phi \\ \frac{\Delta V}{V} \end{bmatrix} \tag{2.9}$$

$$\sigma^T = \begin{bmatrix} 1 & -1 & g_r & g_i \end{bmatrix} \tag{2.10}$$

k_p is chosen to be positive. g_r and g_i are obtained from the linearized relationship (2.6) and are positive as shown in Appendix A.

The matrix $k_p \sigma \sigma^T$ in the equation (2.9) can be compared to the A matrix in the equation (2.1). The changes brought about by the ΔP_{dc} results in a augmentation of the matrix A of equation (2.1) by a symmetric positive semi-definite matrix, which has a beneficial outcome, as discussed previously. However, the perturbation brought about by k_H matrix in (2.9) which is an inherent dependence (not affected by our strategy) is not symmetric positive definite in nature. Although it was observed that for increased gain k_p the change brought by $k_p \sigma \sigma^T$ will mask the effect of k_H.

2.2 Discussion

2.2.1 Choice of Parameters

The value of parameters will affect not only the dynamic behaviour of the system, but also determine the steady state power flows (if washout blocks are not used in the implementation).

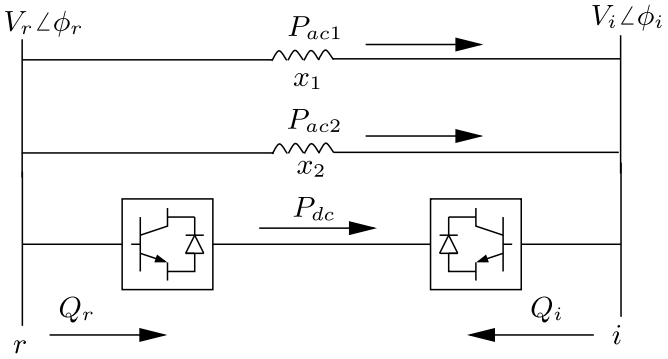

Figure 2.3: Parallel AC-DC System

Although this can be determined by a system study, a guideline for the choice of k_p is to make it comparable to the reactance of a parallel ac line. For example if we have two ac lines in parallel with a dc link as shown in the Fig. 2.3, with steady state power flows given by the equations (2.11)-(2.13). During a contingency, if a parallel ac line "2" trips, the power through the dc link can be modulated with $k_p = \frac{1}{x_2}$. Thus the incremental power change in the dc link following a network disturbance will be at least as much as the parallel ac path (assuming V_r and V_i are at 1pu and non linear dependence of sine function is neglected).

$$P_{ac1} = \frac{V_r V_i \sin(\phi_r - \phi_i)}{x_1} \tag{2.11}$$

$$P_{ac2} = \frac{V_r V_i \sin(\phi_r - \phi_i)}{x_2} \tag{2.12}$$

$$P_{dc} = P_{dc_o} + k_p(\phi_r - \phi_i - \phi^*) \tag{2.13}$$

2.2.2 Power Flow Re-routing

Changes in steady state power flow should generally be effected by a system operator by changing P_{dc_o}, and ϕ^*, V_r^*, and V_i^*. These changes are based on optimal scheduling

and online contingency analysis. The strategy could be changed to achieve changes in power flow as shown in equation (2.14), unless the gains are applied through a washout in which case the steady state power flow through DC link remains unaffected.

$$P_{dc} = P_{dc_o} + k_p(\phi_r - \phi_i) \tag{2.14}$$

2.2.3 Strategies for Multiple HVDC Links

Multiple HVDC links can be controlled individually using strategies given in the previous section. An interesting possibility is the emulation of mutually coupled power flows by the exchange of signals among the HVDC links. For two VSC hvdc links 'A' and 'B' - see Fig 2.4 - a linear strategy with mutual coupling can be arranged by simply introducing coupling terms in the coefficient matrix. An example of a strategy which has mutual coupling in real power flow is given below.

$$\begin{bmatrix} P_{dc_a} \\ P_{dc_b} \end{bmatrix} = \begin{bmatrix} P_{dc_{ao}} \\ P_{dc_{bo}} \end{bmatrix} + \begin{bmatrix} k_{p_a} & k_{p_m} \\ k_{p_m} & k_{p_b} \end{bmatrix} \begin{bmatrix} \phi_{ra} - \phi_{ia} - \phi_a^* \\ \phi_{rb} - \phi_{ib} - \phi_b^* \end{bmatrix} \tag{2.15}$$

It is important to have a symmetric positive definite gain matrix, in order to preserve the beneficial aspects of the strategy. The strategy can also be generalized for more than two links or multi-terminal links.

The main advantage of the exchanging variables between multiple dc links to modulate their power flow is the additional degrees of freedom by which one may control power flows in the network.

2.3 Case Study

Single LCC-HVDC link in a Four Machine System

Consider the case of a single 200 MW LCC based dc link embedded in the well known

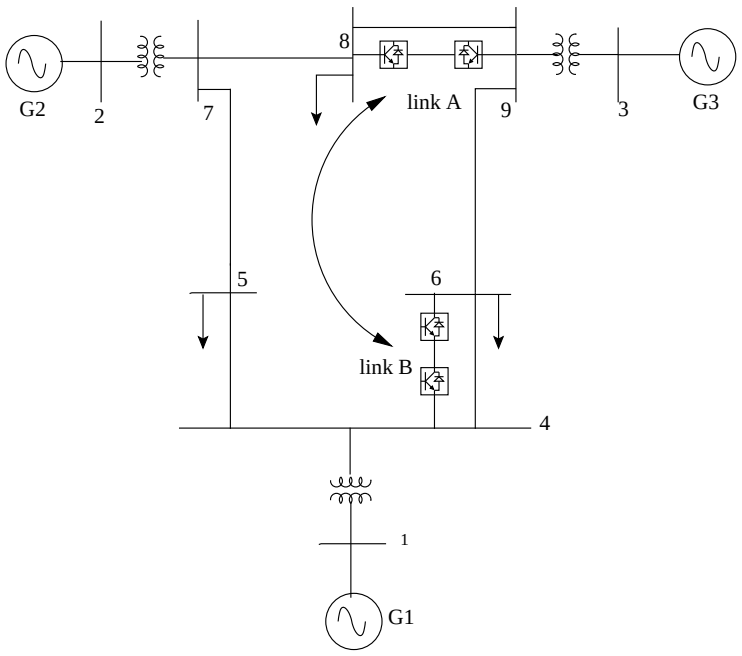

Figure 2.4: Multiple DC links embedded in an ac system

four machine system (data adapted from pp. 1151 of [1]) and is given in Appendix C. A detailed generator model is considered. The generators are equipped with static excitation systems. The loads are of constant impedance type.

The LCC link is controlled as shown in Fig.2.6 using the strategy given in equation (2.7). The link is operated at 75% of its rating in CC-CEA mode and g_r and g_i are evaluated for the corresponding operating condition by the procedure obtained in Appendix A.

The simulated response for a fault in line 7-8 near bus 8, followed by the tripping of the line, is shown in Fig. 2.7. The flow in the dc link increases due to the strategy. Their is a maximum limit of 1.2 pu in the transient power carried by the DC. A decrease in the angular excursion between generator 2 and generator 4 is clearly seen, along with an increase in frequency (indicative of improved synchronizing torques in the system).

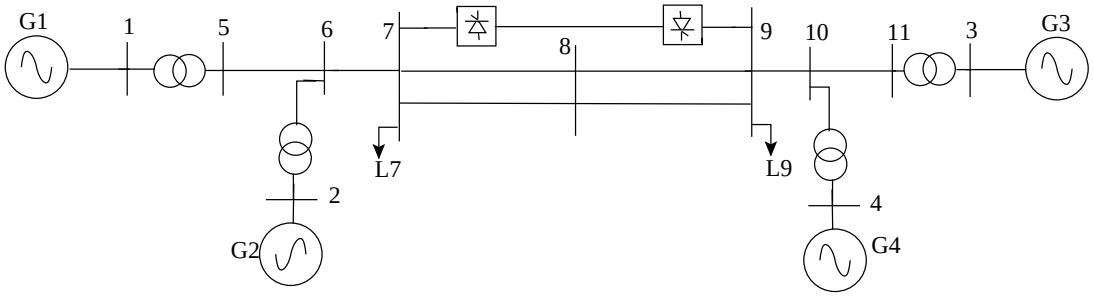

Figure 2.5: 4 Machine System

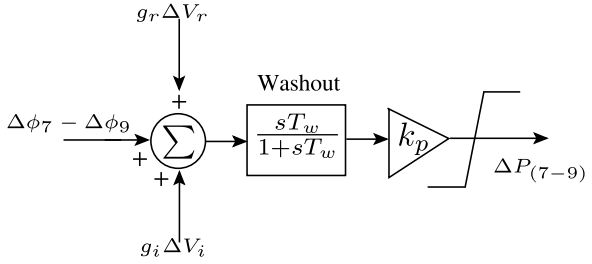

Figure 2.6: Supplementary control for DC link in 4 machine system

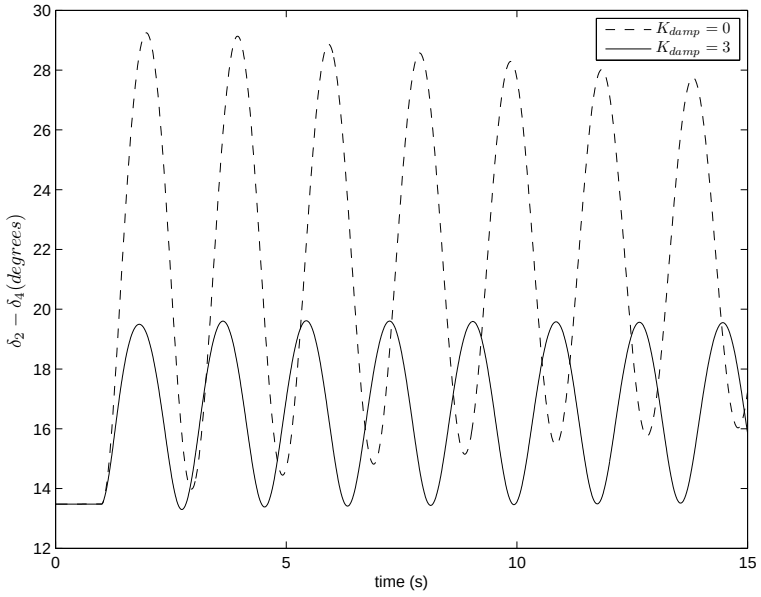

Figure 2.7: Response to a Fault in line 7-8 near bus 8 followed by tripping of the line

2.4 Concluding Remarks

1. So far we have considered only a static approach under which we mimic the powerflow behavior of the AC lines through DC by making the power injection through them as a function of phase angular difference.

2. As brought out by the case study, although post disturbance angular separation decreases, damping of the swings is poor. Therefore, a more detailed analysis is required to examine the impact of the DC power flow strategy on the angular stability of the system.

3. In the next chapter a simplified circuit analogy of a power system is presented which demonstrates to understand dynamics of the system in the AC-DC system.

Chapter 3

Understanding the Impact of Super Line Strategy on Angular Stability:

Using a Circuit Analogy of the Electromechanical System

The previous chapter described a strategy in which DC line mimics an AC line by making the power proportional to the phase angular difference between the converter stations. Also in the previous chapter we only discussed mimicking the dc line as an ac line to introduce synchronizing effect but in order to avoid any oscillatory instabilities damping torque is also required. The objectives of this chapter are:

1. To introduce a circuit analogy for a simplified power system which helps to more easily visualize the control strategy to improve the angular stability by introducing both synchronizing and damping effect with controllable DC link.

2. Extension of the proposed control strategy to the control of multiple and multi-terminal DC links embedded in an ac system.

3. Discuss the impact of local and remote feedback signals on the control strategy

and implementation of the control laws.

4. To develop a formal state space approach in order to quantify the effect of the control strategy.

3.1 Understanding Power Swings: A Circuit Analogy

The control concept in this research can be more easily understood if we consider a circuit analogy [15] of the electro-mechanical model of a power system, wherein the following is assumed.

1. Generators are represented by the classical model (voltage source of constant magnitude behind a transient reactance).

2. Generator mechanical power inputs and load active powers are constant.

3. Transmission losses are neglected.

4. Bus voltage magnitudes are constant(1.0 pu).

The circuit analogy transforms the power flow representation into a circuit representation by using the following analogies:

Power flow through a branch $\Longleftrightarrow$ "Current"

Time derivative of bus voltage phase angle $\Longleftrightarrow$ "Voltage"

By this analogy, the *small-signal* behavior of the simplified model of a power system can be represented by an L-C circuit: From the swing equation, the time derivative of the voltage phase angle (i.e voltage in the analog) across a generator is proportional to the power flow (current in the analog) and therefore is analogous to a capacitor $\mathcal{C}$ (see Fig.3.1a). Similarly, a lossless ac transmission line between buses i and j is analogous to an inductance $\mathcal{L}_{ij}$ because power flow (current in the analog) is proportional to the phase difference (integration of the voltage) across it (see Fig.3.1b).

List of the Main Symbols used in this Chapter	
δ	Generator rotor angle
ω	Generator rotor speed
ω_B	Machine base speed
ϕ	Bus voltage phase angle
ζ	Line current phase angle
ϕ_d	Voltage phase angular difference between the buses to which a two terminal dc link is connected
H	Generator inertia constant
I	Line current magnitude
I_R	Shunt injected reactive current
P_e	Power injected by generators
P_{sh}	Shunt injected real power
P_{ser}	Series injected real power
$P_{\rm dc}$	Two terminal dc link power flow
V	Bus voltage magnitude
V_R	Series injected reactive voltage (voltage in quadrature with current)

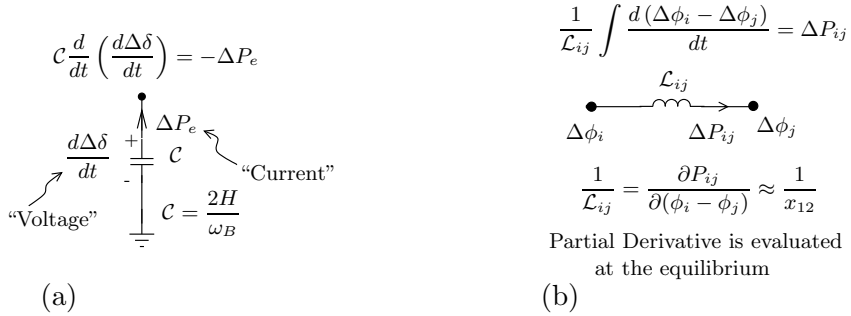

Figure 3.1: Circuit Analogy of (a) Generator (b) AC Transmission Line

The small signal analog circuit of a three machine system [60] is shown in Fig. 3.2. For the given assumptions, the oscillatory modes of the L-C circuit are the swing modes of the original power system. Appendix I shows the comparison of the eigen values for the original and analogous system with multiple HVDC links.

3.2 Control of Power Swings

3.2.1 Local Control Strategy using a DC Link

With this analogy consider the network shown in Fig 3.2. In its *small signal* analog equivalent,

1. The transmission line elements can be transformed to reactances in the equivalent model. This can be justified as follows,
   Since the power equation (between buses i and j) is

$$P_{ij} = \frac{V_i V_j \sin \phi_{ij}}{X}$$

   Assuming V_i and V_j are close to 1.0pu and ϕ_{ij} is small, then small signal equivalent will be

$$\Delta P_{ij} = \frac{\Delta \phi_{ij}}{X}$$

   The small signal equivalent of the above equation can be written as

$$\Delta P_{ij} = \frac{1}{\mathcal{L}_{ij}} \int \frac{d(\Delta \phi_i - \Delta \phi_j)}{dt}$$

   Now in the analog equivalent the above equation can be written as

$$\Delta \mathcal{I}_{ij} = \frac{1}{\mathcal{L}} \int \mathcal{V} dt$$

which is essentially the model of the inductor of value X

2. In order to find an analogous equivalent for the machine, we first consider the swing equation

$$\frac{Md\omega}{dt} = P_m - P_e$$

where

$$M = \frac{2H}{\omega_B}$$

The small signal equivalent of the above equation can be written as

$$M\frac{d\Delta\omega}{dt} = -\Delta P_e$$

Now in the analog equivalent the above equation can be written as

$$\frac{\mathcal{C}d\Delta\mathcal{V}}{dt} = -\Delta\mathcal{I}$$

The above equation can also be written as

$$-\Delta P_e = \mathcal{C}\frac{d}{dt}\left(\frac{d\Delta\phi}{dt}\right)$$

which is essentially the model of the capacitor of value

$$\mathcal{C} = \frac{2H}{\omega_B}$$

Now consider the addition of a DC link as shown in Fig.3.3. The main utility of the circuit analogy is that it suggests a control strategy which can improve angular stability with controllable network elements, say, a DC link[1].

[1]The figure shows a VSC-based DC link, but a Line-Commutated Converter(LCC) based link may also be used.

1. If power flow in the DC link is changed in proportion to the voltage phase angular difference between the buses to which it is connected then the DC line behaves like an AC line, i.e., the effect is the addition of another inductive link $\mathcal{L}$ in the analogous circuit. This reduces angular deviations following disturbances (synchronizing effect).

2. If power flow is changed in proportion to the derivative of the voltage phase angular difference between the buses (i.e., the bus frequency difference), the DC line behaves like a *resistance* $\mathcal{R}$ in the analogous circuit. This creates a damping effect.

Both these effects are beneficial. There are certain advantages which are obvious if such a strategy is used;

1. The control strategy is simple and uses local measurements.

2. The introduction of "resistive" and "inductive" links will *always* enhance damping and synchronizing effects respectively, for all swing modes in the system (except for those modes which are not observable in the phase angular difference at the DC link location).

3. When multiple DC links are present, the same strategy may be applied for each of them (more resistors/inductors get added); their independent actions are not adversarial.

The use of bus frequency difference signal for power swing damping with DC link power control is not new, and has been derived earlier for a two machine system[36]. However, the circuit analogy shows that it is an appropriate strategy even for larger multi-machine systems and multiple links.

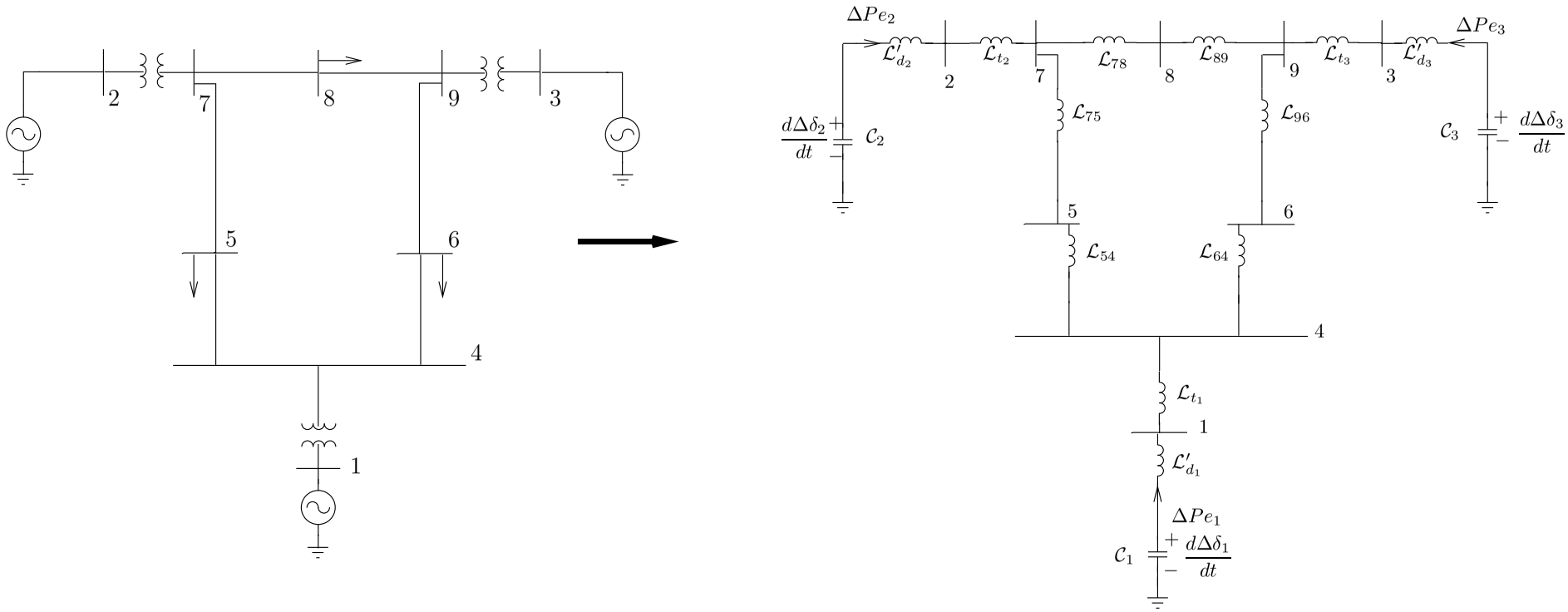

Figure 3.2: Small-signal Analogous Circuit of a Three Machine System

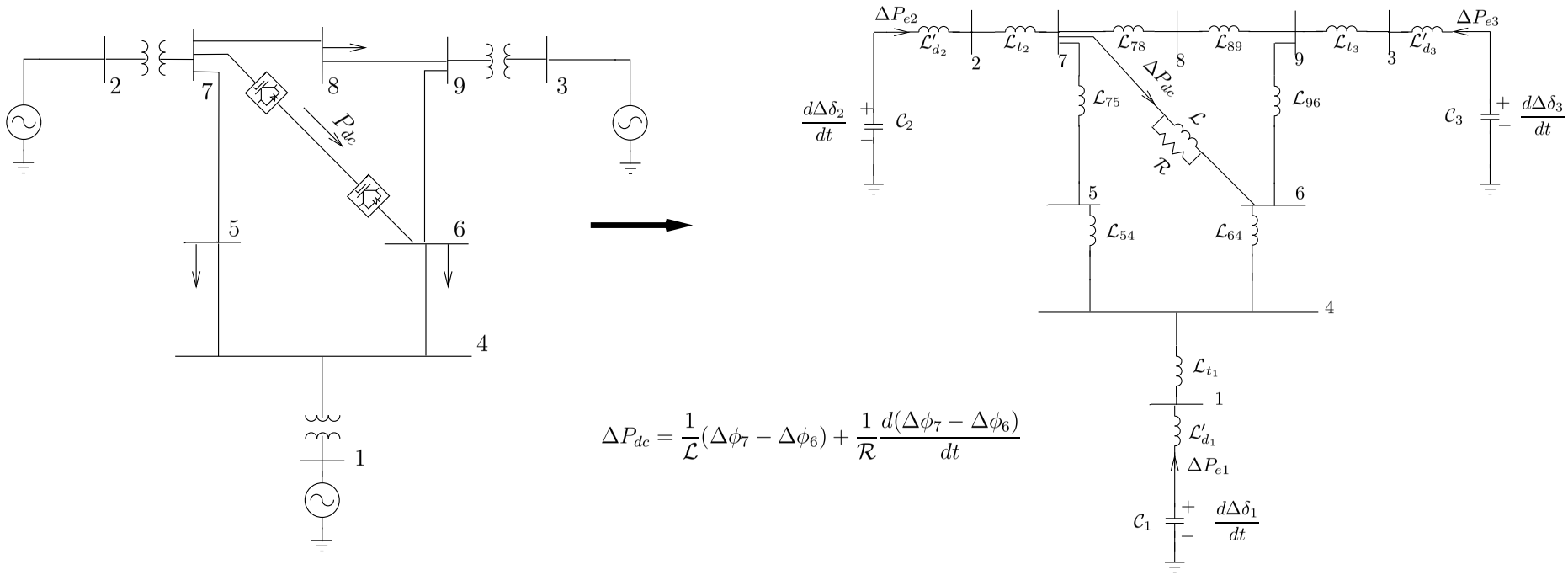

$$\Delta P_{dc} = \frac{1}{\mathcal{L}}(\Delta\phi_7 - \Delta\phi_6) + \frac{1}{\mathcal{R}}\frac{d(\Delta\phi_7 - \Delta\phi_6)}{dt}$$

Figure 3.3: DC link in the System: Local Control Strategy

3.2.2 Multiple DC links: A Restricted Global Strategy

As mentioned in the previous section, the local strategy which emulates the effect of resistance and inductance in the analogous circuit may be used in every DC link present in the system. However, the circuit analogy suggests that with multiple links and global measurements, one may also be able to emulate "mutual inductance" or "mutual resistance". This is depicted in Fig. 3.4 for a three machine system with two DC links. This strategy gives us additional *degrees of freedom* in the form of the parameters $\mathcal{M}$ and $\mathcal{R}_m$ as shown in Fig. 3.4. These may be used to selectively increase the leverage on a particular swing mode.

The matrix shown in Fig. 3.4 should be symmetric positive definite, which also implies that $\mathcal{L}_1, \mathcal{L}_2, \mathcal{R}_1$ and $\mathcal{R}_2$ should be positive. A mutual loss of communication [2], is equivalent to setting $\frac{1}{\mathcal{M}}$ and $\frac{1}{\mathcal{R}_m}$ to zero. Therefore, we essentially revert to the local strategy in case of communication problems. While there will be a quantitative change in the damping and synchronizing effects due to this, it will not cause any harm since the local strategy to which we revert also contributes to positive damping and synchronizing effects.

The strategy for two DC links can be generalized to a larger number of links - the inductance and resistance matrices will have correspondingly larger sizes, but should be symmetric positive definite. If communication from/to a DC link is problematic, then that DC link should use only local measurements and *all* other DC links should not use measurements from that link. Equivalently, all off-diagonal elements of the inductance and resistance matrices corresponding to the link from/to which communication is problematic are set to zero. Even if the values of other matrix elements is unchanged, this will preserve the symmetry and positive definitiveness of the matrices, and therefore the positive damping and synchronizing effects.

[2]Both Transmit and Receive: the loss of reception at location A from location B for a preset time will automatically stop transmission from location A to location B

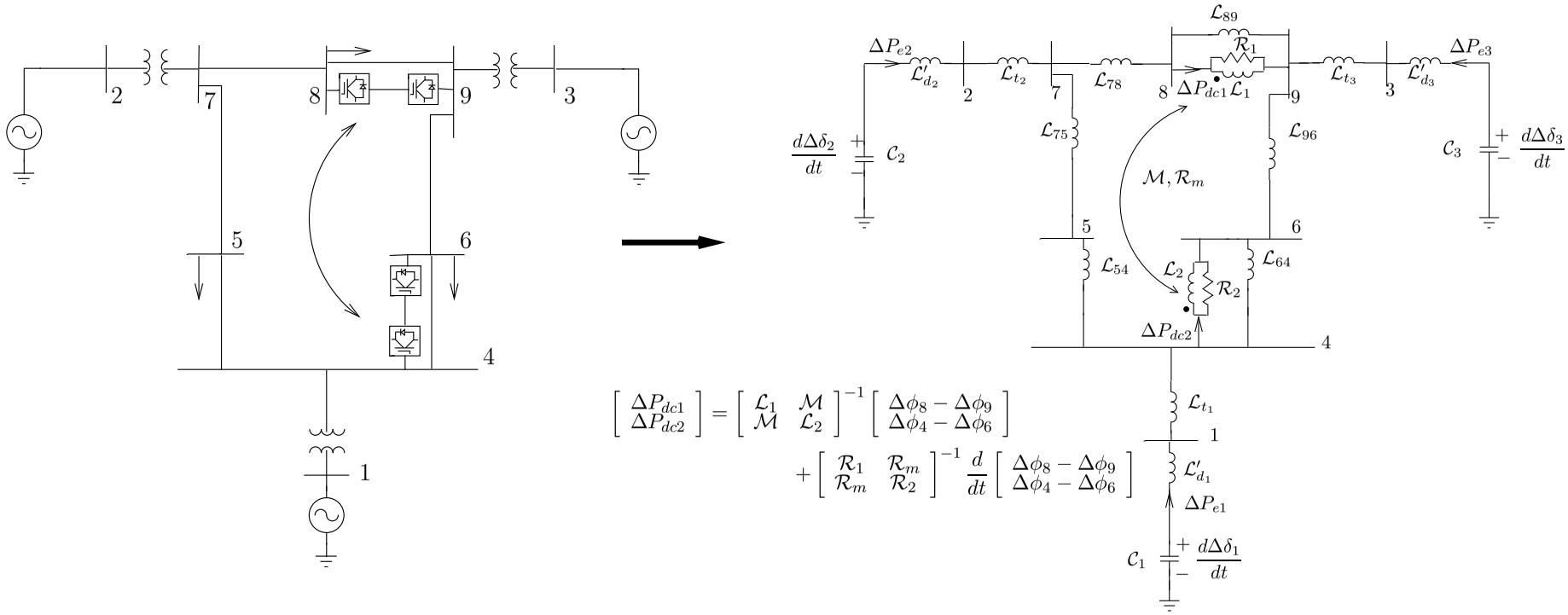

Figure 3.4: Restricted Global Strategy for two DC links

3.2.3 Multi-terminal DC links

With a multi-terminal DC link, we can emulate multiple inductive and resistive links in the analogous circuit as shown in Fig. 3.5. If partial loss of angular information due to communication failure, say between buses 8 and 6 is detected, then $\mathcal{R}_2$ and $\mathcal{L}_2$ should be set to infinity, i.e., the inductor and resistor, $\mathcal{L}_2$ and $\mathcal{R}_2$, are removed. In such a case, the control law will continue to provide a positive damping and synchronizing effect.

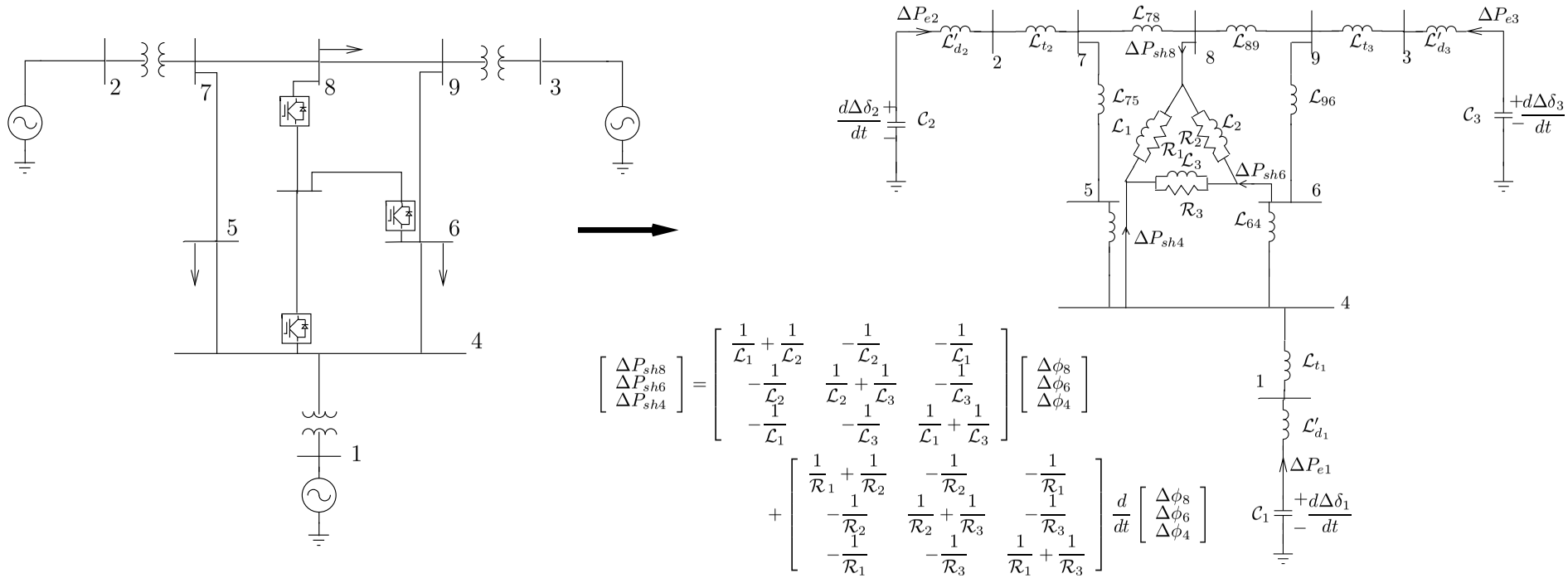

Figure 3.5: Control Strategy for a MTDC link. Note: $\Delta P_{sh8} + \Delta P_{sh6} + \Delta P_{sh7} = 0$, and the shunt power injections are dependent only on angular *differences.*

3.2.4 Extension to FACTS Devices

The utility of the circuit analogy presented in the previous section is limited to suggesting control laws related to real power flows and phase angular differences. Actually, a larger set of actuator-sensor pairs and similar control laws can be identified which introduce damping and synchronizing effects in the system. These can be inferred from a mathematical formulation which also uses the classical generator model as before, but relaxes the assumption of constant voltage magnitude at buses [42]. Series and shunt reactive power devices can therefore be made eligible for similar control strategies using the corresponding actuator-sensor pairs - see Table 3.1 .

One may also extend the restricted global strategy to combine dissimilar devices like a SSSC and a DC link, as shown in Fig. 3.6. For the scheme shown in the figure, the signals ΔI and $\Delta\phi_7 - \Delta\phi_8$ and their time derivatives are used to modulate ΔP_{dc} and ΔV_R using gain matrices. A formal state space analysis using these input-output pairs is needed to prove this.

Table 3.1: Collocated Actuator-Sensor Pairs

Actuator Variable	Sensed Signal	Actuator Description
ΔP_{sh}	$\Delta\phi$	DC converter terminal, STATCOM with energy source.
ΔI_R	ΔV	STATCOM, SVC
ΔP_{ser}	$\Delta\zeta$	SSSC with energy source
ΔV_R	ΔI	TCSC, SSSC

3.3 Limitation of the Circuit Analogy

At first sight, it appeared that the circuit analogy would simplify the design of damping and synchronizing controllers, by allowing circuit theory to be used for designing

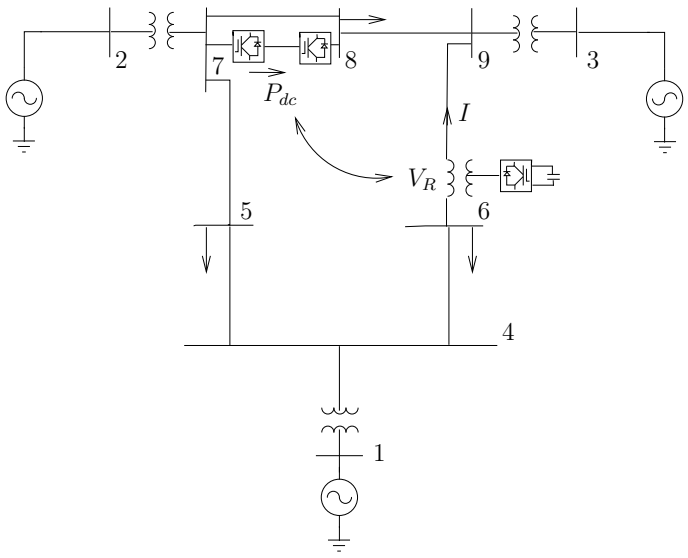

Figure 3.6: The Control Strategy with Dissimilar Devices: DC Link and SSSC

the controllers. However, for testing on large systems, the approximations in this theory, as well as the significantly increased calculations rendered it to be not so usable. Therefore, in the next section we have presented a formal state space analysis to quantify the effect of the control strategy and the degrees of freedom that it provides in terms of eigenvalue movement.

3.4 State Space Analysis

In this section, we present eigenvalue sensitivity expressions to evaluate the proposed control strategy. We use the classical model of the electro-mechanical system with constant real power loads to obtain the expressions. Losses in the electrical network are neglected. The linearized state space equations for the classical model of a power system may be written as follows:

$$\begin{bmatrix} \mathbf{\Delta}\dot{\delta} \\ \mathbf{\Delta}\dot{\omega} \end{bmatrix} = A \begin{bmatrix} \mathbf{\Delta}\delta \\ \mathbf{\Delta}\omega \end{bmatrix} + B\mathbf{u} \tag{3.1}$$

$$\mathbf{y} = C \begin{bmatrix} \mathbf{\Delta}\delta \\ \mathbf{\Delta}\omega \end{bmatrix} + D\mathbf{u} \tag{3.2}$$

where the set of all controllable inputs due to HVDC and FACTS devices are:

$$\mathbf{u} = [\mathbf{\Delta P_{sh}}^T \quad \mathbf{\Delta I_R}^T \quad \mathbf{\Delta P_{ser}}^T \quad \mathbf{\Delta V_R}^T]^T$$

If the measured variables are as follows,

$$\mathbf{y} = [\mathbf{\Delta}\phi^T \quad \mathbf{\Delta V}^T \quad \mathbf{\Delta}\zeta^T \quad \mathbf{\Delta I}^T]^T$$

then the matrices have the following structure [42].

$$A = \begin{bmatrix} [0] & I \\ -M^{-1}A_r & [0] \end{bmatrix} \tag{3.3}$$

$$A_r = A_{11} - [A_{12} \quad A_{13} \quad A_{14} \quad A_{15}]\, J_r \begin{bmatrix} A_{21} \\ A_{31} \\ A_{41} \\ A_{51} \end{bmatrix} \tag{3.4}$$

$$B = -M^{-1} \begin{bmatrix} [0] \\ B_\omega \end{bmatrix} = -M^{-1} \begin{bmatrix} [0] & [0] & [0] & [0] \\ A_{12} & A_{13} & A_{14} & A_{15} \end{bmatrix} J_r \tag{3.5}$$

$$C = -\begin{bmatrix} C_\delta & [0] \end{bmatrix} = -J_r \begin{bmatrix} A_{21} & [0] \\ A_{31} & [0] \\ A_{41} & [0] \\ A_{51} & [0] \end{bmatrix} \tag{3.6}$$

$$J_r = \begin{bmatrix} A_{22} & A_{23} & A_{24} & A_{25} \\ A_{32} & A_{33} & A_{34} & A_{35} \\ A_{42} & A_{43} & A_{44} & A_{45} \\ A_{52} & A_{53} & A_{54} & A_{55} \end{bmatrix}^{-1} = D \tag{3.7}$$

The matrix M is a diagonal matrix with $\frac{2H_i}{\omega_B}$ as its ith diagonal element, where i denotes the machine number. The sub-matrices A_{ij} relate the five sets of variables,
$[\mathbf{\Delta P_e}^T \quad \mathbf{\Delta P_{sh}}^T \quad \mathbf{\Delta I_R}^T \quad \mathbf{\Delta P_{ser}}^T \quad \mathbf{\Delta V_R}^T]^T$
to the variables

$[\mathbf{\Delta}\delta^T \quad \mathbf{\Delta}\phi^T \quad \mathbf{\Delta V}^T \quad \mathbf{\Delta}\zeta^T \quad \mathbf{\Delta I}^T]^T$.

These matrices are obtained from the linearized real and reactive power balance

equations for shunt and series connected devices [42]. For example, A_{23} denotes the Jacobian matrix $[\frac{\partial P_{sh}}{\partial V}]$ which is evaluated at the equilibrium point, and which is obtained from the real power balance equations at every node of the network. It has been shown in [42] that,

(1) For a lossless transmission system, the matrices A_{ij}, A_r and D are symmetric, while $C_\delta = B_\omega^T$.

(2) For a n machine system, the matrix A has $(n-1)$ pairs of purely imaginary eigenvalues (the swing modes). The i^{th} eigenvalue is denoted by λ_i.

(3) The right eigenvectors $\mathbf{e_i}$ and left eigen-vectors $\mathbf{f_i}$ corresponding to the eigenvalue λ_i are related to each other by the following equation.

$$\mathbf{f_i} = \begin{bmatrix} \mathbf{f}_{\delta_\mathbf{i}} \\ \mathbf{f}_{\omega_\mathbf{i}} \end{bmatrix} = h_i \begin{bmatrix} \lambda_i M \mathbf{e}_{\delta_\mathbf{i}} \\ M \mathbf{e}_{\delta_\mathbf{i}} \end{bmatrix} = h_i \begin{bmatrix} M \mathbf{e}_{\omega_\mathbf{i}} \\ M \frac{\mathbf{e}_{\omega_\mathbf{i}}}{\lambda_i} \end{bmatrix} \tag{3.8}$$

where $\mathbf{e}_{\omega_\mathbf{i}}$ and $\mathbf{e}_{\delta_\mathbf{i}}$, and $\mathbf{f}_{\omega_\mathbf{i}}$ and $\mathbf{f}_{\delta_\mathbf{i}}$ denote the right and left eigenvector components corresponding to the rotor speeds and angles respectively. h_i is an arbitrary scalar constant.

(4) Due to the symmetry of A_r and diagonal nature of M, $\mathbf{e}_{\delta_\mathbf{i}}$ may be chosen to be real.

The change in an eigenvalue due to a small perturbation in the A matrix, ΔA, is given by [5]

$$\Delta\lambda_i = \frac{\mathbf{f_i}^T \Delta A \, \mathbf{e_i}}{\mathbf{f_i}^T \mathbf{e_i}} \tag{3.9}$$

Using this equation, let us evaluate the eigenvalue change due to power flow modulation in the dc links.

Consider a system in which there are l two terminal dc links. Other controllable elements (e.g, FACTS) are assumed to be absent. Additionally, if the variations in the reactive power drawn by the dc links due to power modulation are neglected[3],

[3]In Line Commutated Converter(LCC) based links, reactive power drawn at the converter ac

then we have a reduced number of controllable inputs consisting of only shunt power injections at the buses to which the dc links are connected. If dc transmission losses are neglected, then we can relate $\mathbf{u}$ to the dc power flows (P_{dc}) as follows.

$$\mathbf{u} = \begin{bmatrix} \mathbf{\Delta P_{sh}} \\ \mathbf{\Delta I_R} \\ \mathbf{\Delta P_{ser}} \\ \mathbf{\Delta V_R} \end{bmatrix} = \begin{bmatrix} \mathbf{\Delta P_{sh}} \\ \mathbf{0} \\ \mathbf{0} \\ \mathbf{0} \end{bmatrix} = \begin{bmatrix} -R \\ [0] \\ [0] \\ [0] \end{bmatrix} \begin{bmatrix} \Delta P_{\mathrm{dc}_1} \\ \vdots \\ \Delta P_{\mathrm{dc}_l} \end{bmatrix} \tag{3.10}$$

R is a $n \times l$ matrix, where n denotes the number of buses in the network. Note that this matrix relates the controllable shunt active power injections at the ac buses to the dc power flows. $R(i,q) = +1$ and $R(j,q) = -1$ if the q^{th} link is connected to bus i and j, and the dc power flow direction is from i to j. All the other terms of R are zero.

Let us use only the voltage phase angular differences between the ac terminals to which the two terminal dc links are connected, as feedback signals. If the q^{th} link is connected to bus i and j, then the phase angular difference $\phi_{d_q} = \phi_i - \phi_j$. Therefore, this set of signals for the l dc links can be related to $\mathbf{y}$ as follows.

$$\begin{bmatrix} \Delta\phi_{d_1} \\ \vdots \\ \Delta\phi_{d_l} \end{bmatrix} = R^T \mathbf{\Delta}\phi = \begin{bmatrix} R^T & [0]^T & [0]^T & [0]^T \end{bmatrix} \mathbf{y} \tag{3.11}$$

terminals is dependent on the active power flow, while in Voltage Source Converter(VSC) based links it can be regulated independently. Active power usually has greater controllability over a swing mode than the reactive power and it is expected to predominate.

If we use the following control law,

$$\begin{bmatrix} \Delta P_{\mathrm{dc}_1} \\ \vdots \\ \Delta P_{\mathrm{dc}_l} \end{bmatrix} = \alpha K_s \begin{bmatrix} \Delta \phi_{d_1} \\ \vdots \\ \Delta \phi_{d_l} \end{bmatrix} \tag{3.12}$$

where K_s is a matrix gain and α is a scalar multiplying factor, then

$$\mathbf{u} = -\alpha S K_s S^T \mathbf{y} \tag{3.13}$$

where $S^T = \begin{bmatrix} R^T & [0]^T & [0]^T & [0]^T \end{bmatrix}$

If the control law (3.12) is used, then

$$\mathbf{y} = C \begin{bmatrix} \boldsymbol{\Delta}\delta \\ \boldsymbol{\Delta}\omega \end{bmatrix} + D\mathbf{u} = C \begin{bmatrix} \boldsymbol{\Delta}\delta \\ \boldsymbol{\Delta}\omega \end{bmatrix} - \alpha D S K_s S^T \mathbf{y} \tag{3.14}$$

Therefore, (3.1) becomes,

$$\begin{bmatrix} \boldsymbol{\Delta}\dot{\delta} \\ \boldsymbol{\Delta}\dot{\omega} \end{bmatrix} = (A + \Delta A) \begin{bmatrix} \boldsymbol{\Delta}\delta \\ \boldsymbol{\Delta}\omega \end{bmatrix} \tag{3.15}$$

where,

$$\Delta A = -\alpha B S K_s S^T (I + \alpha D S K_s S^T)^{-1} C \tag{3.16}$$

Assuming that α is small, we can approximate ΔA as follows,

$$\Delta A = -\alpha B S K_s S^T C \tag{3.17}$$

From the structure of B and C, shown in (3.5) and (3.6) respectively, it is clear that

the structure of ΔA is as follows.

$$\Delta A = - \begin{bmatrix} [0] & [0] \\ \alpha M^{-1} B_\omega S K_s S^T C_\delta & [0] \end{bmatrix} \tag{3.18}$$

Recognizing that $C_\delta = B_\omega^T$, we obtain (3.19).

$$\Delta A = \alpha \begin{bmatrix} [0] & [0] \\ -M^{-1}(B_\omega S K_s S^T B_\omega^T) & [0] \end{bmatrix} \tag{3.19}$$

Therefore,

$$\Delta\lambda_i = -\alpha \, \frac{\mathbf{f_i}^T B S K_s S^T C \mathbf{e_i}}{\mathbf{f_i}^T \mathbf{e_i}} \tag{3.20}$$

$$= -\alpha \, \frac{\begin{bmatrix} \lambda_i \mathbf{e_{\delta_i}}^T M & \mathbf{e_{\delta_i}}^T M \end{bmatrix} \begin{bmatrix} [0] \\ -M^{-1} B_\omega \end{bmatrix} S K_s S^T \begin{bmatrix} -C_\delta & [0] \end{bmatrix} \begin{bmatrix} \mathbf{e_{\delta_i}} \\ \mathbf{e_{\omega_i}} \end{bmatrix}}{\begin{bmatrix} \lambda_i \mathbf{e_{\delta_i}}^T M & \mathbf{e_{\delta_i}}^T M \end{bmatrix} \begin{bmatrix} \mathbf{e_{\delta_i}} \\ \mathbf{e_{\omega_i}} \end{bmatrix}} \tag{3.21}$$

Since $\lambda_i \mathbf{e_{\delta_i}} = \mathbf{e_{\omega_i}}$,

$$\Delta\lambda_i = -\alpha \, \frac{\mathbf{e_{\delta_i}}^T B_\omega S K_s S^T B_\omega^T \mathbf{e_{\delta_i}}}{2\lambda_i \mathbf{e_{\delta_i}}^T M \mathbf{e_{\delta_i}}} \tag{3.22}$$

For a swing mode, $\lambda_i = j\Omega_i$. Therefore,

$$\Delta\lambda_i = \frac{j\alpha}{2\Omega_i} \left(\frac{\mathbf{e_{\delta_i}}^T B_\omega S K_s S^T B_\omega^T \mathbf{e_{\delta_i}}}{\mathbf{e_{\delta_i}}^T M \mathbf{e_{\delta_i}}} \right) = \frac{j\alpha}{2\Omega_i} \frac{\mathbf{z_i}^T K_s \, \mathbf{z_i}}{\mathbf{e_{\delta_i}}^T M \mathbf{e_{\delta_i}}} \tag{3.23}$$

Note that M is a diagonal matrix with positive values on the diagonal. If $\alpha > 0$ and the matrix K_s is positive definite[4], then quantity in the round brackets in this equation is greater than zero if $\mathbf{z_i}$ is non-zero. Therefore, this control law leads to an

[4]In other words, $\mathbf{r}^T K_s \mathbf{r} > 0$ for all non-zero real vectors $\mathbf{r}$.

increase in the *frequency* of the swing modes which are controllable by the dc links. This is is a manifestation of increased synchronizing effects.

On the other hand, if we use the control law:

$$\begin{bmatrix} \Delta P_{\mathrm{dc}_1} \\ \vdots \\ \Delta P_{\mathrm{dc}_l} \end{bmatrix} = \alpha K_d \frac{\mathrm{d}}{\mathrm{d}t} \begin{bmatrix} \Delta\phi_{d_1} \\ \vdots \\ \Delta\phi_{d_l} \end{bmatrix} = \alpha K_d \begin{bmatrix} \Delta f_{d_1} \\ \vdots \\ \Delta f_{d_l} \end{bmatrix} \tag{3.24}$$

The control law (3.24) implies that $\mathbf{u} = -\alpha S K_d S^T \dot{\mathbf{y}}$.

Therefore, from (3.2) we obtain,

$$\dot{\mathbf{y}} = C \begin{bmatrix} \mathbf{\Delta}\dot{\delta} \\ \mathbf{\Delta}\dot{\omega} \end{bmatrix} + D\dot{\mathbf{u}} \tag{3.25}$$

$$= \begin{bmatrix} [0] & -C_\delta \end{bmatrix} \begin{bmatrix} \mathbf{\Delta}\delta \\ \mathbf{\Delta}\omega \end{bmatrix} - \alpha D S K_d S^T \ddot{\mathbf{y}} \tag{3.26}$$

Therefore,

$$\begin{bmatrix} \mathbf{\Delta}\dot{\delta} \\ \mathbf{\Delta}\dot{\omega} \end{bmatrix} = (A + \Delta A) \begin{bmatrix} \mathbf{\Delta}\delta \\ \mathbf{\Delta}\omega \end{bmatrix} + \alpha^2 B S K_d S^T [D S K_d S^T \ddot{\mathbf{y}}] \tag{3.27}$$

$$\approx (A + \Delta A) \begin{bmatrix} \mathbf{\Delta}\delta \\ \mathbf{\Delta}\omega \end{bmatrix} \tag{3.28}$$

The approximation holds when α is small. Note that,

$$\Delta A = -\alpha B S K_s S^T \begin{bmatrix} [0] & -C_\delta \end{bmatrix} \tag{3.29}$$

From structure of B given in (3.5), we obtain the structure of ΔA, which is as follows.

$$\Delta A = - \begin{bmatrix} [0] & [0] \\ [0] & \alpha M^{-1} B_\omega S K_d S^T C_\delta] \end{bmatrix} \tag{3.30}$$

This leads us to (3.31), since $C_\delta = B_\omega^T$

$$\Delta A = \alpha \begin{bmatrix} [0] & [0] \\ [0] & -M^{-1}(B_\omega S K_d S^T B_\omega^T) \end{bmatrix} \tag{3.31}$$

where the matrices $B_\omega S K_s S^T B_\omega^T$ and $B_\omega S K_d S^T B_\omega^T$ are positive semi-definite.

then

$$\Delta\lambda_i = -\frac{\alpha}{2} \frac{\mathbf{e_{\delta_i}}^T B_\omega S K_d S^T B_\omega^T \mathbf{e_{\delta_i}}}{\mathbf{e_{\delta_i}}^T M \mathbf{e_{\delta_i}}} = -\frac{\alpha}{2} \frac{\mathbf{z_i}^T K_d \mathbf{z_i}}{\mathbf{e_{\delta_i}}^T M \mathbf{e_{\delta_i}}} \tag{3.32}$$

which implies increased damping for all swing modes, if K_d is positive definite and $\alpha > 0$.

Clearly, the control laws affect the synchronizing components (proportional to angle variations) and damping components (proportional to speed variations) of the electrical torque. Note that with positive definite K_d the damping torque of all modes is improved. This is the main idea for designing controllers used in this thesis.

If we wish to improve both synchronizing and damping effects, then the sum of the right hand side of equations (3.12) and (3.24), may be used to modulate the dc power flows.

Note that:

(1) In addition to being positive definite, it is advantageous if the matrices K_s and K_d are chosen to be symmetric positive definite (spd). If K_s and K_d are spd and

have the following form,

$$\begin{bmatrix} \times & \times & \times & \times \\ \times & \times & \times & \times \\ \times & \times & \times & \times \\ \times & \times & \times & \times \end{bmatrix}$$

where '$\times$' denotes an element of the matrix, then the following modified matrix (obtained by setting the off-diagonal elements corresponding to the second row *and* second column to zero), is also spd.

$$\begin{bmatrix} \times & 0 & \times & \times \\ 0 & \times & 0 & 0 \\ \times & 0 & \times & \times \\ \times & 0 & \times & \times \end{bmatrix}$$

This follows from the properties of spd matrices that every diagonal element is positive and every principal submatrix is also spd [66]. In this example, a 4×4 matrix is used and the off-diagonal elements of the second row and column are set to zero, but the property holds true for spd matrices of arbitrary size and for any row (and the corresponding column).

This property implies that if we use a spd gain matrix and if the j^{th} dc link is unexpectedly shut-down or if communication from any dc link to the j^{th} link is down, then the positive definite character of the gain matrix which is important to achieve the desired effects, can be retained by setting the non-local channel gains in the j^{th} link to zero and multiplying with zero, the frequency difference signal from this link which is sent out to the other links. This decision can be taken and implemented locally at the j^{th} link. Thus we can seamlessly revert to local control in case of problems.

Any modification in the gain matrix, as long as it does not alter its spd character

is acceptable in the sense that it will contribute to positive damping and/or synchronizing effects of all modes (although it may not be optimal). Similarly, changes in the network topology or operating conditions will alter B_ω, Ω_i and $\mathbf{e}_{\delta_i}$, but as long as the gain matrix is spd, the sign of $\Delta\lambda_i$ is not altered - see (3.32). Therefore, this strategy is *robust* to loss of remote signals as well as changes in network topology and operating conditions.

(2) The implementation of the strategy is well within the capabilities of present day technology. Measurement of frequency at a location and communication of this signal is a part of PMU/WAMS functionality. With the modern day technology, the phase and frequency signal (both signals approximately in quadrature with each other) can be made available on a continuous basis in every cycle.

(3) As this control strategy requires a limited set of non-local signals, the use of the phasor data concentrator at a central control center for collation of system-wide data is neither necessary nor recommended, as this could add additional delays and possibly reduce reliability. Instead, a direct communication link can be used to exchange signals, as is the commonly the case with most HVDC links.

(4) Unlike other HVDC based damping controllers such as the one incorporated in the Pacific DC Intertie which target only a particular swing mode of interest at the most common operating point, the proposed control strategy provides improved damping for all the swing modes of the system. In addition, it is robust to changes in operating point and network conditions.

3.5 Concluding Remarks

1. The strategy for the control of power flow through dc links embedded in an ac system is presented based on an intuitive circuit analogy of the electro-mechanical model of the power system.

2. The control strategy introduce synchronizing and damping torque respectively if

power flow through the dc link is made proportional to the phase and frequency difference between the buses to which it is connected.

3. The control strategy can also be extended to the multiple dc links which gives us additional *degrees of freedom* to selectively increase the leverage on a particular swing mode.

4. For a multiple dc link, in the event of the loss of communication from a remote link, the strategy reverts back to the local strategy which still ensures positive synchronizing/damping effect.

5. While implementation of the control laws if the steady state change in the dc link power is not desired then appropriate washout blocks can be used.

6. Since the control strategy has been introduced in an intuitive fashion, a formal state space analysis is provided to analyze the eigenvalue movement when the dc power flow is made proportional to the phase and frequency difference signals.

7. A rigorous sensitivity analysis proof has been given in this chapter which explain that the proposed control strategy improves damping and synchronizing effect of all the swing modes of the system regardless of the change in operating point or network condition of the system. Furthermore, it also shows that the proposed strategy is robust to the loss of communication.

Chapter 4

HVDC Superline concept and Robust Control for single/multiple HVDC links embedded in an ac system: Case Studies

The previous chapter proposed a strategy based on intuitive circuit analogy for power system network to control the power flow through the dc link to improve angular stability of the ac-dc system. The proposed control strategy was based on various assumptions such as generators have a classical model (i.e only frequency and rotor angle are the states), generator mechanical power inputs and load active powers are constant, transmission losses are neglected, and bus voltages are constant (1pu). In order to test the efficacy of this control strategy on a realistic system, it was tested on a system without any such assumptions where all the elements were modeled to the fullest possible details. The objectives of the case studies in this chapter are as

below:

1. To validate the strategy on a detailed ac system (with detailed generator models, transmission losses etc.)

2. To investigate the synchronizing and damping torque of the DC link embedded in an ac system controlled by the proposed strategy and its impact on the angular stability.

3. Demonstrate the stabilizing effect by utilizing the degrees of freedom provided by the control of power flow through multiple DC links.

4. To assess the performance of the control strategy during various contingencies such as increased loading, contingency (line removal), and loss of communication.

5. Conduct small signal analysis of the ac-dc system to show the beneficial eigenvalue movement for the proposed control strategy and its validation by the time domain simulations.

4.1 Case Study 1: Two machine system with parallel AC-DC links

A 2 machine system is simulated in PSCAD/EMTDC. From the circuit analogy, a small signal analog circuit equivalent of this system is shown in Fig 4.1. Synchronous machine in Area 1 is delivering power to Area 2 through double circuit AC line and HVDC link. AC transmission lines are rated at 345 kV, 400 km in length at 50 Hz. These transmission lines are modeled using Bergeron Model in PSCAD/EMTDC. HVDC links are modeled using CIGRE benchmark model rated at 1000 MW 500 kV DC. In steady state HVDC link transfers 500 MW power from Area 1 to 2. Fig 4.2 shows the DC current order control implemented in PSCAD/EMTDC. Frequency

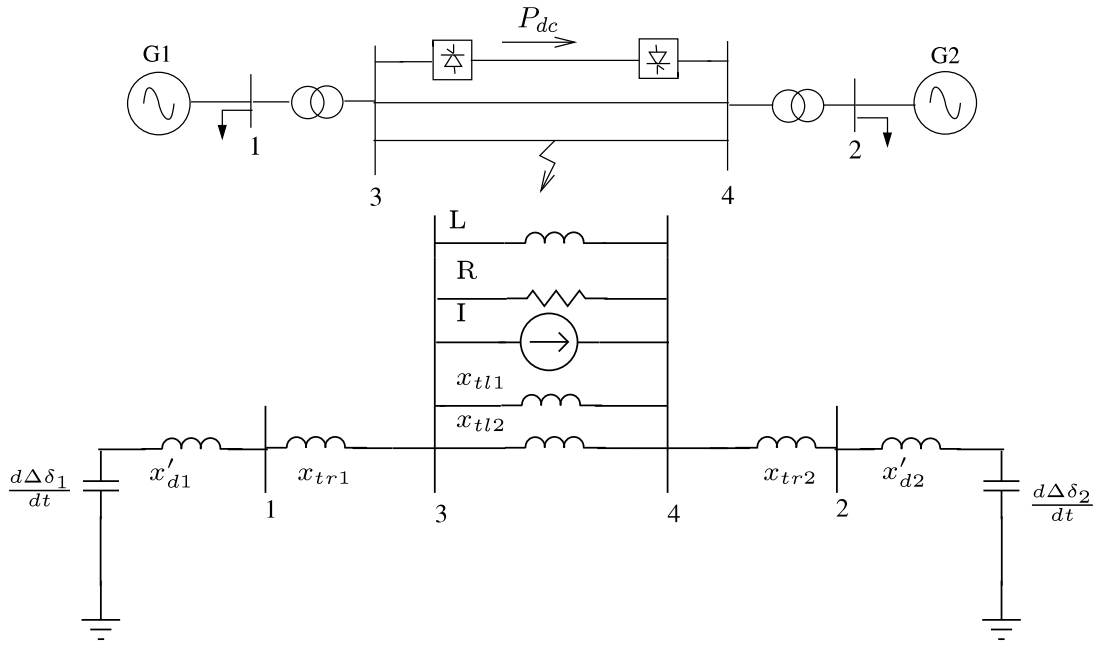

Figure 4.1: Two machine with parallel AC-DC links and its small signal equivalent model

difference at both the converter ends are measured. Gains K_1 and K_2 are selected such that for ± 1rad/sec of frequency difference or 1rad angular difference between the two areas will modulate the DC power by ±1000 MW. Since the strategy is to use overload capacity of HVDC link to provide synchronizing and damping torque, a hard limiter is introduced in the control to limit the current order to ±3% of its steady state capacity (±1030 MW). Both the synchronous machine in area 1 and 2

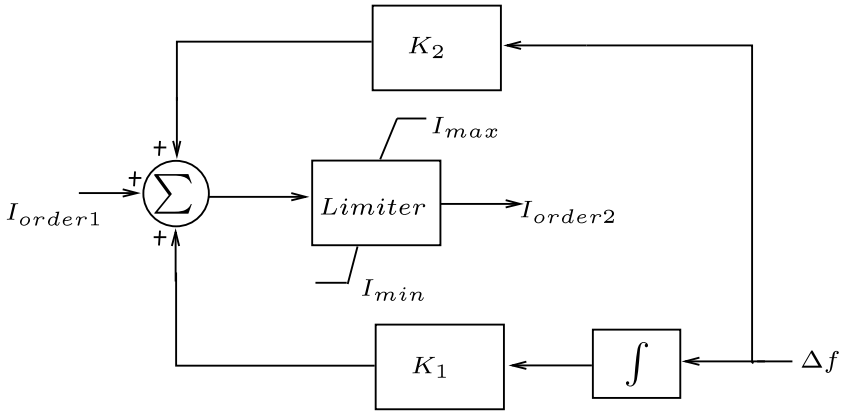

Figure 4.2: Supplementary DC control for synchronizing and damping torque

are rated at 22 kV, with 3080 MVA and 1025 MVA, and three phase resistive load of 1000 MW and 3000 MW respectively.

4.1.1 Effect of Synchronizing and Damping Torque through HVDC Links

In order to show the synchronizing and damping effect through HVDC link on the 2 machine system a three phase fault is applied on one of the transmission line for 3 cycles followed by tripping of the line. These tests are performed with the following HVDC controls

1. With synchronizing torque only.
2. With damping torque only
3. With both synchronizing and damping torque

From Fig 4.3 it can be observed that when the HVDC link is in synchronizing torque control mode, the system can sustain the fault without losing synchronism, whereas when the HVDC link is in damping control mode, the system could not sustain this fault and loses synchronism. This is mainly because in the latter case the rotor angle deviation is more due to which the machines lose synchronism compared to the HVDC link with synchronizing torque control where the rotor angular deviation is lesser and the machines remains in synchronism. The system shows better performance with both the components of the torque.

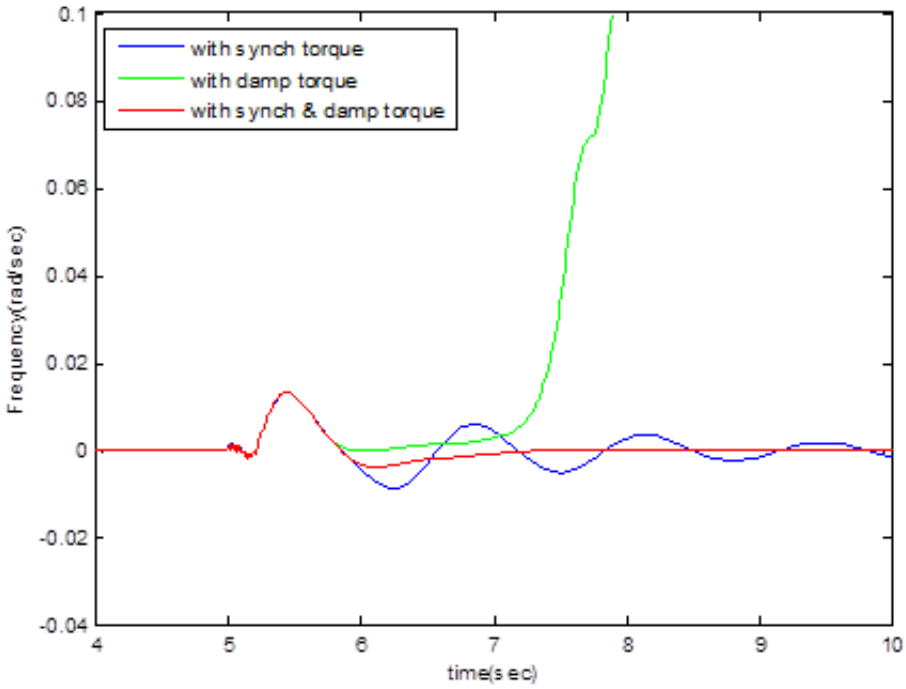

Figure 4.3: Longer Duration of Fault

4.2 Case Study 2: Three machine System

An illustrative example based on the three machine system is shown in Fig.4.4.

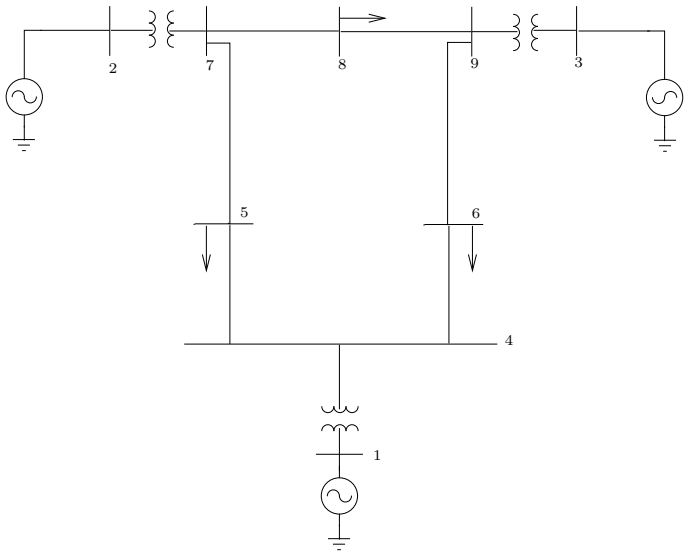

Figure 4.4: Three Machine System

A detailed generator model is considered. The generators are equipped with static excitation systems with AVRs which are modeled by a single time constant transfer function and gain, 250 pu/pu and 0.05s respectively. The loads are of constant impedance type and the transmission lines have resistance losses. The two swing modes of the system obtained using small signal analysis are described in Table 4.1.

Table 4.1: Swing Modes of the Three Machine System: Base Case

Mode Description	Eigenvalues
Swing Mode I: Generators 2 and 3 swing against Generator 1	-0.0556 + j 8.6550
Swing Mode II Generator 3 swings against Generator 2, with low participation of Generator 1	-0.1353 +j 13.2844

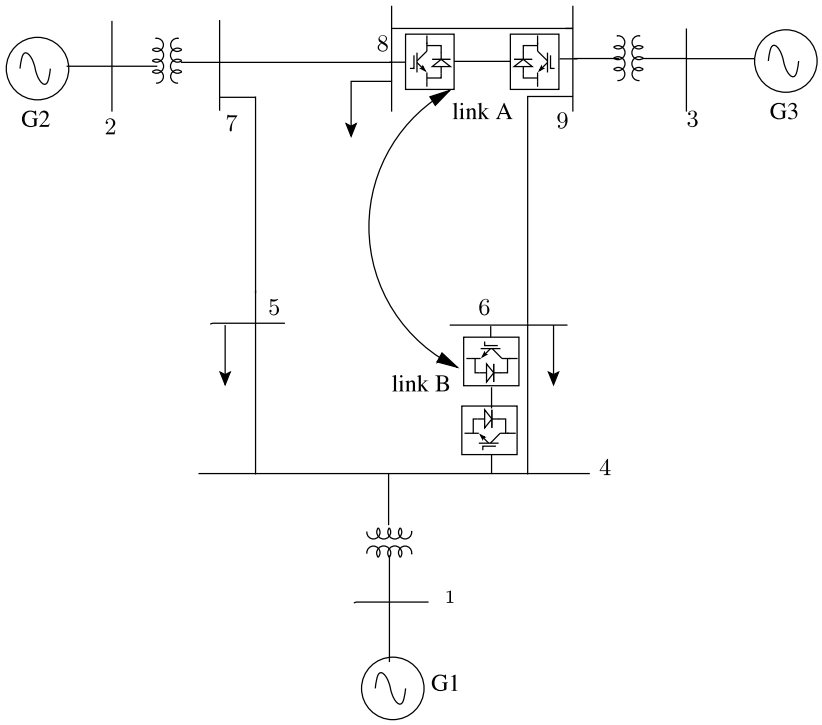

Figure 4.5: Three Machine System with two VSC DC links

Two VSC based DC links are introduced in the system as shown in Fig. 4.5 in order to study the effects of the control strategy. The quiescent power flow in both links is

set to zero, so that the study can be done for the same equilibrium condition as before. The small-signal analysis program models the dc links as controllable power injections at the buses to which they are connected. The reactive power injections by the DC links are assumed to be regulated to zero by the VSCs. Since our objective here is to analyze the movement of the electromechanical modes which are low frequency modes using small signal analysis, we can ignore the details of modeling the VSC because small signal analysis of such detailed VSCs will result in high frequency modes. Instead we can simply model them as static loads with equal magnitude and opposite sign (-P for the rectifier end and +P for the inverter end) power injections at the converter buses. Any power modulation through these dc links based on the proposed strategy can be added to the steady state power flow to achieve stabilizing effects.

We consider three sets of gain matrices to illustrate the utility of the degrees of freedom. The primary concern in this system is the damping of the swing modes. Therefore, we consider only the "resistance" matrix - the "inductance" matrix is set to zero, i.e., $\mathcal{L}_1 = \mathcal{L}_2 = \mathcal{M} = 0$. Also, the time constant in the approximate implementation of the derivative of phase angle is assumed to be small: $T = 10$ ms. In a later case study with the 16 machine system, we have also explored the synchronizing torque enhancement.

Note that the above approach is guaranteed to increase damping of all modes as long as the gain matrix K_d is spd. However, another concern is that the control scheme must be robust to a loss of communication between the two links, in this case the controller matrix structure reverts to a diagonal one. The diagonal elements of K_d (local gains) can be selected in the conventional manner based on local damping controller design principles [61]. This ensures that with the loss of communication the system behavior would be the same as that of two individually tuned HVDC systems.The off-diagonal elements can then be selected with the constraint that K_d

remain spd. The "resistance" matrices in Cases I and II given below are spd in nature as their eigenvalues are positive ($\mu_1 = 1.0, \mu_2 = 0.1$). Case III denotes the case where communication is lost (the mutual term becomes equal to zero) resulting in a local strategy - the eigenvalues of the gain matrix are ($\mu_1 = 0.28, \mu_2 = 0.82$).

Case I: $\mathcal{R}_1 = 0.28, \mathcal{R}_2 = 0.82, \mathcal{R}_m = -0.36$

Case II: $\mathcal{R}_1 = 0.82, \mathcal{R}_2 = 0.36, \mathcal{R}_m = 0.36$

Case III: $\mathcal{R}_1 = 0.28, \mathcal{R}_2 = 0.82, \mathcal{R}_m = 0$

The gains units are in pu/(rad/s) on a 100 MVA base.

In Case I, we chose the elements of the gain matrix such that the damping effect on Swing Mode I is preferentially higher. In Case II, we preferentially try to increase the damping effect on Swing Mode II. This effect is shown in Table.4.2. Note that in both these cases, damping for both the swing modes have improved but to different extents. Case III denotes the case where communication is lost (the mutual terms becomes zero) resulting in a control scheme that uses only local signals.

In Case III, where remote signals are lost, an improvement in damping from the no-damping-controller case of Table.4.2 is still observed, although the damping of mode I is not as good as in Case I.

Table 4.2: Effect of Restricted Global Strategy: Base Loading

Case	Swing Mode I	Swing Mode II
No Control	-0.0556 + j 8.6550	-0.1353 +j 13.2844
I	-0.1848 + j 8.7604	-0.2283 + j 13.3222
II	-0.0732 + j 8.6595	-0.4582 + j 13.8626
III	-0.1550 + j 8.7201	-0.3425 + j 13.5031

The results of the study done at a different loading condition (a 50% increase in the load at the buses 5, 6 and 8) are shown in Table 4.3. The results for a different network topology - line 5-7 is removed are shown in Table 4.4. The same set of gains

as in Case I is used. Although the gains are not specifically designed for these cases, they always work to improve the damping, attesting to the robustness of the control law.

Table 4.3: Effect of Control Strategy: Increased Loading

Case	Swing Mode I	Swing Mode II
Without Damping Controller	-0.1665 + j 8.4615	-0.3497 +j 13.1670
Gains as in Case I	-0.3015 + j 8.5734	-0.4547 + j 13.1996

Table 4.4: Effect of Control Global Strategy: Line 5-7 Removed

Case	Swing Mode I	Swing Mode II
Without Damping Controller	0.1071 + j 6.7523	-0.2657 + j 13.2076
Gains as in Case I	-0.3354 + j7.0279	-0.3712 + j 13.2634

We now present a detailed simulation result to verify the conclusions. The modeling is done on PSCAD. The two DC links are rated at 100 MW each, have "inner" real and reactive current controls and use a PWM switching scheme. Reactive power injections by the links are regulated to zero. The control strategy discussed in the previous paragraphs is used to modulate the power flows of the DC links.

A disturbance is given in the form of a single phase to ground fault near bus 7 which is cleared in 60 ms by tripping line 5-7. The resulting swings without a damping controller are unstable - the growing oscillation of 1 Hz is clearly seen in Fig. 4.6. However, application of the damping controller is able to damp the oscillations (Fig. 4.7) as predicted by the eigenvalues of Table 4.4. From Fig.4.8 we can observe that the small signal response (with control for line 5-7 removed) matches reasonably in terms of the swing frequency and damping with the EMTDC simulation validating

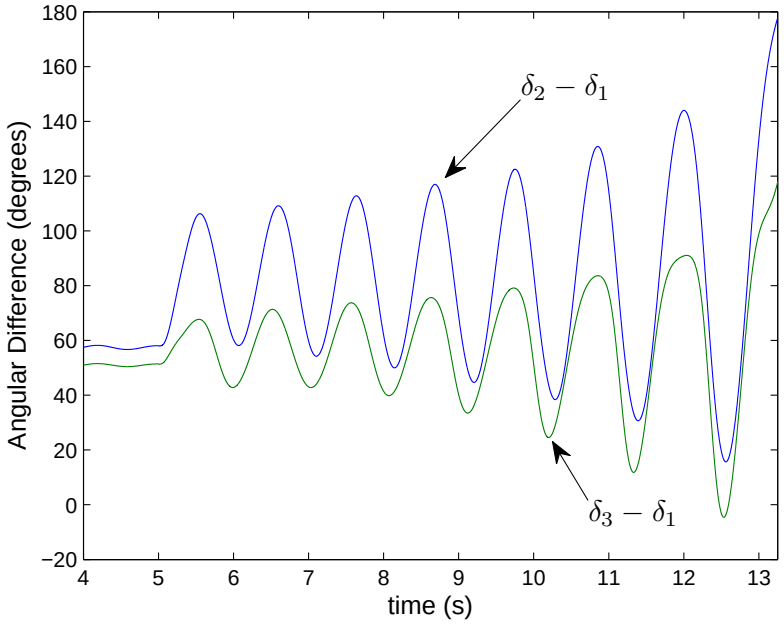

Figure 4.6: Response for a fault on line 5-7, followed by line tripping (No damping controller).

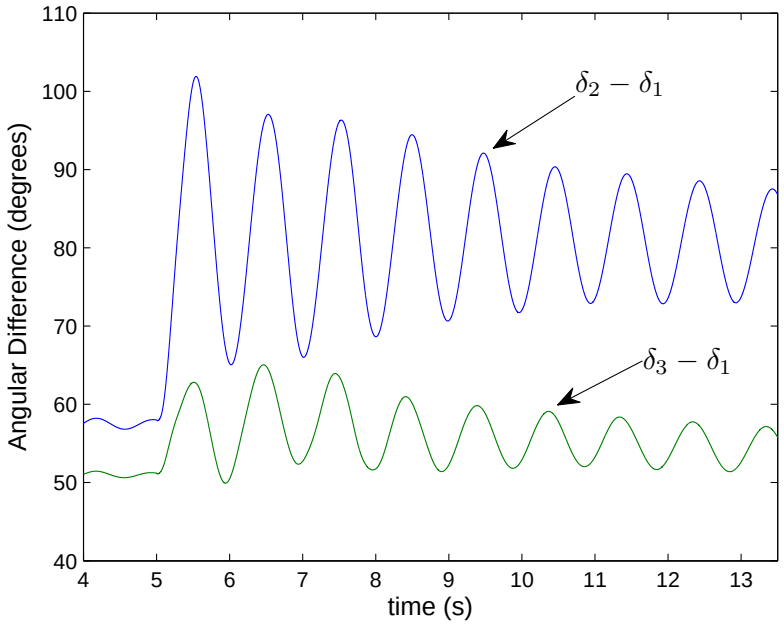

Figure 4.7: Response for a fault on line 5-7, followed by line tripping (damping controller present).

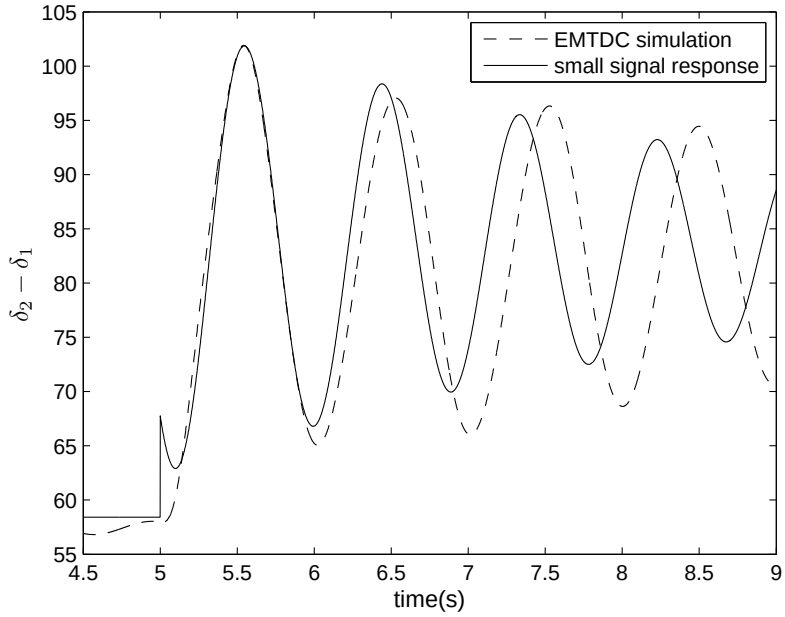

Figure 4.8: Comparison of EMTDC and Small Signal Results.

the small signal model. The swing frequency for the EMTDC is approximately 6.3 rad/sec while is slightly lower that the one obtained from small signal analysis is 7.03 rad/sec, but damping is same.

4.3 Case Studies: 16 machine System

The 16 machine system which is used to test the control strategy is shown in Fig. 4.9. Two VSC dc links are introduced in the system at bus 41-36 and 52-37, as shown in the figure. These are rated at 1000 MW and 1500 MW respectively. The reactive power injections at the dc link terminals are maintained at zero. The base-case powerflow, generator and network data are adapted from [5]. The generators are modeled in detail along with their excitation systems. The small-signal and transient stability analysis programs used in this section model the dc links as controlled power injections at the converter stations. The damping controller for the dc links is shown in Fig.4.10 with $\alpha = 1$, $T_w = 20$ s, while the compensator is disabled by setting

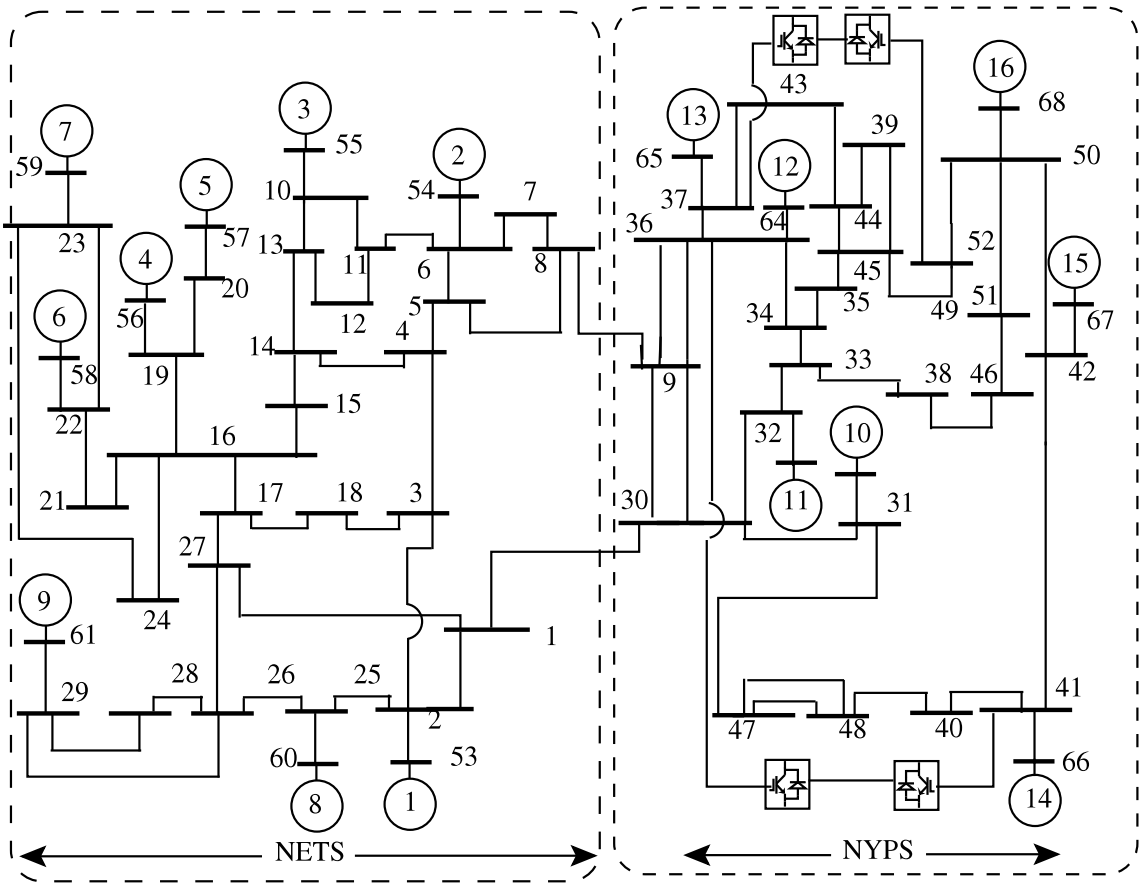

Figure 4.9: 16 machine 58 bus NETS-NYPS test system.

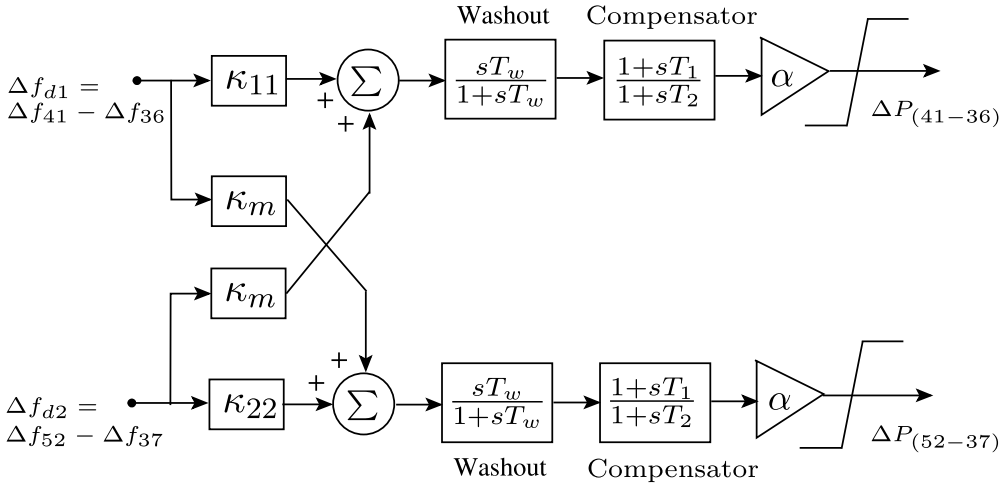

Figure 4.10: Damping Controllers for the dc links across buses 41-36 and 52-37

$T_1 = T_2$.

4.3.1 Eigenvalue Analysis and Gain Matrix Selection

The low frequency swing modes that are controllable by power modulation in the dc links are shown in Table 5.1. The elements of the 2×2 gain matrix (κ_{11}, κ_{22}, and

Table 4.5: Low frequency Swing Modes Controllable by the two dc links: Base Case (No control)

Mode Description/Generators with high participation	Eigenvalues
Swing Mode I: Generators 13 and 15 swing against 14 and 16	-0.009 ± j 4.692
Swing Mode II: Generators 12 swings against 13	-0.113± j 4.248
Swing Mode III: Generator 14 swings against 16	-0.003 ± j 3.364
Swing Mode IV: Generators 9 and 13 swing against 14 and 15	-0.080 ± j 2.497

$\kappa_m = \kappa_{12} = \kappa_{21}$), are selected using an exhaustive optimization where the objective function is to find the gains which give the best damping for the swing mode of interest for the normal operating point. In this analysis, the normal operating point is considered as one where all dc converters are operating at the rated condition. The optimized gains are expressed in pu/(rad/s), on a 100 MVA base and are given below:

Case NC: No Control, i.e, the gain matrix is a zero matrix

Case I: $\kappa_{11} = 3.45,\ \kappa_{22} = 1.32,\ \kappa_m = 2$

Case II: $\kappa_{11} = 3.35,\ \kappa_{22} = 3.96,\ \kappa_m = -2$

Case III: $\kappa_{11} = 3.35,\ \kappa_{22} = 3.96,\ \kappa_m = 0$

Gains in Case I of Table 4.6 are optimized to preferentially damp Swing Mode IV, i.e., make the negative real part most negative. As can be seen, this decreases

Table 4.6: Eigenvalues (Base Network Condition)

Case	Swing Mode I	Swing Mode II	Swing Mode III	Swing Mode IV
NC	-0.009 ± j 4.692	-0.113 ± j 4.248	-0.002 ± j 3.365	-0.080 ± j 2.497
I	-0.104 ± j 4.430	**-1.125 ± j 4.136**	-0.102± j 3.379	**-0.925 ± j 2.975**
II	-0.212 ± j 4.590	-0.288 ± j 4.343	**-1.246 ± j 3.461**	-0.343 ± j 2.526
III	-0.117 ± j 4.451	-0.892 ± j 4.466	-0.689 ± j 3.402	-0.656 ± j 2.646

from -0.08 to -0.925. Incidentally, it was observed from modal analysis that Modes II and IV have residue angles in a close range, therefore with an increase in damping of Swing Mode IV, damping of Swing Mode II also increases from -0.113 to -1.125. Gains in Case II of Table 4.6 are optimized to preferentially damp Swing Mode III where damping increases from -0.002 to -1.246. Here κ_m has a negative value. Thus, κ_m can be chosen to achieve targeted damping of modes depending on which of them are found to be critically damped during actual operation. Case III is a special case where the system is originally as in Case II, but there is an interruption in communication between the two links. This is represented by setting κ_m to zero. As can be seen in Table 4.6, with the loss of communication, damping of Swing Mode III is still better compared to the uncontrolled case (-0.689 in Case III as compared to -0.002 in NC). This shows that the proposed control shown in the paper is robust to the loss of communication.

4.3.2 Robustness of the Proposed Approach

We now test the proposed control strategy for different network conditions. The eigenvalues when line 39-45 is removed and when line 8-9 is removed are shown in Table 4.7 and 4.8. Although the gain matrices in Case I and II are optimized for the normal operating point to damp Mode III and IV respectively with the lines in service, the damping remains high and relatively unchanged. For example, the real part of the Swing Mode III is -1.246 (see Case II in Table 4.6) and with the line $39-45$ removed it is -1.255 (see Case II in Table 4.7). With the loss of communication, the

real part of the Swing Mode III is -0.689 (see Case III in Table 4.6) and with the line $39-45$ removed it is -0.694 (see Case III in Table 4.7).

Therefore, the proposed control strategy is also robust with the change in the operating point.

Table 4.7: Eigenvalues: Line 39-45 Removed

Case	Swing Mode I	Swing Mode II	Swing Mode III	Swing Mode IV
NC	-0.008 ± j 4.687	-0.114 ± j 4.242	-0.002 ± j 3.356	-0.079 ± j 2.493
I	-0.104 ± j 4.432	**-1.137 ± j 4.111**	-0.099 ± j 3.369	**-0.931 ± j 2.978**
II	-0.203 ± j 4.586	-0.297 ± j 4.335	**-1.255 ± j 3.454**	-0.342 ± j 2.519
III	-0.117 ± j 4.453	-0.899 ± j 4.448	-0.694 ± j 3.398	-0.658 + j 2.641

Table 4.8: Eigenvalues: Line 8-9 Removed

Case	Swing Mode I	Swing Mode II	Swing Mode III	Swing Mode IV
NC	-0.007 ± j 4.689	-0.077 ± j 3.803	-0.012 ± j 3.310	-0.110 ± j 2.294
I	-0.223 ± j 4.380	**-1.643 ± j 3.800**	-0.104 ± j 3.507	**-0.903 ± j 2.566**
II	-0.188 ± j 4.639	-0.431 ± j 3.803	**-1.225 ± j 3.457**	-0.265 ± j 2.317
III	-0.245 ± j 4.424	-1.017 ± j 4.131	-0.739 ± j 3.282	-0.413 ± j 2.436

4.3.3 Validation by Time-Domain Simulation

We now validate the small signal analysis results shown in the previous section by time-domain simulations to assess the performance of the damping controller for different sets of optimized gains. A three-phase fault is applied on line 39-45 near bus 45, which is cleared in 4 cycles by tripping that line. The response of rotor angle difference between generators 14 and 16 is shown in Fig. 4.11 along with the power flow in the dc links in Fig. 4.12. Without the damping controller, we observe poor damping of the Mode III. As seen from Fig.4.11, that with the controller of Case II in place, damping of Mode III remains high and agrees with the conclusion based on eigenvalue analysis earlier in this section. Similarly, if communication is lost, as in Case III, the damping though less than that with the gains in Case II, is nevertheless better than that for the uncontrolled case.

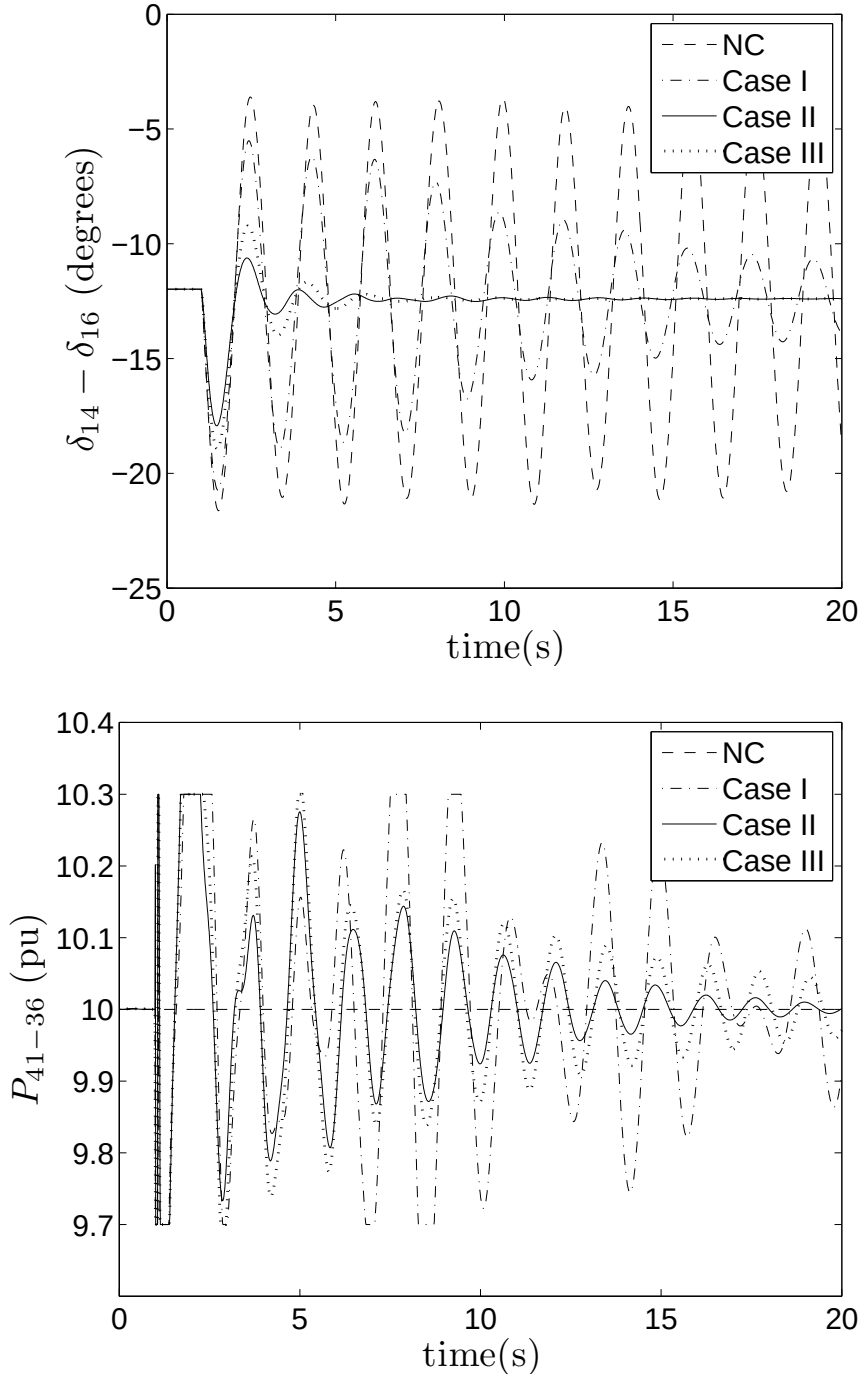

Figure 4.11: Response for a fault near bus 45, followed by tripping of line 39-45.

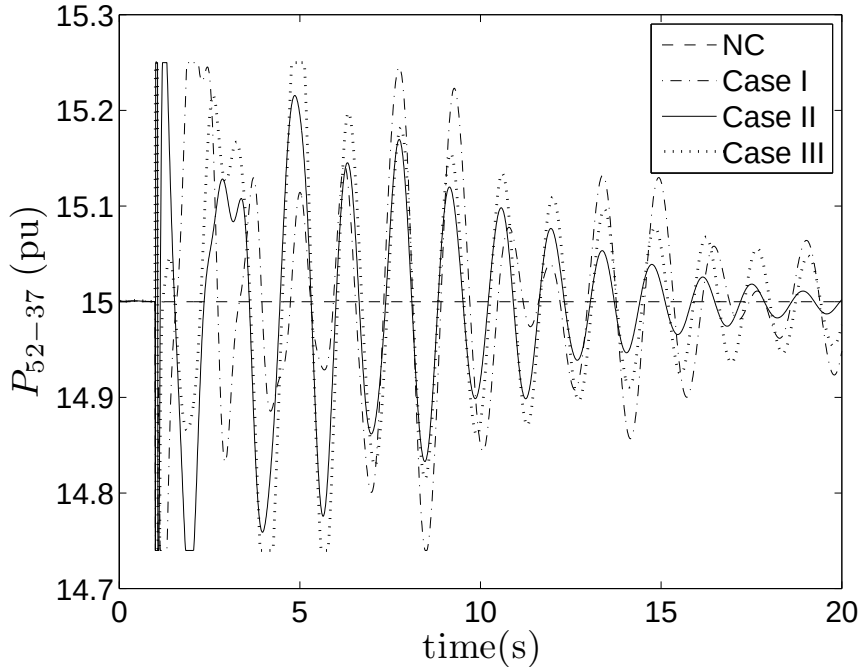

Figure 4.12: Power Flow through DC line for a fault near bus 45, followed by tripping of line 39-45.

Fig.4.13 shows the response for a fault near bus 8 which is cleared by tripping line 8-9. The lowest frequency Swing Mode IV is excited by this disturbance, which is observable in the rotor angle difference between generators 9 and 15. Since Case I gains are optimized to provide best damping effect for the lowest Swing Mode IV, the time-domain simulation validates the result predicted by the eigen-analysis.

4.3.4 Effect of Communication Delay

Delays in communicating the remote frequency difference signals will result in phase delays in these signals at the swing mode frequencies. These delays may be variable, but delays below a certain value can be converted to fixed delays by buffering the signals. The phase lag at a swing mode frequency caused due to a transport delay T_d is given by ΩT_d, where Ω is the radian frequency of the swing mode. For example, a 50 ms delay will cause a phase lag of about 11.5^o at 4 rad/s.

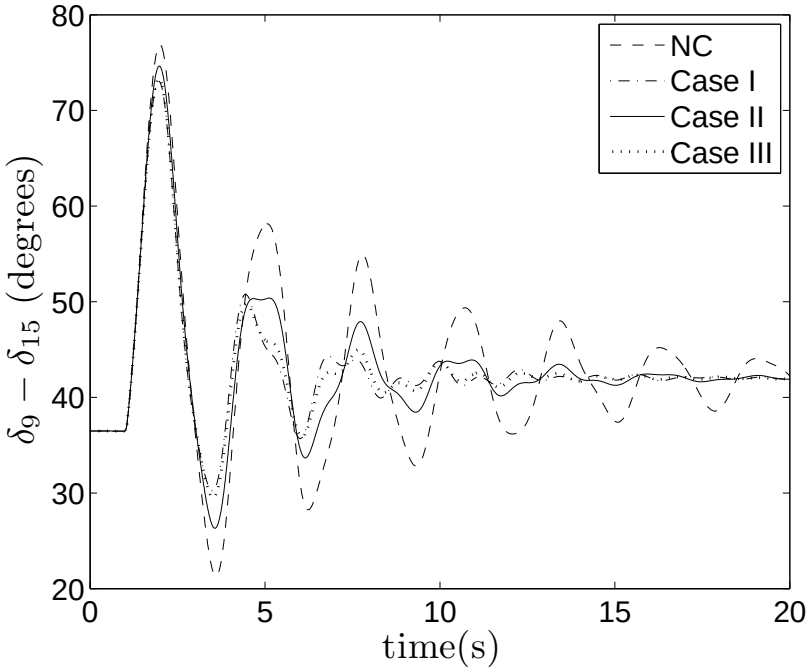

Figure 4.13: Response for a fault near bus 8, followed by the tripping of line 8-9.

Small and equal phase lags in the local and the remote channels of a damping controller will contribute to synchronizing effects. However, since the transport delays are not present in the local signal, the phase compensation parameters for the remote and the local channels may have to be different, unlike in Fig. 4.10. For small transport delays, one may be able to achieve an acceptable overall performance with minor adjustments in the design, but it is pragmatic to revert to the purely local strategy if delays are large.

We now consider the effect of a 100 ms delay in the non-local channel for the controller shown in Fig. 4.10. The gains corresponding to Case I are used. No phase compensation is used. The response of all rotor angles with reference to the centre-of-inertia angle (δ_{COI}) are shown in Fig. 4.14 with and without the delay. It is clear that for this disturbance, the delay in the non-local channel does not cause a significant difference in the performance of the controller.

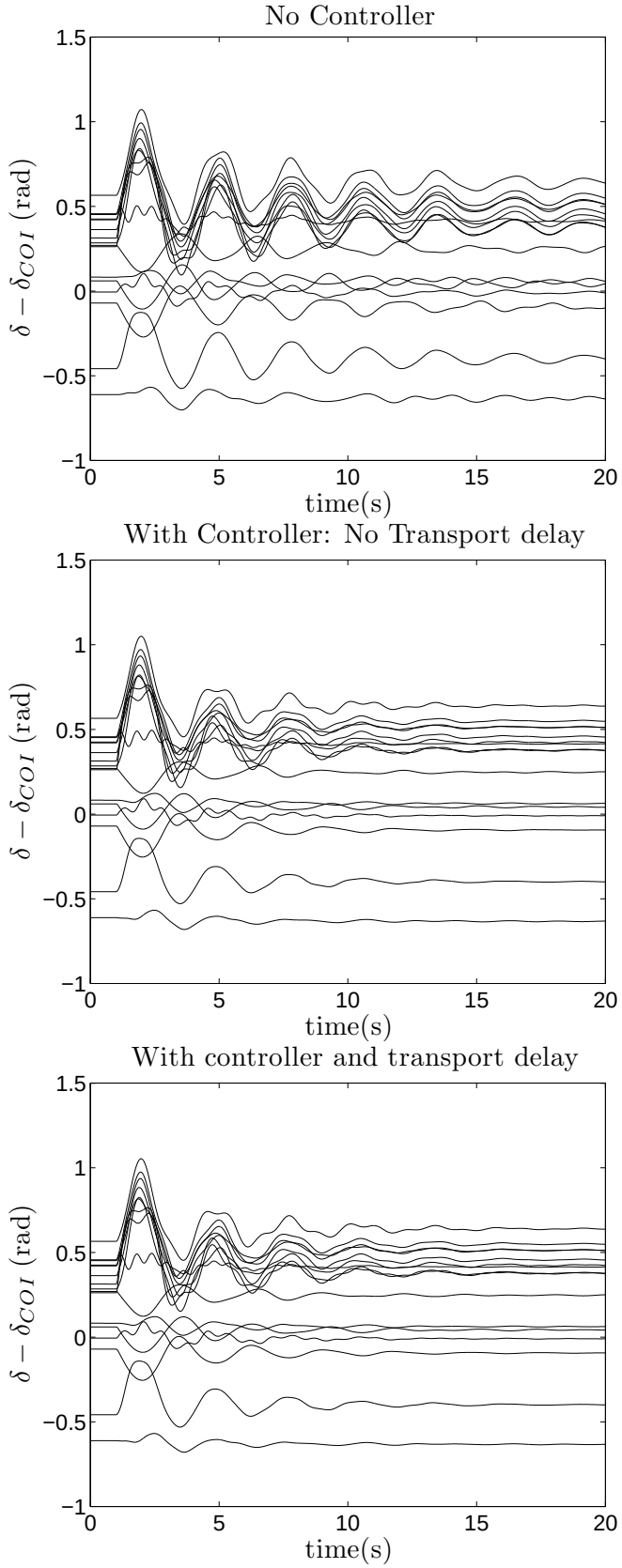

Figure 4.14: Response for a fault near bus 8, followed by the tripping of line 8-9, with and without a communication delay of 100 ms. Gains are as in Case I.

4.3.5 Line Commutated Converter dc links

We now consider the effect of introducing LCC links instead of VSC links. The power ratings are the same as before. The load-flow is slightly different, as the LCC links draw reactive power at the ac terminals which is partially compensated using filters. The reactive power is a function of the real power flow, and varies when a damping controller modulates the dc power. Nonetheless, since the controllability of swing modes by reactive power variation is expected to be smaller than active power, we expect that the changes will be marginal.

Table 4.9: Effect on Low-Frequency Swing Modes (LCC links)

Case	Swing Mode I	Swing Mode II	Swing Mode III	Swing Mode IV
NC	-0.004 ± j 4.716	-0.102 ± j 4.257	-0.005 ± j 3.421	-0.073 ± j 2.515
I	-0.327 ± j 4.848	-0.248 ± j 4.220	-0.316± j 3.433	**-0.959 ± j 2.305**
II	-0.185 ± j 4.753	-0.280 ± j 4.192	**-0.966 ± j 3.524**	-0.329 ± j 2.462
III	-0.296 ± j 4.794	-0.337 ± j 4.208	-0.610 ± j 3.517	-0.621 ± j 2.382

Table 4.10: Eigenvalues (LCC links): Line 39-45 Removed

Case	Swing Mode I	Swing Mode II	Swing Mode III	Swing Mode IV
NC	-0.004 ± j 4.709	-0.103 ± j 4.253	-0.006 ± j 3.413	-0.072 ± j 2.512
I	-0.321 ± j 4.838	-0.249 ± j 4.214	-0.312 ± j 3.430	**-0.963 ± j 2.304**
II	-0.184 ± j 4.745	-0.279 ± j 4.190	**-0.956 ± j 3.515**	-0.330 ± j 2.461
III	-0.293 ± j 4.785	-0.336 ± j 4.204	-0.605 ± j 3.511	-0.623 + j 2.379

Table 4.11: Eigenvalues(LCC Links): Line 8-9 Removed

Case	Swing Mode I	Swing Mode II	Swing Mode III	Swing Mode IV
NC	-0.002 ± j 4.711	-0.059 ± j 3.839	-0.007 ± j 3.345	-0.106 ± j 2.309
I	-0.339 ± j 4.832	-0.302 ± j 3.913	-0.450 ± j 2.910	**-0.826 ± j 2.389**
II	-0.193 ± j 4.731	-0.509 ± j 3.747	**-0.827 ± j 3.452**	-0.258 ± j 2.291
III	-0.311 ± j 4.776	-0.549 ± j 3.984	-0.589 ± j 3.119	-0.469 ± j 2.311

The effect of the strategy is brought out in Tables 4.9- 4.11. As in the case of the VSC links, the introduction of the controller brings in additional damping in all

the cases. The effect on various modes can be changed by changing the elements of the gain matrix (Cases I, II and III), as before. This is also confirmed by simulation studies, the results of which are shown in Figs. 4.15 and 4.17.

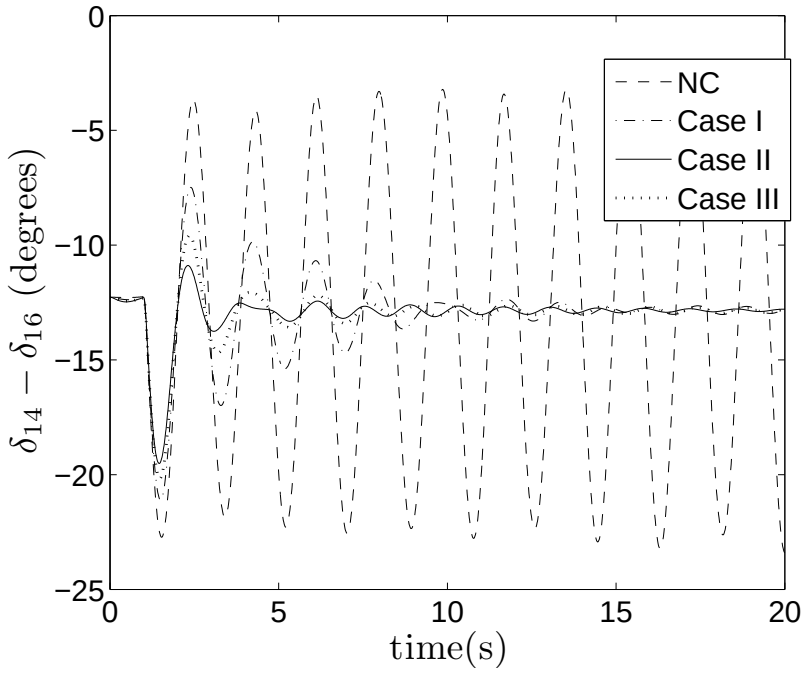

Figure 4.15: Response for a fault near bus 45, followed by tripping of line 39-45; System with LCC links.

4.4 Concluding Remarks

In this chapter we tested the efficacy of the proposed control strategy on the detailed systems using small signal analysis and time domain simulations. The effectiveness of the proposed control strategy to mimic dc line as an ac line (by introducing both synchronizing and torque through dc), and using spd gain matrices to ensure positive synchronizing and damping for all the swing modes was confirmed.

- A 3 machine case study with multiple DC links is simulated using MATLAB/SIMULINK based small signal and transient stability program.

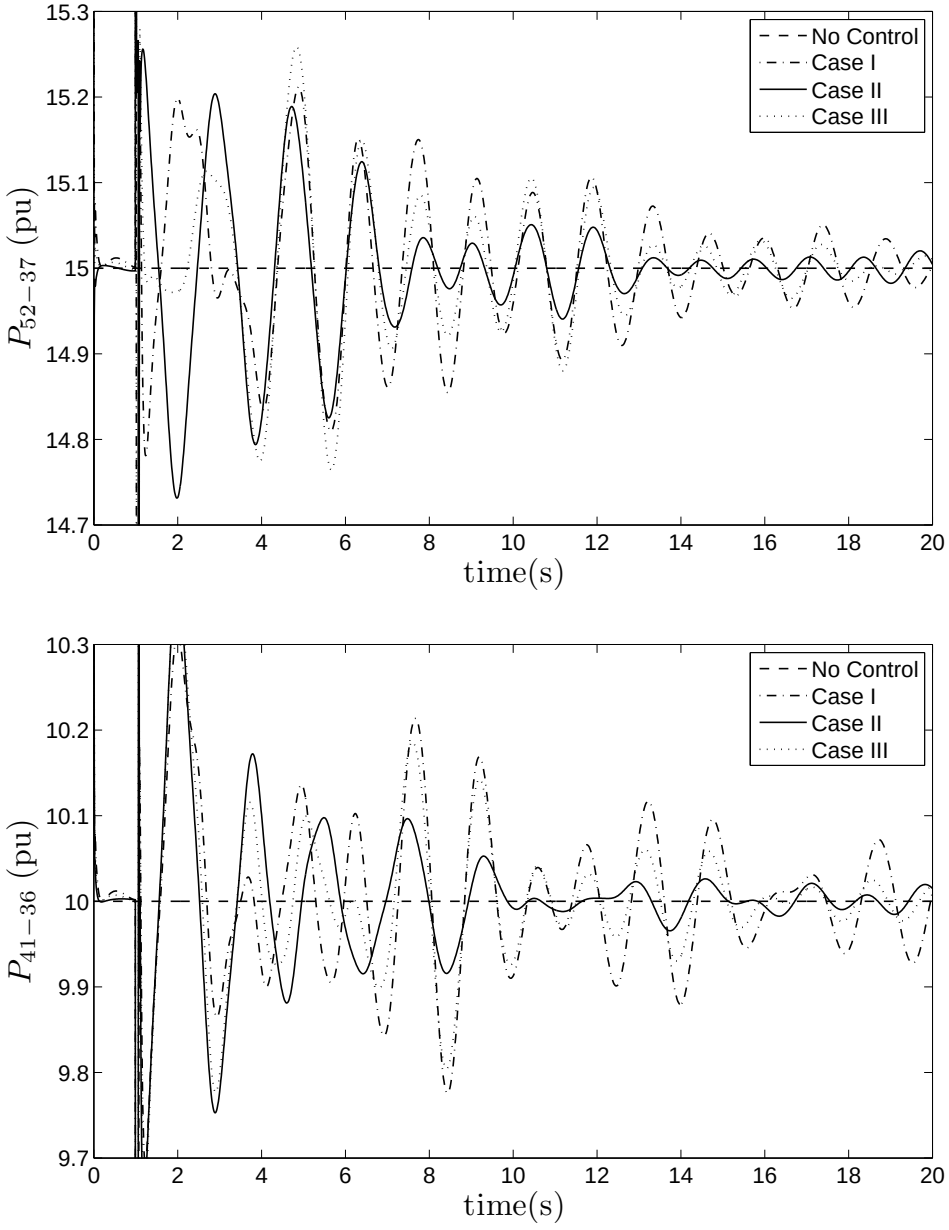

Figure 4.16: Power modulation in LCC dc links for a fault near bus 45, followed by tripping of line 39-45

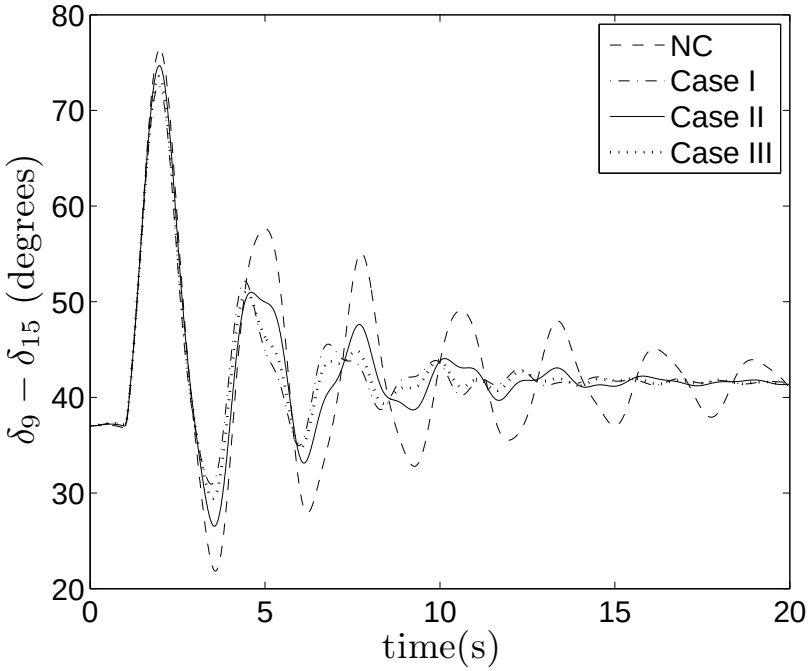

Figure 4.17: Response for a fault near bus 8, followed by the tripping of line 8-9; System with LCC links.

  - Choosing symmetric positive definite gain matrices ensured positive synchronizing and damping effect.
  - As shown by the eigen value analysis, multiple DC links provided extra degrees of freedom to put more leverage on the damping of the selective modes.
  - Eigenvalue study also shows that the proposed control strategy is robust towards the change in the network topology, and loss of communication.
  - The results are validated using electromagnetic transient simulation.

- A similar study is carried out on a larger 16 machine 68 bus system with two embedded VSC links into the system. Both eigenvalue analysis and transient simulation shows an improvement in the system stability with the controlled power flow through the DC links.

Chapter 5

Asynchronous System connected by HVDC links

Our discussion in the previous chapters was mainly focused on improving the angular stability of the AC-DC system by controlling the power flow through the HVDC links embedded in a synchronous system. A great advantage of HVDC systems is that they allow the ac networks on the sending and receiving ends to be asynchronous, i.e, the phase angle difference may change continuously or the frequency of these systems can be different. Although this means that disturbances on one side are isolated from the other, it also implies that left to themselves, i.e., operated in constant power mode, they do not actively aid in damping power system oscillations either. Various configurations in which asynchronous DC links connecting synchronous grids is shown below in Fig. 5.1.

Asynchronous dc links, as shown in Figs. 5.1(a), 5.1(b) and 5.1(c), can regulate the power exchange between grids. If power modulation is introduced, they can also be used to damp power swings and/or reduce transient and steady-state deviations in frequency by emulating inertia and power-frequency regulation(droop). Such a

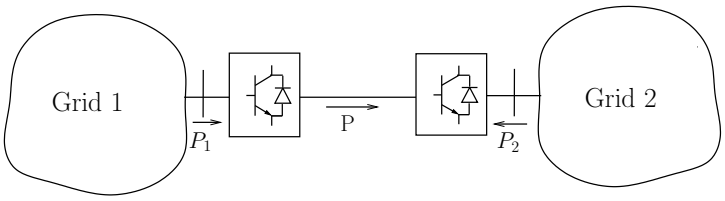

(a) Asynchronous dc link connecting two synchronous grids

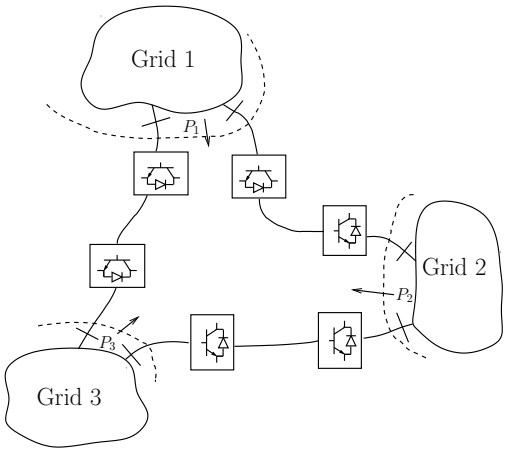

(b) Asynchronous dc links connecting several synchronous grids

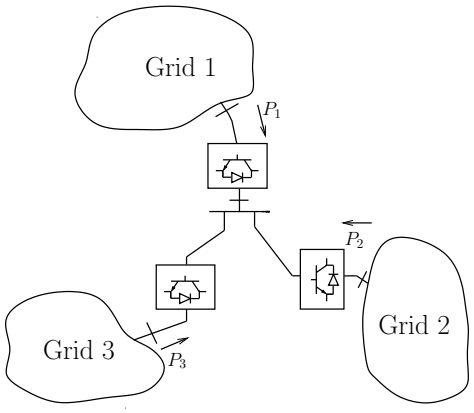

(c) Multi-terminal asynchronous dc links connecting several synchronous grids

Figure 5.1: Asynchronous dc links

strategy should ensure that the interconnected grids assist each other without causing excessive stress to either of them. A description of some practical schemes for controlling asynchronous links are given in [35, 63, 64, 65].

5.1 Review of Some Control Schemes for Asynchronous Links

The aim of this section is to discuss the implications of adopting various control strategies to improve the angular stability of the synchronous grids connected by asynchronous HVDC link.

- Consider the asynchronous connection shown in Fig. 5.1(a). A do-nothing strategy from the point of view of damping oscillations is to keep the two grids decoupled from one another as shown in Fig. 5.2(a) by having a constant dc power flow.

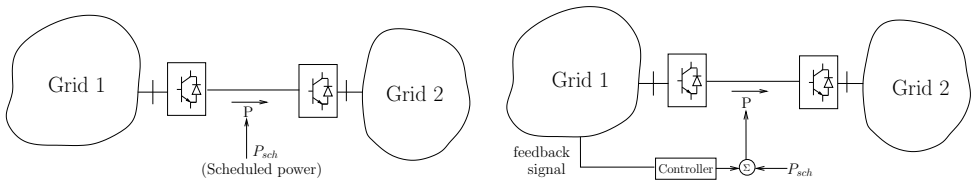

(a) Strict Power Regulation (No coupling will result)

(b) Control with feedback from only one grid

Figure 5.2: Control Strategies for Asynchronous Links

- If the strategy shown in Fig. 5.2(b) is used, then although the disturbances in Grid 1 become observable in Grid 2, they are uncorrelated to the dynamics of Grid 2 and thereby cause no change in the modal characteristics of that grid (assuming both the grids have different modal characteristics). This control strategy only assists Grid 1, and Grid 2 is expected to be tolerant to the reflected disturbances in Grid 1. Any attempt to damp a targeted swing mode in say Grid 2 by modulating the dc power mainly depends on the observability of that swing mode in the feedback signal which is used to modulate the dc power. If in addition to the targeted swing mode, some other un-targeted swing modes are also observable in the feedback signal then the dc power modulation may affect the damping of these un-targeted modes too. Therefore, the effect of the control strategy on the numerous swing modes of the grids needs a careful evaluation.

- Another area of interest is the improvement in frequency deviation followed by a load or generation loss (common mode). We know that the rate of change of frequency in any grid depends on the inertia of the system, i.e. a system with high inertia will observe lesser frequency deviations compared to a area with low inertia. Consider three cases here:

  - In Case I, consider a low inertia Grid 2 asynchronously connected to a Grid 1 with high inertia. In this case, control the dc power infeed into grid 2 to minimize frequency deviation. This dc power control will result

in frequency deviation in Grid 1, but since this Grid has high inertia, the rate of change of frequency deviations will be low.

- In Case II, consider the two grids with comparable inertia. In this case, any attempt to reduce the frequency deviation in one grid will result in a similar rate of change of frequency deviation in the other grid. Therefore, in this scenario a droop control may be used where one grid (say Grid 1) can allow a limited dc power modulation to reduce the sudden frequency deviation in Grid 2 while suffering limited deviation in its own frequency.
- In Case III, consider two grids with weak inertia. If a strategy like the one above is followed, some assistance to Grid 2 can be still be provided, but this should be done cautiously as it could result in a severe drop in frequency in Grid 1.

The objectives of this chapter are as follows:

- To propose a control strategy for dc power modulation such that damping of the targeted mode should not worsen the damping of the un-targeted modes but rather improve it.
- To propose a **simple** droop control strategy which will improve the frequency deviation in a grid with relatively small impact on the other grid.
- To develop a generalized control strategy for single and multiple asynchronous links.
- To develop a mathematical characterization of the effect of the control strategies on the interconnected grids.

5.2 Proposed Control Strategy for Emulating Inertia and Power-Frequency Droop

This section describes that how a simple control strategy can be formulated for a single or multiple asynchronous links to improve the inertia and damping of the synchronous grids.

5.2.1 Single Asynchronous link

Consider an asynchronous link connecting two grids, as shown in Fig.5.1(a). Let us assume that all the generators in each grid are assumed to be coherent within the grid, and each represented by one single equivalent generator, and their respective frequencies are f_1 and f_2. If losses are neglected, then $P_1 = -P_2 = P_s + \Delta P$, where P_s is the scheduled power and ΔP is the output of the frequency droop/inertia controller.

Consider the following strategy[1]:

$$\Delta P = \alpha_1 \frac{\mathrm{d}\Delta f_1}{\mathrm{d}t} - \alpha_2 \frac{\mathrm{d}\Delta f_2}{\mathrm{d}t} + \beta_1 \Delta f_1 - \beta_2 \Delta f_1 \tag{5.1}$$

The prefix Δ denotes the change from the nominal value.

Note: $\alpha_1, \alpha_2, \beta_1, \beta_2$ are all greater than or equal to zero. The equation (5.1) can be re-written as follows.

$$\begin{bmatrix} \Delta P_1 \\ \Delta P_2 \end{bmatrix} = A_2 \frac{\mathrm{d}}{\mathrm{d}t} \begin{bmatrix} \Delta f_1 \\ \Delta f_2 \end{bmatrix} + B_2 \begin{bmatrix} \Delta f_1 \\ \Delta f_2 \end{bmatrix} \tag{5.2}$$

[1]Only the basic strategy is shown here, without the implementation details. In practice, a transfer function which approximates the derivative block (e.g, $\frac{s}{1+sT}$) will be used. In addition, limiters, filters and washout blocks may be used to restrict the bandwidth and steady state output of the controller.

where,

$$A_2 = \begin{bmatrix} 1 & -1 \\ -1 & 1 \end{bmatrix} \begin{bmatrix} \alpha_1 & 0 \\ 0 & \alpha_2 \end{bmatrix}$$

$$B_2 = \begin{bmatrix} 1 & -1 \\ -1 & 1 \end{bmatrix} \begin{bmatrix} \beta_1 & 0 \\ 0 & \beta_2 \end{bmatrix}$$

Suppose that there is a sudden step power imbalance at $t = 0$ s in each of the grid which are initially in steady-state. In such a case, the rate of change of frequencies at $t = 0^+$ s can be obtained by combining 5.2 with the equation of motion[1].

$$\begin{bmatrix} \frac{2H_1}{f_{B_1}} + \alpha_1 & -\alpha_2 \\ -\alpha_1 & \frac{2H_2}{f_{B_2}} + \alpha_2 \end{bmatrix} \begin{bmatrix} \frac{\mathrm{d}\Delta f_1}{\mathrm{d}t} \\ \frac{\mathrm{d}\Delta f_2}{\mathrm{d}t} \end{bmatrix} = \begin{bmatrix} \rho_1 \\ \rho_2 \end{bmatrix}$$

where, ρ_1 and ρ_2 denote the power imbalances in the grids. (H_1, f_{B_1}) and (H_2, f_{B_2}) are the inertias and base frequencies of the grids.

Note that if $\alpha_1 > 0$ and $\alpha_2 = 0$, then the effective inertia of only Grid 1 undergoes a positive change while the Grid 2 effective inertia will decrease. Thus Grid 2 by bearing a frequency deviation is effectively helping to reduce frequency deviation in Grid 1. This is not a necessary deleterious in nature if Grid 2 is a strong system with higher inertia compared to Grid 1. However, as discussed in the earlier sections that if the inertia of two Grids is comparable then the control parameters α_1 and α_2 can be appropriately chosen to introduce a droop control to share the burden of reducing frequency deviation in both the grids.

The steady state frequency can be obtained from the following equation.

$$\begin{bmatrix} D_1 + \beta_1 & -\beta_2 \\ -\beta_1 & D_2 + \beta_2 \end{bmatrix} \begin{bmatrix} \Delta f_1 \\ \Delta f_2 \end{bmatrix} = \begin{bmatrix} \rho_1 \\ \rho_2 \end{bmatrix} \tag{5.3}$$

D_1 and D_2 are the damping factors due to frequency-dependent loads and governors.

As described in Appendix B that if the control matrix for dc power modulation is selected to be positive semi definite in nature, then it will always result in the positive damping of all the swing modes, here again if $\beta_1 \geq 0$ and $\beta_2 \geq 0$, and $\beta_1 = \beta_2$, then the control matrix in equation 5.3 will be positive definite in nature, which will result in a positive damping for all the controllable swing modes through dc power modulation in both the Grids.

5.2.2 Multiple/Multi-terminal Asynchronous links connecting many grids

The strategy for one link can be extended to the three grids shown in Figs. 5.1(b) and 5.1(c)[2].

$$\begin{bmatrix} \Delta P_1 \\ \Delta P_2 \\ \Delta P_3 \end{bmatrix} = A_3 \frac{\mathrm{d}}{\mathrm{d}t} \begin{bmatrix} \Delta f_1 \\ \Delta f_2 \\ \Delta f_3 \end{bmatrix} + B_3 \begin{bmatrix} \Delta f_1 \\ \Delta f_2 \\ \Delta f_3 \end{bmatrix} \tag{5.4}$$

The matrices A_3 and B_3 are of the following form where matrix A introduces inertia effect and matrix B introduces damping effect.

$$A = \begin{bmatrix} \gamma_{12}+\gamma_{13} & -\gamma_{12} & -\gamma_{13} \\ -\gamma_{12} & \gamma_{12}+\gamma_{23} & -\gamma_{23} \\ -\gamma_{13} & -\gamma_{23} & \gamma_{13}+\gamma_{23} \end{bmatrix} \times \begin{bmatrix} \alpha_1 & 0 & 0 \\ 0 & \alpha_2 & 0 \\ 0 & 0 & \alpha_3 \end{bmatrix}$$

$$B = \begin{bmatrix} \zeta_{12}+\zeta_{13} & -\zeta_{12} & -\zeta_{13} \\ -\zeta_{12} & \zeta_{12}+\zeta_{23} & -\zeta_{23} \\ -\zeta_{13} & -\zeta_{23} & \zeta_{13}+\zeta_{23} \end{bmatrix} \times \begin{bmatrix} \beta_1 & 0 & 0 \\ 0 & \beta_2 & 0 \\ 0 & 0 & \beta_3 \end{bmatrix}$$

[2]In practice, any two of the three powers ($\Delta P_1, \Delta P_2$, ΔP_3) are specified and the third $\Delta P_3 \approx -\Delta P_1 - \Delta P_2$. This is because the links have very low losses and are assumed to have no energy storage.

The parameters $(\gamma_{12}, \gamma_{23}, \gamma_{31})$ and $(\zeta_{12}, \zeta_{23}, \zeta_{31})$, may be chosen based on the relative ratings of the links between the grids. For example, if the asynchronous link between Grid 2 and Grid 3 in Fig. 5.1(b) is of a low rating, then γ_{23} may be chosen to be smaller relative to the other parameters. The parameters $(\gamma_{12}, \gamma_{23}, \gamma_{31})$, $(\zeta_{12}, \zeta_{23}, \zeta_{31})(\alpha_1, \alpha_2, \alpha_3)$ and $(\beta_1, \beta_2, \beta_3)$ can be appropriately chosen as positive definite to ensure the positive improvement in the inertia and damping of the subsequent grids respectively.

One can intuitively understand the effect of these strategies by considering the circuit analogy of the electro-mechanical system, wherein the bus frequency is the 'voltage' and power is the 'current'. It is evident from Figs. 5.3(a) and 5.3(b) that the effect of the inertia-emulation strategy is to pull together the grids, transiently, through the inter-grid 'capacitances'. Similarly power-frequency droop has a resistive effect.

This strategy can easily be extended to a larger number of asynchronously connected grids.

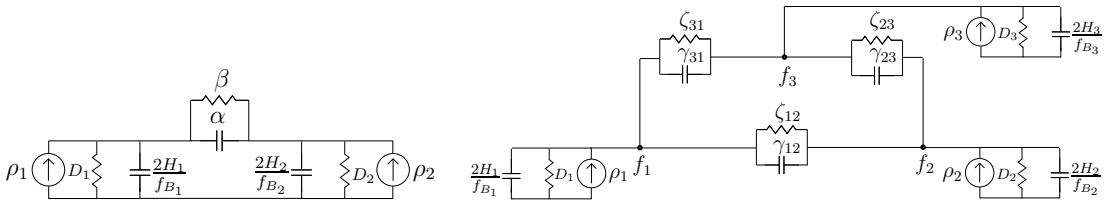

(a) Single Asynchronous Link (b) Multiple Asynchronous Links

Figure 5.3: Circuit Analogy of the Control Strategy for Inertia Emulation

5.3 Case Studies

In order to demonstrate the efficacy of the proposed control as described in the above section, a test system shown if Fig.5.4 is simulated in Simulink. Modeling of the HVDC systems in power flow and stability studies is based on the discussion in [1].

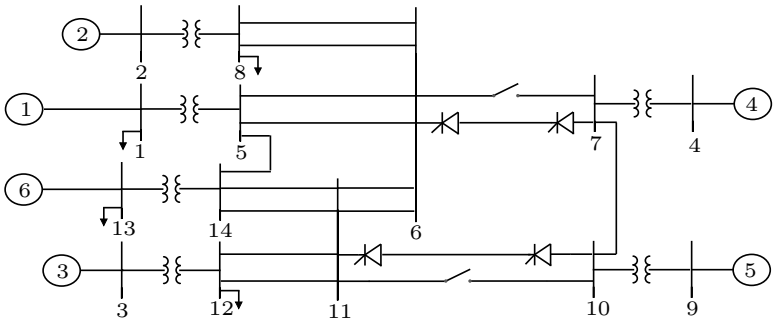

Figure 5.4: Test System - I for Asynchronous Link Controls

Two synchronous grids are connected by two LCC based HVDC links. Details of the system are given in Appendix F. The test system is inspired by the Nelson River scheme in Manitoba with generation in the north (generators 4 and 5) and consumption in the south (generators 1,2,3, and 6). The two areas are completely asynchronous. Also, the frequency in the sending end in nelson river system can transiently differ by up to 10 Hz from the nominal. This is because no local loads are connected there.

5.3.1 Performance of the test system with the proposed control to emulate inertia and power frequency droop

The objective of this section is to implement the dc power modulation control for the two LCC HVDC links as described in equation 5.1 for the test system. The power through the DC links is modulated proportional to the sending and receiving end frequencies to introduce damping to the swing modes in both the grids and its derivative to reduce frequency deviation in both the grids. Since both the links are of the same rating the value of the gain parameters are chosen as $\alpha_1 = \alpha_2 = 0.1$, and $\beta_1 = \beta_2 = 0.1$ which ensures positive definite nature of the control matrices and hence positive inertia and damping effects. Table 5.1 shows the eigenvalues of the system with and without the proposed control. The table shows that the frequencies

of the swing modes with controller have reduced compared to the frequencies of the swing modes in Table 5.1, this can be seen as an apparent increase in inertia of the system due to the inter-grid "capacitances". Damping of the modes in both the grids have also increased due to the resistive effect brought by the frequency dependance of power.

Table 5.1: Swing Modes of the Test System with Proposed Control

Mode Description	Without Control	With Proposed Control
Swing Mode I: Generator 1 against Generator 6	-0.1409 ± j 13.5491	-0.2846 ± j 13.0314
Swing Mode II Generators 1 and 6 against Generators 2 and 3	-0.6069 ± j 12.5668	-1.0443 ± j 11.6639
Swing Mode III Generators 1 against 6 against Generators 2 against 3	-0.3459 ± j 12.1020	-1.0663 ± j 11.3804
Swing Mode IV Generator 4 against Generator 5	-0.4948 ± j 3.6837	-0.5124 ± j 3.6583

- The simulated response for a fault at generator 2 bus followed by tripping of the same generator is shown in Fig 5.5-5.8.
- Fig.5.5 shows the reduction in the power order through the dc links due to the given fault.
- Without the controller in action, dc link power drop results in a sudden frequency deviations in the generators 1,4,5, and 6.
- With the inertia controller in action for both the grids, frequency deviations are reduced. This contingency also triggered a swing mode of approximately 12.56 rad/sec in the generator 3 as shown in Fig.5.8 which is well damped with the damping controller in action.

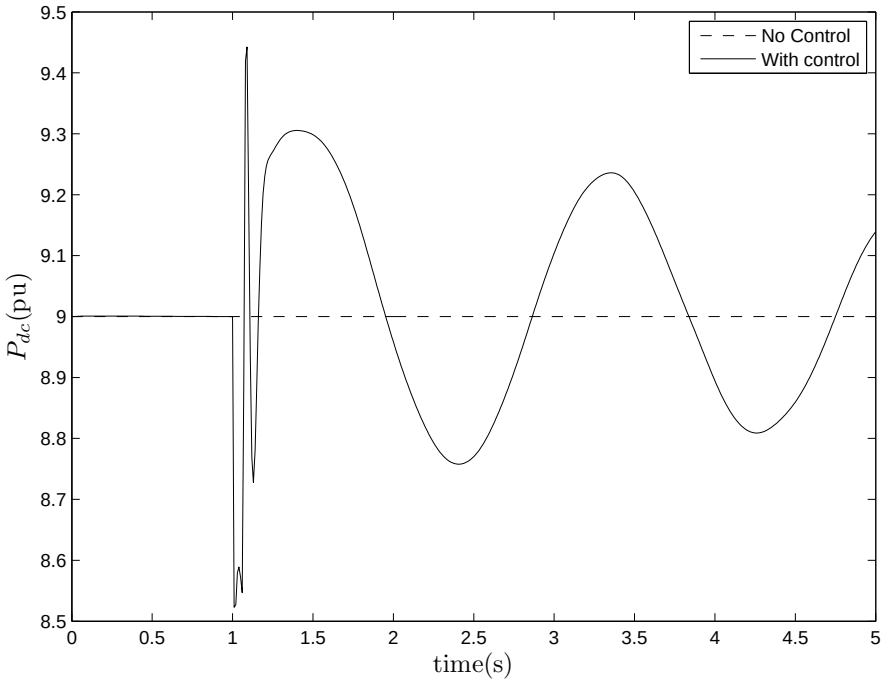

Figure 5.5: Power through the DC links

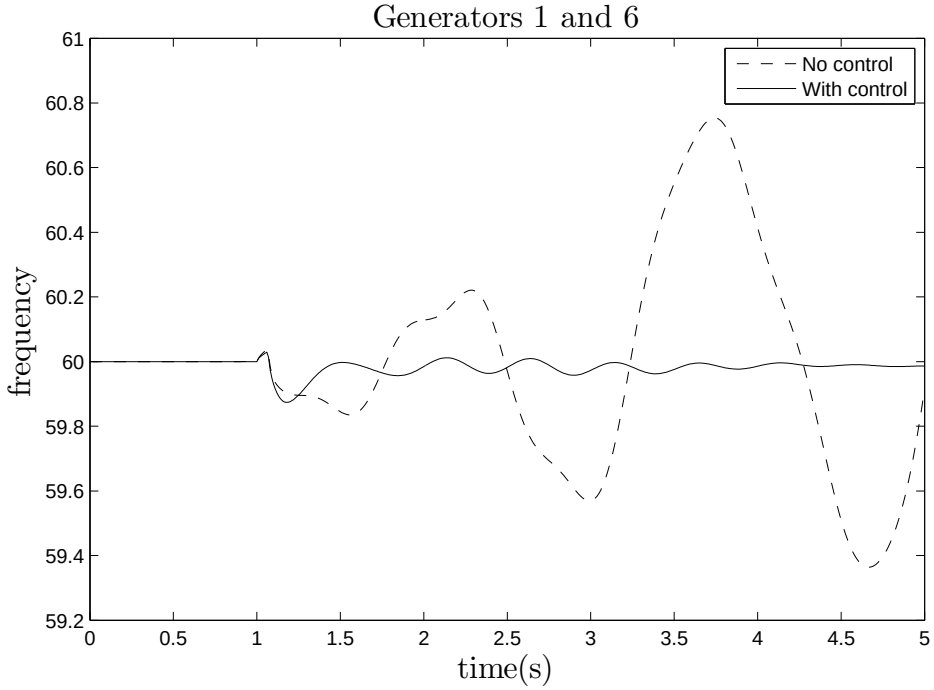

Figure 5.6: Frequencies of the Generators 1 and 6

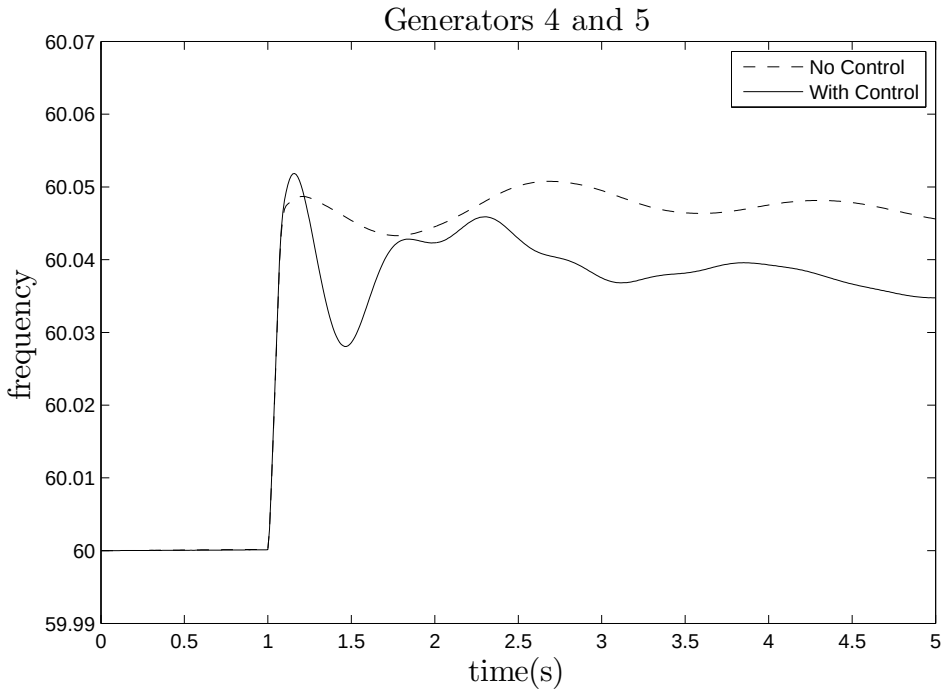

Figure 5.7: Frequencies of the Generators 4 and 5

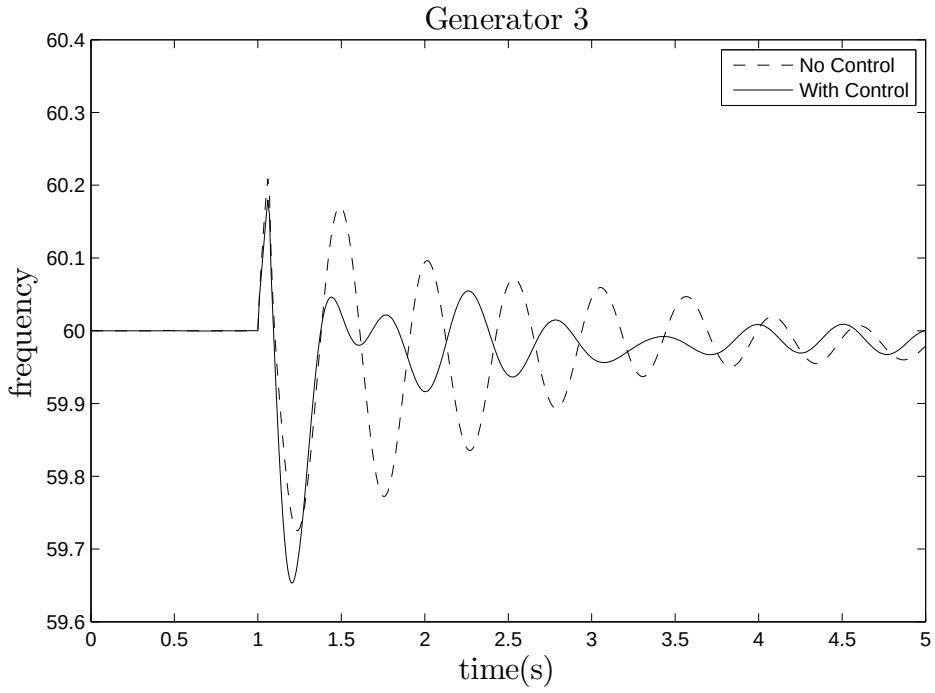

Figure 5.8: Frequency of the Generator 3

Chapter 6

Conclusions and Future Work

Wide area measurement signals based controllers for HVDC and FACTS devices has attracted the attention of many researchers to improve angular stability of the ac system. However, if several wide area signals are used, it becomes difficult to intuitively understand the effect of various parameters in the controller. Furthermore, it becomes a challenge to ensure the robustness of the control strategy with the change in the network topology and loss of communication. The objective of this thesis was to investigate a control strategy for multi-infeed and multi-terminal dc links embedded in the ac system which

- Is robust to the loss of communication, and changes in the network topology.
- Always improves damping for all the swing modes of the system.
- Can be easily adapted to achieve targeted damping of the critical swing modes.
- Uses a limited set of local and non-local signals to ensure the intuitive understanding of the parameters on the controller.

6.1 The Main Contributions of this Thesis

The main contributions of this thesis are the following:

- Detailed literature survey is provided which critically explains state of the art research conducted since 1960's in the HVDC based power modulation to enhance the ac system stability.

- An intuitive "circuit analogy" for the detailed power system is presented in Chapter 3 which captures the information regarding the electromechanical modes of the detailed system through a simple circuit with R-L-C elements. The main utility of the circuit analogy is that it suggests a control strategy which can improve angular stability with controllable network elements, say, a DC link. It describes that:

  - If power flow in the DC link is changed in proportion to the voltage phase angular difference between the buses to which it is connected then the DC line behaves like an AC line, i.e., the effect is the addition of another inductive link in the analogous circuit. This reduces angular deviations following disturbances (synchronizing effect).

  - If power flow is changed in proportion to the derivative of the voltage phase angular difference between the buses (i.e., the bus frequency difference), the DC line behaves like a resistance in the analogous circuit. This creates a damping effect.

  - With multiple HVDC links, there are additional degrees of freedom to design the control matrix. If the control matrix is chosen to be symmetric positive definite (spd) it always results in improvement of the damping of all the swing modes. Furthermore, since mutual resistance and inductance could be emulated with multiple HVDC links by exchanging the remote

signals, the control matrix was appropriately designed to provide increased damping on certain modes. In case the remote signals are lost, mutual resistance/inductance in the control matrix become zero and the control strategy falls back to using only local signals. Furthermore, this loss of communication between dc links does not destroy the symmetric positive definiteness and the control matrix which still introduces improved damping of all the modes.

- Since the proposed control (based on circuit analogy) in Chapter 3 was based on the following assumptions:
  - The ac system is modeled using simple classical model
  - Transmission losses are neglected
  - Bus voltages are essentially at 1pu.

  It was important to validate the efficacy of the proposed control method on the detailed system where the above mentioned assumptions are approximate. Therefore, a formal state space explanation is shown in Appendix B which analyzes the eigenvalue movement of the system when the dc power flow is made proportional to the phase and frequency difference signals. Detailed three machine and sixteen machine case studies were simulated in MATLAB/Simulink to validate the proposed control strategy. Small signal and time-domain simulations were performed on these system to test the methodology explained in the thesis. The results showed that, as expected, the proposed strategy yields **guaranteed** positive damping for all swing modes, and is robust to changes in operating conditions and network topology. During the loss of the remote signals, the local strategy as expected confirmed to provide positive damping. It was also seen, that although the proposed method increases damping of all modes, gain

matrix elements can be selected to increase damping for some modes more than others. This was done by trial and error, and not by optimization.

- While designing the real power control through the dc links, we assumed that the corresponding change in the reactive power is zero. This is particularly true in case of the VSC dc links where real and reactive power can be independently controlled. However, in the case of the LCC dc link the real and reactive power are coupled i.e., reactive power increases monotonically but non-linearly as real power is increased. A small signal analysis for both the VSC and LCC dc links showed that the resultant small signal gain matrix can easily be chosen to be a symmetric positive definite matrix in the case of VSC, but in the case of LCC links it is not spd in nature (due to the corresponding reactive power modulation). However, through simulation it was seen that this problem essentially exists only when the LCC operate at low power order, as the real power order increases it masks the effect brought by the reactive power modulation and the gain matrix is approximately spd in nature.

- As far as the impact of the time delays on the performance of the proposed strategy is concerned, when tested on the sixteen machine system, the damping was seen to be relatively unaffected by time delays as large as 100ms. However, if time delays are a concern a dedicated communication link could be used, instead of relying on phasor data concentrators.

- The proposed control strategy was also extended for the case of synchronous grids connected asynchronously by a dc link. By the circuit analogy concept it was shown that the derivative of the frequency signals can be used to emulate the inertia effect which transiently pulls the grids together to reduce the sudden deviation in the grid frequencies followed by a disturbance. In the circuit analogy this effect is represented by a "capacitor". Furthermore, it was also shown

that by the proposed control strategy, we can ensure improved damping for all the controllable swing modes of the system. A test system similar to the Nelson River Bipole Scheme was simulated in MATLAB/Simulink with the proposed control to demonstrate the small signal and time domain simulation results.

6.2 Future Work

This thesis mainly looked at modulating the real power through the HVDC links proportional to specific set of feedback signals in order to introduce additional synchronizing, damping torque and inertia. However, the proposed strategy was restricted in the sense that only real power modulation proportional to the phase difference (and frequency difference) was explored. It would be of interest to test the methodology proposed in the paper with the reactive power modulation and its effect on the ac system stability. Also other shunt/series FACTS devices can be explored with different pair of feedback signals such as shunt injected reactive current/voltage magnitude, series injected power/Line current phase angle, and series injected reactive voltage/voltage magnitude.

Bibliography

[1] P. Kundur, "*Power System Stability and Control*", Tata McGraw-Hill Inc,New Delhi 2008.

[2] D.R. Davidson, D.N. Ewart, and L.K. Kirchmayer, "Long Term Dynamic Response of Power system-An Analysis of Major Disturbance," *IEEE Trans.*, Vol. PAS-94, pp.819-826, May/June 1975.

[3] S.B. Crary, *Power System Stability, Vol.I: Steady State Stability*, John Wiley and Sons, 1945.

[4] B. Chaudhuri and B. C. Pal, "Robust damping of multiple swing modes employing global stabilizing signals with a TCSC," *in proc. IEEE Transactions on Power Systems*, vol. 19, no. 1, pp. 499-506, Feb. 2004.

[5] G. Rogers, *Power System Oscillations*, Kluwer Academic Publishers, Norwell, MA, 2000.

[6] Junbo Zhang; Chung, C.Y.; Shuqing Zhang; Yingduo Han, "Practical Wide Area Damping Controller Design Based on Ambient Signal Analysis," in Power Systems, IEEE Transactions on , vol.28, no.2, pp.1687-1696, May 2013

[7] Cepeda, J.; Echeverria, D.; Arguello, G., "Cenace's experiences on implementing a wide area monitoring system (WAMS) in the Ecuadorian power system," in Central America and Panama Convention (CONCAPAN XXXIV), 2014 IEEE , vol., no., pp.1-7, 12-14 Nov. 2014

[8] J. He, C. Lu, X. Wu, P. Li and J. Wu, "Design and experiment of wide area HVDC supplementary damping controller considering time delay in China southern power grid," *IET Generation, Transmission & Distribution*, vol. 3, no. 1, pp. 17-25, 2009.

[9] Narain. G. Hingorani, Laszlo Gyugyi, *Understanding FACTS: Concepts and Technology of Flexible AC Transmission Systems*, IEEE Press 2013.

[10] Liu Wen-xia; Fan Yong-feng; Zhang Li-xin; Zhang Xin; Que Hua-kun, "WAMS information security assessment based on evidence theory," in Sustainable Power Generation and Supply, 2009. SUPERGEN '09. International Conference on , vol., no., pp.1-5, 6-7 April 2009

[11] Yunqi Kan; Zhaoyang Qu, "Notice of Retraction Design data structure for WAMS datastream mining base on GPS time scale," in Mobile Congress (GMC), 2010 Global , vol., no., pp.1-3, 18-19 Oct. 2010

[12] Shaobu Wang; Wenzhong Gao; Jianhui Wang; Jin Lin, "Synchronized Sampling Technology-Based Compensation for Network Effects in WAMS Communication," in Smart Grid, IEEE Transactions on , vol.3, no.2, pp.837-845, June 2012

[13] Cai, J.Y.;Zhenyu Huang; Hauer, J.; Martin, K., "Current Status and Experience of WAMS Implementation in North America," in Transmission and Distribution Conference and Exhibition: Asia and Pacific, 2005 IEEE/PES , vol., no., pp.1-7, 2005

[14] E.W. Kimbark, *Direct Current Transmission*, John Wiley and Sons Inc., 1971.

[15] K.R. Padiyar, "*HVDC Power Transmission Systems*", New Age International Publishers,New Delhi 2010.

[16] M. Szechtman, et al, "First Benchmark Model for HVDC Control Studies," Electra, Vol. 135, April 1991, pp 55-73

[17] C. V. Thio, J. B. Davies, and K. L. Kent, "Commutation failures in HVDC transmission systems," IEEE Transactions on Power Delivery, vol. 11, no. 2, pp. 946957, Apr. 1996

[18] N. Flourentzou, V. G. Agelidis, G. D. Demetriades, "VSC-based HVDC power transmission systems: an overview," IEEE Trans. Power electronics, vol. 24, no. 3, pp. 592-602, 2009.

[19] Zhou, J.Z.; Gole, A.M., "VSC transmission limitations imposed by AC system strength and AC impedance characteristics," in AC and DC Power Transmission (ACDC 2012), 10th IET International Conference on , vol., no., pp.1-6, 4-5 Dec. 2012

[20] Gnanarathna, U.N.; Gole, A.M.; Jayasinghe, R.P., "Efficient Modeling of Modular Multilevel HVDC Converters (MMC) on Electromagnetic Transient Simulation Programs," in Power Delivery, IEEE Transactions on , vol.26, no.1, pp.316-324, Jan. 2011

[21] Gnanarathna, U.N.; Chaudhary, S.K.; Gole, A.M.; Teodorescu, R., "Modular multi-level converter based HVDC system for grid connection of offshore wind power plant," in AC and DC Power Transmission, 2010. ACDC. 9th IET International Conference on , vol., no., pp.1-5, 19-21 Oct. 2010

[22] de Toledo, P.F.; Jiuping Pan; Srivastava, K.; WeiGuo Wang; Chao Hong, "Case Study of a Multi-Infeed HVDC System," in Power System Technology and IEEE Power India Conference, 2008. POWERCON 2008. Joint International Conference on , vol., no., pp.1-7, 12-15 Oct. 2008.

[23] Cresap, R.L.; Mittelstadt, W.A.; Scott, D.N.; Taylor, C.W., "Operating Experience with Modulation of the Pacific HVDC Intertie," in Power Apparatus and Systems, IEEE Transactions on , vol.PAS-97, no.4, pp.1053-1059, July 1978

[24] Grund, C.E.; Hauer, J.F.; Crane, L.P.; Carlson, D.L.; Wright, S.E., "Square Butte HVDC modulation system field tests," in Power Delivery, IEEE Transactions on , vol.5, no.1, pp.351-357, Jan 1990

[25] Patterson, W.A., "The Eel River HVDC scheme A 320 MW asynchronous interconnection between the New Brunswick Electric Power Commission and Hydro-Qubec employing thyristor valves," in Electrical Engineering Journal, Canadian , vol.2, no.1, pp.9-16, Jan. 1977.

[26] Mortensen, K.; Larsen, E.V.; Piwko, R.J., "Field Tests and Analysis of Torsional Interaction Between the Coal Creek Turbine-Generators and the CU HVdc System," in Power Apparatus and Systems, IEEE Transactions on , vol.PAS-100, no.1, pp.336-344, Jan. 1981

[27] Kuffel, P.; Kent, K.L.; Mazur, G.B.; Weekes, M.A., "Development and validation of detailed controls models of the Nelson River Bipole 1 HVDC system," in Power Delivery, IEEE Transactions on , vol.8, no.1, pp.351-358, Jan 1993

[28] Mazur, G.; Carryer, R.; Ranade, S.T.; Web, T., "Converter Control and Protection of the Nelson River HVDC Bipole 2 Commissioning and First Year of Commercial Operation," in Power Apparatus and Systems, IEEE Transactions on , vol.PAS-100, no.1, pp.327-335, Jan. 1981

[29] McNichol, John; Ranade, S.T.; Ring, H.; Meyl, D., "Parallel Operation of Nelson River HVDC Bipoles 1 and 2 Control System - Simulator Studies," in Power Apparatus and Systems, IEEE Transactions on , vol.PAS-101, no.3, pp.653-661, March 1982

[30] E. Uhlmann, "Stabilisation of an A. C. link by a parallel D. C. link," Direct Current, pp. 89-94, August 1964.

[31] Peterson, H.A.; Krause, P.C., "Damping of Power Swings in a Parallel AC and DC System," in Power Apparatus and Systems, IEEE Transactions on , vol.PAS-85, no.12, pp.1231-1239, Dec. 1966

[32] H. A. Peterson, D. K. Reitan, and A. G. Phadke, "Parallel operation of AC and DC power transmission," 1964 IEEE International Cony. Rec., vol. 12, pt. 3, pp. 84-89.

[33] K.W.V.; David, A.K.; Hammad, A.E., "A robust co-ordinated control scheme for HVDC transmission with parallel AC systems," in Power Delivery, IEEE Transactions on , vol.9, no.3, pp.1710-1716, Jul 1994

[34] R.L. Cresap, D.N. Scott, W.A.. Mittelstadt, and C.W. Taylor, "Damping of the Pacific AC Intertie Oscillations via Modulation of the Parallel Pacific HVDC Intertie," CIGRE Paper 14-05, Paris, 1978.

[35] IEEE Committee Report, "Dynamic Performance Characteristics of North American HVDC Systems for Transient and Dynamic Stability Evaluations," in Power Engineering Review, IEEE , vol.PER-1, no.7, pp.41-42, July 1981.

[36] T. Smed and G.Andersson, "Utilizing HVDC to Damp Power Oscillations", " *in proc. Power Delivery, IEEE Transactions on*, Vol. 8, No. 2, 1993, 620-627

[37] Vovos, N.A.; Galanos, G.D., "Damping of Power Swings in AC Tie Lines Using a Parallel DC Link Operating at Constant Reactive Power Control," in Power Apparatus and Systems, IEEE Transactions on , vol.PAS-98, no.2, pp.416-425, March 1979

[38] Grund, C.E.; Pohl, R.V.; Reeve, J., "Control Design of an Active and Reactive Power HVDC Modulation System with Kalman Filtering," in Power Engineering Review, IEEE , vol.PER-2, no.10, pp.61-61, Oct. 1982

[39] Lu. J, Thorp. J.S and Chiang. H.D., "Modal control of large flexible space structures using collocated actuators and sensors," *Automatic Control, IEEE Transactions on*, vol.37, no.1, pp.143-148, Jan 1992.

[40] Jing Ma, Tong Wang, James S. Thorp, A. G. Phadke and Zengping Wang "Application of Wide-area Collocated Control Technique for Damping Inter-area Oscillations Using Flexible AC Transmission Systems Devices", *Electric Power Components and Systems, 2011*, 39:13, 1452-1467.

[41] Samuelsson, O., "Load Modulation for Damping of Electro-Mechanical Oscillations", Panel paper, *IEEE Power Engineering Society Winter Meeting*, Jan 28-Feb 1, 2001, Columbus, OH, USA.

[42] Mhaskar, U.P and Kulkarni, A.M., "Power oscillation damping using FACTS devices: modal controllability, observability in local signals, and location of transfer function zeros", *IEEE TPWRS*, vol.21, no.1, pp. 285- 294, Feb. 2006.

[43] Taylor C.W., Erickson D. C., Martin K. E., "WACS Wide-area stability and voltage control system: R&D and online demonstration," Proceedings of the IEEE, Vol. 93, No. 5, pp. 892-906, 2005

[44] Li Peng; Wu Xiaochen; Lu Chao; Shi Jinghai; Hu Jiong; He Jingbo; Zhao Yong; Aidong Xu, "Implementation of CSG's Wide-Area Damping Control System: Overview and experience," in Power Systems Conference and Exposition, 2009. PSCE '09. IEEE/PES , vol., no., pp.1-9, 15-18 March 2009

[45] Cigr Working Group C4.601. "Wide area monitoring and control for transmission capability enhancement," Paris, Aug. 2007

[46] I. Kamwa, J. Bland, G. Trudel, R. Grondin, C. Lafond, D. McNabb, "Wide-Area monitoring and control at Hydro-Qubec: past, present and Future," in Proc. IEEE PES General Meeting, Montral, June 18-22, 2003

[47] Meyer B., Trotignon M. "Recommendations for the improvement of the Brazilian power system security following the 11th March 1999 outage based on EFD experience," EDF report, 1999.

[48] Zima M, Larsson M, Korba P, et al. "Design aspects for wide-area monitoring and control systems," Proceedings of the IEEE, 2005, 93(5):980-996

[49] Jingbo He; Chao Lu; Xiaoming Jin; Peng Li, "Analysis of time delay effects on wide area damping control," in Circuits and Systems, 2008. APCCAS 2008. IEEE Asia Pacific Conference on , vol., no., pp.758-761, Nov. 30 2008-Dec. 3 2008

[50] J. Y. Zhang, Y. Z. Sun, "Effect of Delayed Input on Oscillation Damping Using Wide Area Power System Stabilizer" in Proc. IEEE Transmission and Distribution Conference & Exhibition: Asia and Pacific, 2005, pp. 1-4

[51] H. Wu et al., The impact of time delay on robust control design in power systems, in Proc. IEEE PES Winter Meeting, vol. 2, 2002, pp. 2731.

[52] P. Park, "A delay-dependent stability criterion for systems with uncertain time-invariant delays," IEEE transactions on automatic control, vol.44, pp: 876-877, April 1999

[53] Lei Wu; Infield, D.G., "Towards an Assessment of Power System Frequency Support From Wind PlantModeling Aggregate Inertial Response," in Power Systems, IEEE Transactions on , vol.28, no.3, pp.2283-2291, Aug. 2013

[54] Jiebei Zhu; Booth, C.D.; Adam, G.P.; Roscoe, A.J.; Bright, C.G., "Inertia Emulation Control Strategy for VSC-HVDC Transmission Systems," in Power Systems, IEEE Transactions on , vol.28, no.2, pp.1277-1287, May 2013

[55] Ruifeng Yan; Saha, T.K., "Frequency response estimation method for high wind penetration considering wind turbine frequency support functions," in Renewable Power Generation, IET , vol.9, no.7, pp.775-782, 9 2015

[56] Wang-Hansen, M.; Josefsson, R.; Mehmedovic, H., "Frequency Controlling Wind Power Modeling of Control Strategies," in Sustainable Energy, IEEE Transactions on , vol.4, no.4, pp.954-959, Oct. 2013

[57] Delille, G.; Francois, B.; Malarange, G., "Dynamic Frequency Control Support by Energy Storage to Reduce the Impact of Wind and Solar Generation on Isolated Power System's Inertia," in Sustainable Energy, IEEE Transactions on , vol.3, no.4, pp.931-939, Oct. 2012

[58] P. Agnihotri, A.M. Kulkarni, A.M. Gole, "Robust Global Control Strategies for Improvement of Angular Stability using FACTS and HVDC Devices", *International Journal of Emerging Electric Power Systems, 2013*, vol.14, no.1, pp. 95-104.

[59] R.A. Horn, C.R. Johnson, "Matrix Analysis," Cambridge University Press, pp 397, 1985.

[60] P. M. Anderson and A. A. Fouad, "*Power System Control and Stability*", Ames, IA: Iowa State Univ. Press, 1977.

[61] J. H. Chow, J. J. Sanchez-Gasca, H. Ren, and S. Wang "Power system damping controller design using multiple input signals," *IEEE Control Systems Magazine*, vol. 20, no. 4, pp. 82-90, 2000.

[62] E. V. Larsen, J.J. Sanchez-Gasca, and J. H. Chow, Concepts for design of FACTS controllers to damp power swings, " *IEEE Transactions on Power Systems*, Vol. 10, No. 2, pp. 948-956, 1995

[63] Jagdish Chand, "Auxiliary Power Controls on the Nelson River HVDC Scheme," *Power Systems, IEEE Transactions on*, Vol. 7, No. 1, Feb 1992, 398-402

[64] W.A. Patterson, "External control systems on Eel River HVDC"

[65] Report of Panel Discussion, "HVDC Controls for System Dynamic Performance," *Power Systems, IEEE Transactions on*, vol. 6, no.2, pp.3356,3364, May 1991.

[66] R.A. Horn, C.R. Johnson, *Matrix Analysis*, Cambridge University Press, pp 397, 1985.

[67] D. J. Trudnowski and J. W. Pierre, "Overview of algorithms for estimating swing modes from measured responses, " *in proc. IEEE Power and Energy Society General Meeting*, Calgary, 2009.

[68] V. Pradhan, A.M. Kulkarni, S.A. Khaparde, "A Composite Strategy for Power Oscillation Damping Control Using Local and Wide Area Feedback Signals," Accepted for publication in " *IEEE Transactions on Power Systems*, Digital Object Identifier 10.1109/TPWRS.2015.2454294

Appendices

Appendix A

Small signal analysis of Line Commutated Converter

Here,
P_r=Real power at the rectifier end
Q_r=Reactive power at the rectifier end
V_r=Line-line ac Voltage at the rectifier end
K_r=1.35
I_d=DC line current
V_{dr}=DC Voltage at the rectifier end
V_{dor}=ideal no load voltage at the rectifier end
ϕ_r=Power factor at the rectifier end
R_r=Commutation resistance at the rectifier end
R_i=Commutation resistance at the inverter end
R_{dc}=DC resistance
P_i=Real power at the inverter end
Q_i=Reactive power at the inverter end
V_i=Line-line ac Voltage at the inverter end
K_i=1.35
V_{di}=DC Voltage at the inverter end
V_{doi}=ideal no load voltage at the inverter end
ϕ_i=Power factor at the inverter end
R_i=DC line resistance at the inverter end
α=delay angle
γ=extinction advance angle

Real and reactive power at the converter buses are related as:

$$\begin{bmatrix} Q_r \\ Q_i \end{bmatrix} = P_r \begin{bmatrix} \tan\phi_r \\ \tan\phi_i \end{bmatrix} \tag{A.1}$$

$$\begin{bmatrix} \Delta Q_r \\ \Delta Q_i \end{bmatrix} = \Delta P_r \begin{bmatrix} \tan\phi_{ro} \\ \tan\phi_{io} \end{bmatrix} + P_{ro} \begin{bmatrix} \sec^2\phi_{ro}\Delta\phi_r \\ \sec^2\phi_{io}\Delta\phi_i \end{bmatrix} \tag{A.2}$$

$$\cos\phi_r = \frac{V_{dr}}{V_{dor}} \tag{A.3}$$

$$-\sin\phi_{ro}\Delta\phi_r = \frac{\Delta V_{dr}}{V_{doro}} - \frac{\Delta V_{dro}\Delta V_{dor}}{V_{doro}^2} \tag{A.4}$$

$$\Delta\phi_r = -\frac{\Delta V_{dr}}{V_{doro}\sin\phi_{ro}} - \frac{\Delta V_{dro}\Delta V_{dor}}{V_{doro}^2\sin\phi_{ro}} \tag{A.5}$$

$$\Delta\phi_i = -\frac{\Delta V_{di}}{V_{doio}\sin\phi_{io}} + \frac{\Delta V_{dio}\Delta V_{doi}}{V_{doio}^2\sin\phi_{io}} \tag{A.6}$$

$$\Delta V_{dor} = K_r\frac{\Delta V_r}{V_{ro}} \tag{A.7}$$

$$\Delta V_{doi} = K_i\frac{\Delta V_i}{V_{io}} \tag{A.8}$$

$$\begin{bmatrix} \Delta Q_r \\ \Delta Q_i \end{bmatrix} = \Delta P_r \begin{bmatrix} \tan\phi_{ro} \\ \tan\phi_{io} \end{bmatrix} - \begin{bmatrix} \frac{P_{ro}\sec^2\phi_{ro}}{V_{doro}\sin\phi_{ro}} & 0 \\ 0 & \frac{P_{ro}\sec^2\phi_{ro}}{V_{doro}\sin\phi_{ro}} \end{bmatrix} \begin{bmatrix} \Delta V_{dr} \\ \Delta V_{di} \end{bmatrix} \tag{A.9}$$

$$+ \begin{bmatrix} \frac{P_{ro}\sec^2\phi_{ro}V_{dro}K_r}{V_{doro}\sin\phi_{ro}} & 0 \\ 0 & \frac{P_{ro}\sec^2\phi_{io}}{V_{doio}\sin\phi_{io}} \end{bmatrix} \begin{bmatrix} \frac{\Delta V_r}{V_{ro}} \\ \frac{\Delta V_i}{V_{io}} \end{bmatrix} \tag{A.10}$$

$$A_1 = \begin{bmatrix} \tan\phi_{ro} \\ \tan\phi_{io} \end{bmatrix} \tag{A.11}$$

$$A_2 = \begin{bmatrix} \frac{P_{ro}\sec^2\phi_{ro}V_{dro}K_r}{V_{doro}\sin\phi_{ro}} & 0 \\ 0 & \frac{P_{ro}\sec^2\phi_{io}}{V_{doio}\sin\phi_{io}} \end{bmatrix} \tag{A.12}$$

$$A_3 = \begin{bmatrix} \frac{P_{ro}\sec^2\phi_{ro}}{V_{doro}\sin\phi_{ro}} & 0 \\ 0 & \frac{P_{ro}\sec^2\phi_{ro}}{V_{doro}\sin\phi_{ro}} \end{bmatrix} \tag{A.13}$$

$$V_{dr} = V_{dor}\cos\alpha - R_r I_d \tag{A.14}$$

$$V_{di} = V_{doi}\cos\gamma - R_i I_d \tag{A.15}$$

$$\begin{bmatrix} \Delta V_{dr} \\ \Delta V_{di} \end{bmatrix} = \begin{bmatrix} \Delta V_{dor}\cos\alpha_o \\ \Delta V_{doi}\cos\gamma_o \end{bmatrix} - \begin{bmatrix} R_r \\ R_i \end{bmatrix} \Delta I_d \tag{A.16}$$

$$\begin{bmatrix} \Delta V_{dor}\cos\alpha_o \\ \Delta V_{doi}\cos\gamma_o \end{bmatrix} = \begin{bmatrix} K_r\cos\alpha_o & 0 \\ 0 & K_i\cos\gamma_o \end{bmatrix} \begin{bmatrix} \frac{\Delta V_r}{V_{ro}} \\ \frac{\Delta V_i}{V_{io}} \end{bmatrix} - \begin{bmatrix} \Delta V_{dor}\sin\alpha_o & 0 \\ 0 & \Delta V_{doi}\sin\gamma_o \end{bmatrix} \begin{bmatrix} \Delta\alpha \\ \Delta\gamma \end{bmatrix} \tag{A.17}$$

If the DC link is operated in Mode 1 Rectifier is in CC mode and inverter in CEA

control mode hence $\Delta\gamma = 0$

$$\begin{bmatrix}\Delta V_{dr}\\ \Delta V_{di}\end{bmatrix} = \begin{bmatrix} K_r\cos\alpha_o & 0\\ 0 & K_i\cos\gamma_o\end{bmatrix}\begin{bmatrix}\frac{\Delta V_r}{V_{ro}}\\ \\ \frac{\Delta V_i}{V_{io}}\end{bmatrix} - \begin{bmatrix}\Delta V_{dor}\sin\alpha_o\\ 0\end{bmatrix}\Delta\alpha - \begin{bmatrix}\frac{R_r}{R_{dc}} & \frac{-R_i}{R_{dc}}\\ \frac{R_i}{R_{dc}} & \frac{-R_i}{R_{dc}}\end{bmatrix}\begin{bmatrix}\Delta V_{dr}\\ \Delta V_{di}\end{bmatrix} \tag{A.18}$$

$$A_4 = \begin{bmatrix} K_r\cos\alpha_o & 0\\ 0 & K_i\cos\gamma_o\end{bmatrix} \tag{A.19}$$

$$A_5 = \begin{bmatrix}\Delta V_{dor}\sin\alpha_o\\ 0\end{bmatrix} \tag{A.20}$$

$$A_6 = \begin{bmatrix}\frac{R_r}{R_{dc}} & \frac{-R_i}{R_{dc}}\\ \frac{R_i}{R_{dc}} & \frac{-R_i}{R_{dc}}\end{bmatrix} \tag{A.21}$$

$$P_r = \frac{V_{dr}^2 - V_{dr}V_{di}}{R_{dc}} \tag{A.22}$$

$$\Delta P_r = \begin{bmatrix}\frac{2V_{dro}}{R_{dc}} - \frac{V_{dio}}{R_{dc}} & \frac{V_{dro}}{R_{dc}}\end{bmatrix}\begin{bmatrix}\Delta V_{dr}\\ \Delta V_{di}\end{bmatrix} \tag{A.23}$$

$$A_7 = \begin{bmatrix}\frac{2V_{dro}}{R_{dc}} - \frac{V_{dio}}{R_{dc}} & \frac{V_{dro}}{R_{dc}}\end{bmatrix} \tag{A.24}$$

$$\Delta P_r = A_7\begin{bmatrix}\Delta V_{dr}\\ \Delta V_{di}\end{bmatrix} \tag{A.25}$$

$$\Delta P_r = A_7A_4\begin{bmatrix}\frac{\Delta V_r}{V_{ro}}\\ \\ \frac{\Delta V_i}{V_{io}}\end{bmatrix} - A_7A_5\Delta\alpha - A_7A_6\begin{bmatrix}\Delta V_{dr}\\ \Delta V_{di}\end{bmatrix} \tag{A.26}$$

$$\Delta\alpha = \frac{-1}{A_7A_5}\left[\Delta P_r - A_7A_4\begin{bmatrix}\frac{\Delta V_r}{V_{ro}}\\ \\ \frac{\Delta V_i}{V_{io}}\end{bmatrix} + A_7A_6\begin{bmatrix}\Delta V_{dr}\\ \Delta V_{di}\end{bmatrix}\right] \tag{A.27}$$

$$[I + A_6]\begin{bmatrix}\Delta V_{dr}\\ \Delta V_{di}\end{bmatrix} = \left[A_4 - \frac{A_5A_7A_4}{A_7A_5}\right]\begin{bmatrix}\frac{\Delta V_r}{V_{ro}}\\ \\ \frac{\Delta V_i}{V_{io}}\end{bmatrix} + \frac{A_5}{A_7A_5}\Delta P_r + \frac{A_5A_7A_6}{A_7A_5}\begin{bmatrix}\Delta V_{dr}\\ \Delta V_{di}\end{bmatrix} \tag{A.28}$$

$$\left[I + A_6 - \frac{A_5A_7A_6}{A_7A_5}\right]\begin{bmatrix}\Delta V_{dr}\\ \Delta V_{di}\end{bmatrix} = A_8\begin{bmatrix}\frac{\Delta V_r}{V_{ro}}\\ \\ \frac{\Delta V_i}{V_{io}}\end{bmatrix} + A_9\Delta P_r \tag{A.29}$$

$$A_{10} = \left[I + A_6 - \frac{A_5 A_7 A_6}{A_7 A_5} \right] \tag{A.30}$$

$$\begin{bmatrix} \Delta V_{dr} \\ \Delta V_{di} \end{bmatrix} = A_{10}^{-1} A_8 \begin{bmatrix} \frac{\Delta V_r}{V_{ro}} \\ \frac{\Delta V_i}{V_{io}} \end{bmatrix} + A_{10}^{-1} A_9 \Delta P_r \tag{A.31}$$

$$A_{11} = A_{10}^{-1} A_8 \tag{A.32}$$

$$A_{12} = A_{10}^{-1} A_9 \tag{A.33}$$

$$\begin{bmatrix} \Delta Q_r \\ \Delta Q_i \end{bmatrix} = \left[A_1 + A_3 A_{12} \right] \Delta P_r + \left[A_2 + A_3 A_{11} \right] \begin{bmatrix} \frac{\Delta V_r}{V_{ro}} \\ \frac{\Delta V_i}{V_{io}} \end{bmatrix} \tag{A.34}$$

$$\begin{bmatrix} \Delta Q_r \\ \Delta Q_i \end{bmatrix} = \begin{bmatrix} g_r \\ g_i \end{bmatrix} \Delta P_r + H \begin{bmatrix} \frac{\Delta V_r}{V_{ro}} \\ \frac{\Delta V_i}{V_{io}} \end{bmatrix} \tag{A.35}$$

If the DC link is operated in Mode 2 Rectifier is in CIA mode and inverter in CC control mode hence $\Delta\alpha = 0$

$$\begin{bmatrix}\Delta V_{dr}\\ \Delta V_{di}\end{bmatrix} = \begin{bmatrix} K_r\cos\alpha_o & 0\\ 0 & K_i\cos\gamma_o\end{bmatrix}\begin{bmatrix}\frac{\Delta V_r}{V_{ro}}\\ \frac{\Delta V_i}{V_{io}}\end{bmatrix} - \tag{A.36}$$

$$\begin{bmatrix}0\\ \Delta V_{dor}\sin\gamma_o\end{bmatrix}\Delta\gamma - \begin{bmatrix}\frac{R_r}{R_{dc}} & \frac{-R_i}{R_{dc}}\\ \frac{R_i}{R_{dc}} & \frac{-R_i}{R_{dc}}\end{bmatrix}\begin{bmatrix}\Delta V_{dr}\\ \Delta V_{di}\end{bmatrix} \tag{A.37}$$

$$A_{13} = \begin{bmatrix}0\\ \Delta V_{dor}\sin\gamma_o\end{bmatrix} \tag{A.38}$$

$$\Delta P_r = A_7A_4\begin{bmatrix}\frac{\Delta V_r}{V_{ro}}\\ \frac{\Delta V_i}{V_{io}}\end{bmatrix} - A_7A_{13}\Delta\gamma - A_7A_6\begin{bmatrix}\Delta V_{dr}\\ \Delta V_{di}\end{bmatrix} \tag{A.39}$$

$$\Delta\gamma = \frac{-1}{A_7A_{13}}\left[\Delta P_r - A_7A_4\begin{bmatrix}\frac{\Delta V_r}{V_{ro}}\\ \frac{\Delta V_i}{V_{io}}\end{bmatrix} + A_7A_6\begin{bmatrix}\Delta V_{dr}\\ \Delta V_{di}\end{bmatrix}\right] \tag{A.40}$$

$$[I + A_6]\begin{bmatrix}\Delta V_{dr}\\ \Delta V_{di}\end{bmatrix} = \left[A_4 - \frac{A_{13}A_7A_4}{A_7A_{13}}\right]\begin{bmatrix}\frac{\Delta V_r}{V_{ro}}\\ \frac{\Delta V_i}{V_{io}}\end{bmatrix} + \frac{A_{13}}{A_7A_{13}}\Delta P_r + \frac{A_{13}A_7A_6}{A_7A_{13}}\begin{bmatrix}\Delta V_{dr}\\ \Delta V_{di}\end{bmatrix} \tag{A.41}$$

$$\left[I + A_6 - \frac{A_{13}A_7A_6}{A_7A_{13}}\right]\begin{bmatrix}\frac{\Delta V_r}{V_{ro}}\\ \frac{\Delta V_i}{V_{io}}\end{bmatrix} = A_{14}\begin{bmatrix}\frac{\Delta V_r}{V_{ro}}\\ \frac{\Delta V_i}{V_{io}}\end{bmatrix} + A_{15}\Delta P_r \tag{A.42}$$

$$A_{16} = \left[I + A_6 - \frac{A_{13}A_7A_6}{A_7A_{13}}\right] \tag{A.43}$$

$$\begin{bmatrix}\Delta V_{dr}\\ \Delta V_{di}\end{bmatrix} = A_{16}^{-1}A_{14}\begin{bmatrix}\frac{\Delta V_r}{V_{ro}}\\ \frac{\Delta V_i}{V_{io}}\end{bmatrix} + A_{16}^{-1}A_{15}\Delta P_r \tag{A.44}$$

$$A_{17} = A_{16}^{-1}A_{14} \tag{A.45}$$

$$A_{18} = A_{16}^{-1}A_{15} \tag{A.46}$$

$$\begin{bmatrix}\Delta Q_r\\ \Delta Q_i\end{bmatrix} = [A_1 + A_3A_{18}]\Delta P_r + [A_2 + A_3A_{17}]\begin{bmatrix}\frac{\Delta V_r}{V_{ro}}\\ \frac{\Delta V_i}{V_{io}}\end{bmatrix} \tag{A.47}$$

$$\begin{bmatrix}\Delta Q_r \\ \Delta Q_i\end{bmatrix} = \begin{bmatrix}g_r \\ g_i\end{bmatrix} \Delta P_r + H \begin{bmatrix}\frac{\Delta V_r}{V_{ro}} \\ \\ \frac{\Delta V_i}{V_{io}}\end{bmatrix} \tag{A.48}$$

We consider Example 10.2 in [1], where a bipolar dc link with a rating of 1000 MW and ± 250 kV is given. The ac side voltage is 220 kV. The line resistance is 10Ω/line. Each converter has a 12-pulse bridge with $R_c = \frac{3}{\pi} X_c = 12\Omega$. The parameters of the linearized equation 2.6 are calculated for four operating points as given below.

1. DC link is operated with rectifier on CC control with $\alpha = 18.16^\circ$ and inverter on CEA control with $\gamma = 18.167^\circ$. The inverter end voltage is 500 kV and inverter end power is 1000 MW. The results are shown on a 1000 MVA, 220 kV base.
$$\begin{bmatrix}\Delta Q_{dc_r} \\ \Delta Q_{dc_i}\end{bmatrix} = \begin{bmatrix}0.81 \\ 0.91\end{bmatrix} \Delta P_{dc} + \begin{bmatrix}2.43 & -2.93 \\ 0 & -0.61\end{bmatrix} \begin{bmatrix}\frac{\Delta V_r}{V_{ro}} \\ \\ \frac{\Delta V_i}{V_{io}}\end{bmatrix}$$

2. If the rectifier end AC voltage is dropped by 20%, and transformer taps are unchanged then rectifier control will reach $\alpha_{min} = 5^\circ$, and inverter operates in CC mode with $\gamma = 37.23^\circ$.
$$\begin{bmatrix}\Delta Q_{dc_r} \\ \Delta Q_{dc_i}\end{bmatrix} = \begin{bmatrix}0.71 \\ 1.1\end{bmatrix} \Delta P_{dc} + \begin{bmatrix}2.3 & -2.22 \\ 0 & -0.25\end{bmatrix} \begin{bmatrix}\frac{\Delta V_r}{V_{ro}} \\ \\ \frac{\Delta V_i}{V_{io}}\end{bmatrix}$$

3. If the inverter end AC voltage is dropped by 15%, mode 1 is possible i.e. rectifier operates at CC mode with $\alpha = 15.8^\circ$ and inverter operates at CEA mode with $\gamma = 18.16^\circ$. The transformer taps are changed to ensure α is within limits and inverter side dc voltage is nearly 500 kV.
$$\begin{bmatrix}\Delta Q_{dc_r} \\ \Delta Q_{dc_i}\end{bmatrix} = \begin{bmatrix}0.76 \\ 0.88\end{bmatrix} \Delta P_{dc} + \begin{bmatrix}2.78 & -2.77 \\ 0 & -0.55\end{bmatrix} \begin{bmatrix}\frac{\Delta V_r}{V_{ro}} \\ \\ \frac{\Delta V_i}{V_{io}}\end{bmatrix}$$

4. If the power is reduced by 50% i.e to 500 MW, then with $\alpha = 18^\circ$ and $\gamma = 18.16^\circ$ we obtain,
$$\begin{bmatrix}\Delta Q_{dc_r} \\ \Delta Q_{dc_i}\end{bmatrix} = \begin{bmatrix}0.59 \\ 0.74\end{bmatrix} \Delta P_{dc} + \begin{bmatrix}1.27 & -1.44 \\ 0 & -0.15\end{bmatrix} \begin{bmatrix}\frac{\Delta V_r}{V_{ro}} \\ \\ \frac{\Delta V_i}{V_{io}}\end{bmatrix}$$

Appendix B

4-machine, 2-area System Data

Table B.1: Machine bus data

Bus No.	Voltage (pu)	Power generation (MW)
1	1.03	700
2	1.01	700
3	1.03	719
4	1.01	700

Table B.2: Load bus data

Bus No.	Real load (MW)	Reactive load (MVAr)	Shunt Load Q_C (MVAr)
7	967	100	200
9	1767	100	350

Table B.3: Line data

From Bus	To Bus	Resistance (pu)	Reactance (pu)	B(total)/Tap Ratio
5	6	.0025	.025	.04375
6	7	.0010	.010	.01750
7	8	.0110	.110	.1925
7	8	.0110	.110	.1925
8	9	.0110	.110	.1925
8	9	.0110	.110	.1925
9	10	.0010	.010	.01750
10	11	.0025	.025	.04375
1	5	.00	.01667	1.000
6	2	.00	.01667	1.000
10	4	.00	.01667	1.000
11	3	.00	.01667	1.000

Table B.4: Machine data

Gen. No.	xd	xd′	xd″	Tdo′	Tdo″	xq	xq′	xq″	Tqo′	Tqo″	H
1	0.2000	0.0333	0.0278	8.00	0.03	0.189	0.061	0.0277	0.4	0.05	58.500
2	0.2000	0.0333	0.0278	8.00	0.03	0.189	0.061	0.0277	0.4	0.05	58.500
3	0.2000	0.0333	0.0278	8.00	0.03	0.189	0.061	0.0277	0.4	0.05	55.575
4	0.2000	0.0333	0.0278	8.00	0.03	0.189	0.061	0.0277	0.4	0.05	55.575

Table B.5: Static excitation system data

Gen. No.	KA	TA	EFDMIN	EFDMAX
1	200	0.02	-6	6
2	200	0.02	-6	6
3	200	0.02	-6	6
4	200	0.02	-6	6

Table B.6: HVDC data

Link. No.	Rec/Inv bus	Br/Bi	Trmax/Timax	Trmin/Timin	Tnr/Tni	Xcr/Xci	Alphamin/Gammamin	Nr/Ni	Bshr/Bshi
1	7	1	1	0	1.0	0.001077	5	100	1.25
1	9	1	1	0	1.0	0.001077	17	100	1.25

Table B.7: HVDC data contd...

Link. No.	Rec bus	Inv bus	Vdis	Idc	Pdr	Im	Rdc	Alprmin	Alprmax	cn	pn	Vbase (kV)	Vdrs(initial)
1	7	9	0.226	2.0	1.5	0.2	0.00283	10	20	0	1	230	0.226

cn -set 1 if the dc link is on link current specification else 0.
pn -set 1 if the dc link is on rectifier-end power specification else 0.

Table B.8: Load Flow Results

Bus No.	VbO	thetaO	PGO	QGO	PLO	QLO
1	1.03	15.62	7.0	1.85	0.0	0.0
2	1.01	5.99	7.0	2.34	0.0	0.0
3	1.03	0.0	7.15	1.759	0.0	0.0
4	1.01	-9.93	7.0	2.019	0.0	0.0
5	1.0	9.21	0.0	0.0	0.0	0.0
6	0.97	-0.65	0.0	0.0	0.0	0.0
7	0.96	-8.7	0.0	0.0	9.67	1.0
8	0.95	-16.72	0.0	0.0	0.0	0.0
9	0.97	-24.5	0.0	0.0	17.67	1.0
10	0.98	-16.52	0.0	0.0	0.0	0.0
11	1.0	-6.52	0.0	0.0	0.0	0.0

Table B.9: DC Link Results

Parameter	Rectifier	Inverter
Bus no 7 9 D.C.Voltage(pu)	0.243438	0.226000
Transformer tap Position(pu)	0.190000	0.177680
Control Angles(Deg)	12.216950	17.000000
Commutation overlap Angles(Deg)	9.694762	8.292635
Real Power flow(pu)	1.500000	1.392553
Reactive power consumption(pu)	0.479281	0.549403
Power factor	0.952557	0.930221
Current in the D.C.Link(pu)	6.161740	

Appendix C

3-machine System Data

Table C.1: Machine bus data

Bus No.	Voltage (pu)	Power generation (MW)
1	1.04	716.6
2	1.025	163
3	1.025	85

Table C.2: Load bus data

Bus No.	Real load (MW)	Reactive load (MVAr)
5	125	50
6	90	30
8	100	35

Table C.3: Line data

From Bus	To Bus	Resistance (pu)	Reactance (pu)	B(total)/Tap Ratio
9	8	.0119	.1008	.209
9	6	.039	.170	.358
8	7	.0085	.072	.149
7	5	.032	.161	.306
7	5	.032	.161	.306
6	4	.017	.092	.158
5	4	.010	.085	.176
4	1	.000	.0576	1.000
3	9	.000	.0586	1.000
2	7	.000	.0625	1.000

Table C.4: Machine data

Gen. No.	xd	xd′	xd″	Tdo′	Tdo″	xq	xq′	xq″	Tqo′	Tqo″	H
1	0.1460	0.0608	0.0608	8.96	1.00	0.0969	0.0969	0.0969	1.000	1.00	23.640
2	0.8958	0.1198	0.1198	6.00	1.00	0.8645	0.1969	0.1969	0.535	1.00	6.400
3	1.3125	0.1813	0.1813	5.89	1.00	1.2578	0.2500	0.2500	0.600	1.00	3.010

Table C.5: Static excitation system data

Gen. No.	KA	TA	EFDMIN	EFDMAX
1	200	0.05	-6	6
2	200	0.05	-6	6
3	200	0.05	-6	6

Table C.6: Load Flow Results

Bus No.	VbO	thetaO	PGO	QGO	PLO	QLO
1	1.040000	0.000000	0.702077	0.081056	0.000000	0.000000
2	1.025000	6.411725	1.630000	-0.108612	0.000000	0.000000
3	1.025000	3.043622	0.850000	-0.178211	0.000000	0.000000
4	1.036241	-2.150494	0.000000	0.000000	0.000000	0.000000
5	1.021993	-3.362176	0.000000	0.000000	1.250000	0.500000
6	1.021952	-4.166801	0.000000	0.000000	0.900000	0.300000
7	1.036399	0.908625	0.000000	0.000000	0.000000	0.000000
8	1.024067	-1.546160	0.000000	0.000000	1.000000	0.350000
9	1.036328	0.355897	0.000000	0.000000	0.000000	0.000000

Appendix D

16-machine System Data

Table D.1: Machine bus data

Bus No.	Voltage (pu)	Power generation (pu)
53	1.045000	2.500000
54	0.980000	5.450000
55	0.983000	6.500000
56	0.997000	6.320000
57	1.011000	5.052000
58	1.050000	7.000000
59	1.063000	5.600000
60	1.030000	5.400000
61	1.025000	8.000000
62	1.010000	5.000000
63	1.000000	10.000000
64	1.015600	13.500000
65	1.011000	35.914193
66	1.000000	17.850000
67	1.000000	10.000000
68	1.000000	40.000000

Table D.2: Load bus data

Bus No.	Real load (pu)	Reactive load (pu)
1	2.527	1.1856
3	3.22	0.02
4	5	1.84
7	2.34	0.84
8	5.22	1.77
9	1.04	1.25
12	0.09	0.88
15	3.2	1.53
16	3.29	0.32
18	1.58	0.3
20	6.8	1.03
21	2.74	1.15
23	2.48	0.85
24	3.09	-0.92
25	2.24	0.47
26	1.39	0.17
27	2.81	0.76
28	2.06	0.28
29	2.84	0.27
33	1.12	0
36	11.02	-0.1946
37	75	3
39	2.67	0.126
40	0.6563	0.2353
41	0	2.5
42	11.5	2.5
44	2.6755	0.0484
45	2.08	0.21
46	1.507	0.285
47	2.0312	0.3259
48	2.412	0.022
49	1.64	0.29
50	1	-1.47
51	3.37	-1.22
52	9.7	1.23

Table D.3: Line data

From Bus	To Bus	Resistance (pu)	Reactance (pu)	B(total)/Tap Ratio
1	2	0.0035	0.0411	0.6987
1	30	0.0008	0.0074	0.48
2	3	0.0013	0.0151	0.2572
2	25	0.007	0.0086	0.146
3	4	0.0013	0.0213	0.2214
3	18	0.0011	0.0133	0.2138
4	5	0.0008	0.0128	0.1342
4	14	0.0008	0.0129	0.1382
5	6	0.0002	0.0026	0.0434
5	8	0.0008	0.0112	0.1476
6	7	0.0006	0.0092	0.113
6	11	0.0007	0.0082	0.1389
7	8	0.0004	0.0046	0.078
8	9	0.0023	0.0363	0.3804
9	30	0.0019	0.0183	0.29
10	13	0.0004	0.0043	0.0729
10	11	0.0004	0.0043	0.0729
13	14	0.0009	0.0101	0.1723
14	15	0.0018	0.0217	0.366
15	16	0.0009	0.0094	0.171
16	17	0.0007	0.0089	0.1342
16	19	0.0016	0.0195	0.304
16	24	0.0003	0.0059	0.068
17	18	0.0007	0.0082	0.1319
17	27	0.0013	0.0173	0.3216
21	22	0.0008	0.014	0.2565
22	23	0.0006	0.0096	0.1846
23	24	0.0022	0.035	0.361
25	26	0.0032	0.0323	0.531
26	27	0.0014	0.0147	0.2396
26	28	0.0043	0.0474	0.7802
26	29	0.0057	0.0625	1.029
28	29	0.0014	0.0151	0.249
9	30	0.0019	0.0183	0.29
9	36	0.0022	0.0196	0.34
9	36	0.0022	0.0196	0.34
36	37	0.0005	0.0045	0.32

Table D.4: Line data

From Bus	To Bus	Resistance (pu)	Reactance (pu)	B(total)/Tap Ratio
34	36	0.0033	0.0111	1.45
33	34	0.0011	0.0157	0.202
32	33	0.0008	0.0099	0.168
30	31	0.0013	0.0187	0.333
30	32	0.0024	0.0288	0.488
1	31	0.0016	0.0163	0.25
31	38	0.0011	0.0147	0.247
33	38	0.0036	0.0444	0.693
38	46	0.0022	0.0284	0.43
46	49	0.0018	0.0274	0.27
1	47	0.0013	0.0188	1.31
47	48	0.0025	0.0268	0.4
47	48	0.0025	0.0268	0.4
48	40	0.002	0.022	1.28
37	43	0.0005	0.0276	0
35	45	0.0007	0.0175	1.39
39	45	0	0.0839	0
43	44	0.0001	0.0011	0
44	45	0.0025	0.073	0
45	51	0.0004	0.0105	0.72
52	42	0.004	0.06	2.25
50	51	0.0009	0.0221	1.62
50	52	0.0012	0.0288	2.06
49	52	0.0076	0.1141	1.16
42	41	0.004	0.06	2.25
41	40	0.006	0.084	3.15
1	27	0.032	0.32	0.41
16	21	0.0008	0.0135	0.2548
2	53	0	0.0181	1.025
19	20	0.0007	0.0138	1.06
12	13	0.0016	0.0435	1.06
12	11	0.0016	0.0435	1.06
41	66	0	0.0015	1
32	63	0	0.013	1.04

Table D.5: Line data

From Bus	To Bus	Resistance (pu)	Reactance (pu)	B(total)/Tap Ratio
31	62	0	0.026	1.04
42	67	0	0.0015	1
52	68	0	0.003	1
36	64	0	0.0075	1.04
37	65	0	0.0033	1.04
25	60	0.0006	0.0232	1.025
35	34	0.0001	0.0074	0.946
39	44	0	0.0411	1
6	54	0	0.025	1.07
23	59	0.0005	0.0272	1
29	61	0.0008	0.0156	1.025
22	58	0	0.0143	1.025
19	56	0.0007	0.0142	1.07
20	57	0.0009	0.018	1.009
10	55	0	0.02	1.07

Table D.6: Machine data

Gen. No.	xd	xd'	xd''	Tdo'	Tdo''	xq	xq'	xq''	Tqo'	Tqo''	H
53	0.1000	0.0310	0.0310	10.2	0.05	0.069	0.0310	0.0310	1.50	0.04	42.0
54	0.2950	0.0697	0.0697	6.56	0.05	0.282	0.0697	0.0697	1.50	0.04	30.2
55	0.2495	0.0531	0.0531	5.70	0.05	0.237	0.0531	0.0531	1.50	0.04	35.8
56	0.2620	0.0436	0.0436	5.69	0.05	0.258	0.0436	0.0436	1.50	0.04	28.6
57	0.3300	0.0660	0.0660	5.40	0.05	0.310	0.0660	0.0660	0.44	0.04	26.0
58	0.2540	0.0500	0.0500	7.30	0.05	0.241	0.0500	0.0500	0.40	0.04	34.8
59	0.2950	0.0490	0.0490	5.66	0.05	0.292	0.0490	0.0490	1.50	0.04	26.4
60	0.2900	0.0570	0.0570	6.70	0.05	0.280	0.0570	0.0570	0.41	0.04	24.3
61	0.2106	0.0570	0.0570	4.79	0.05	0.205	0.0570	0.0570	1.96	0.04	34.5
62	0.1690	0.0457	0.0457	9.37	0.05	0.115	0.0457	0.0457	1.50	0.04	31.0
63	0.1280	0.0180	0.0180	4.10	0.05	0.123	0.0180	0.0180	1.50	0.04	28.2
64	0.1010	0.0310	0.0310	7.40	0.05	0.095	0.0310	0.0310	1.50	0.04	92.3
65	0.0296	0.0055	0.0055	1000	0.05	0.0055	0.0055	0.0055	1.5	0.04	248.0
66	0.018	0.00285	0.00285	1000	0.05	0.00285	0.00285	0.00285	1.5	0.04	300.0
67	0.018	0.00285	0.00285	1000	0.05	0.00285	0.00285	0.00285	1.5	0.04	300.0
68	0.0356	0.0071	0.0071	1000	0.05	0.0071	0.0071	0.0071	1.5	0.04	225.0

Table D.7: Static excitation system data

Gen. No.	KA	TA	EFDMIN	EFDMAX
65	2	0.5	-6	6
66	2	0.5	-6	6
67	2	0.5	-6	6
68	2	0.5	-6	6
62	2	0.5	-6	6
63	2	0.5	-6	6
64	2	0.5	-6	6
53	2	0.5	-6	6
54	2	0.5	-6	6
55	2	0.5	-6	6
56	2	0.5	-6	6
57	2	0.5	-6	6
58	2	0.5	-6	6
59	2	0.5	-6	6
60	2	0.5	-6	6
61	2	0.5	-6	6

Table D.8: HVDC data

Link. No.	Rec/Inv bus	Br/Bi	Trmax/Timax	Trmin/Timin	Tnr/Tni	Xcr/Xci	Alphamin/Gammamin	Nr/Ni	Bshr/Bshi
1	52	1	5.15	0.85	1.0	0.0144	5	27	6.0
1	37	1	5.15	0.85	1.0	0.0144	15	19	6.0
2	41	1	5.15	0.85	1.0	0.0144	5	27	4.0
2	36	1	5.15	0.85	1.0	0.0144	15	19	4.0

Table D.9: HVDC data contd...

Link. No.	Rec bus	Inv bus	Vdis	Idc	Pdr	Im	Rdc	Alprmin	Alprmax	cn	pn	Vbase (kV)	Vdrs(initial)
1	52	37	2.0	7.5	15.0	0.75	0.006	10	20	0	1	500	1
2	41	36	2.0	5.0	10.0	0.50	0.006	10	20	0	1	500	1

cn -set 1 if the dc link is on link current specification else 0.
pn -set 1 if the dc link is on rectifier-end power specification else 0.

Table D.10: Load Flow Results

Bus No.	VbO	thetaO	PGO	QGO	PLO	QLO
1	1.060907	6.647982	0.000000	0.000000	2.527000	1.185600
2	1.052023	8.325495	0.000000	0.000000	0.000000	0.000000
3	1.033235	5.332714	0.000000	0.000000	3.220000	0.020000
4	1.006454	4.234682	0.000000	0.000000	5.000000	1.840000
5	1.007909	5.192599	0.000000	0.000000	0.000000	0.000000
6	1.009975	5.867693	0.000000	0.000000	0.000000	0.000000
7	1.000402	3.631064	0.000000	0.000000	2.340000	0.840000
8	0.999972	3.104251	0.000000	0.000000	5.220000	1.770000
9	1.041452	2.781999	0.000000	0.000000	1.040000	1.250000
10	1.018879	8.354390	0.000000	0.000000	0.000000	0.000000
11	1.014621	7.507875	0.000000	0.000000	0.000000	0.000000
12	1.055893	7.528181	0.000000	0.000000	0.090000	0.880000
13	1.016176	7.688124	0.000000	0.000000	0.000000	0.000000
14	1.013911	6.143738	0.000000	0.000000	0.000000	0.000000
15	1.017455	6.029592	0.000000	0.000000	3.200000	1.530000
16	1.033734	7.555116	0.000000	0.000000	3.290000	0.320000
17	1.036872	6.470088	0.000000	0.000000	0.000000	0.000000
18	1.034178	5.611681	0.000000	0.000000	1.580000	0.300000
19	1.050201	12.128648	0.000000	0.000000	0.000000	0.000000
20	0.990518	10.694249	0.000000	0.000000	6.800000	1.030000
21	1.032760	10.178556	0.000000	0.000000	2.740000	1.150000
22	1.050267	14.846930	0.000000	0.000000	0.000000	0.000000
23	1.045111	14.559610	0.000000	0.000000	2.480000	0.850000
24	1.038910	7.725952	0.000000	0.000000	3.090000	-0.920000
25	1.060148	9.574598	0.000000	0.000000	2.240000	0.470000
26	1.056416	8.075910	0.000000	0.000000	1.390000	0.170000
27	1.043804	6.201112	0.000000	0.000000	2.810000	0.760000
28	1.052169	11.192568	0.000000	0.000000	2.060000	0.280000
29	1.051038	13.821645	0.000000	0.000000	2.840000	0.270000
30	1.055484	6.144487	0.000000	0.000000	0.000000	0.000000
31	1.058831	8.624504	0.000000	0.000000	0.000000	0.000000
32	1.052269	10.930913	0.000000	0.000000	0.000000	0.000000
33	1.058024	7.531981	0.000000	0.000000	1.120000	0.000000
34	1.067890	2.750159	0.000000	0.000000	0.000000	0.000000
35	1.016442	2.717010	0.000000	0.000000	0.000000	0.000000

Table D.11: Load Flow Results

Bus No.	VbO	thetaO	PGO	QGO	PLO	QLO
36	1.045382	-0.458455	0.000000	0.000000	11.020000	-0.194600
37	1.030558	-6.645579	0.000000	0.000000	75.000000	3.000000
38	1.057570	8.672060	0.000000	0.000000	0.000000	0.000000
39	1.008076	-8.267066	0.000000	0.000000	2.670000	0.126000
40	1.071068	15.124160	0.000000	0.000000	0.656300	0.235300
41	0.999169	43.649710	0.000000	0.000000	0.000000	2.500000
42	0.999194	38.288585	0.000000	0.000000	11.500000	2.500000
43	1.016760	-7.439683	0.000000	0.000000	0.000000	0.000000
44	1.016172	-7.469630	0.000000	0.000000	2.675500	0.048400
45	1.020589	2.632308	0.000000	0.000000	2.080000	0.210000
46	1.034526	9.599242	0.000000	0.000000	1.507000	0.285000
47	1.076350	7.391545	0.000000	0.000000	2.031200	0.325900
48	1.079413	9.283698	0.000000	0.000000	2.412000	0.022000
49	1.014073	12.772037	0.000000	0.000000	1.640000	0.290000
50	1.014515	19.132122	0.000000	0.000000	1.000000	-1.470000
51	1.024917	6.550268	0.000000	0.000000	3.370000	-1.220000
52	0.994181	38.043092	0.000000	0.000000	9.700000	1.230000
53	1.045000	10.695323	2.500000	1.130179	0.000000	0.000000
54	0.980000	14.253134	5.450000	1.819302	0.000000	0.000000
55	0.983000	16.280509	6.500000	1.967087	0.000000	0.000000
56	0.997000	17.332590	6.320000	1.063487	0.000000	0.000000
57	1.011000	15.856183	5.052000	1.620169	0.000000	0.000000
58	1.050000	20.170913	7.000000	2.189340	0.000000	0.000000
59	1.063000	22.396902	5.600000	0.979741	0.000000	0.000000
60	1.030000	16.291549	5.400000	-0.012207	0.000000	0.000000
61	1.025000	20.621477	8.000000	0.038979	0.000000	0.000000
62	1.010000	15.712177	5.000000	0.001126	0.000000	0.000000
63	1.000000	18.157159	10.000000	-0.263674	0.000000	0.000000
64	1.015600	4.718802	13.500000	2.075858	0.000000	0.000000
65	1.011000	0.000000	36.367478	8.441850	0.000000	0.000000
66	1.000000	45.142451	17.850000	0.802018	0.000000	0.000000
67	1.000000	39.133597	10.000000	0.620504	0.000000	0.000000
68	1.000000	44.916336	40.000000	4.358314	0.000000	0.000000

Table D.12: DC Link 52-37 Results

Parameter	Rectifier	Inverter
Bus no	52	37
D.C.Voltage(pu)	2.044031	2.000000
Transformer tap Position(pu)	1.637037	1.562779
Control Angles(Deg)	12.604627	15.000000
Commutation overlap Angles(Deg)	15.257477	14.174955
Real Power flow(pu)	15.000000	14.676884
Reactive power consumption(pu)	5.928991	6.273079
Power factor	0.929987	0.919531
Current in the D.C.Link(pu)	7.338442	

Table D.13: DC Link 41-36 Results

Parameter	Rectifier	Inverter
Bus no	41	36
D.C.Voltage(pu)	2.029563	2.000000
Transformer tap Position(pu)	1.637037	1.516203
Control Angles(Deg)	18.292307	15.000000
Commutation overlap Angles(Deg)	9.069386	10.494655
Real Power flow(pu)	10.000000	9.854338
Reactive power consumption(pu)	4.296218	3.760753
Power factor	0.918795	0.934276
Current in the D.C.Link(pu)	4.927169	

Appendix E

Asynchronous System Data

Table E.1: Machine bus data

Bus No.	Voltage (pu)	Power generation (pu)
1	1.02	10.29
2	1.00	2
3	1.00	2
4	1.00	9
13	1.02	9
9	1.02	10

Table E.2: Load bus data

Bus No.	Real load (pu)	Reactive load (pu)
8	12	2
12	12	2
1	9	0.5
13	9	0.5

Table E.3: Line data

From Bus	To Bus	Resistance (pu)	Reactance (pu)	B(total)/Tap Ratio
6	7	1000.00740	.08260	0.0
10	11	1000.00740	.08260	0.0
8	6	0.00185	0.02065	0.275
8	6	0.00185	0.02065	0.275
6	11	0.0064	0.0711	0.948
6	11	0.0064	0.0711	0.948
11	12	0.00185	0.02065	0.275
11	12	0.00185	0.02065	0.275
7	10	0.00185	0.02065	0.275
5	6	.00740	.08260	1.10
5	6	.00740	.08260	1.10
14	11	.00740	.08260	1.10
14	11	.00740	.08260	1.10
5	14	0.00740	.08260	1.10
1	5	.00	.0006	1.000
2	8	.00	.06	1.000
3	12	.00	.06	1.000
4	7	.00	.012	1.000
9	10	.00	.012	1.000
13	14	.00	.0006	1.000

Table E.4: Machine data

Gen. No.	xd	xd′	xd″	Tdo′	Tdo″	xq	xq′	xq″	Tqo′	Tqo″	H
1	0.01	0.001	0.0008	7	0.04	0.008	0.003	0.0008	2	0.17	42.2
2	0.1	0.01	0.008	7	0.04	0.08	0.03	0.008	2	0.17	6.42
3	0.1	0.01	0.008	7	0.04	0.08	0.03	0.008	2	0.17	6.42
4	0.1	0.017	0.013	5.23	0.09	0.062	0.02	0.018	0.59	0.1	300
5	0.1	0.017	0.013	5.23	0.09	0.062	0.02	0.018	0.59	0.1	300
6	0.01	0.001	0.0008	7	0.04	0.008	0.003	0.0008	2	0.17	42.2

Table E.5: Static excitation system data

Gen. No.	KA	TA	EFDMIN	EFDMAX
1	200	0.02	-6	6
2	200	0.02	-6	6
3	200	0.02	-6	6
4	200	0.02	-6	6
9	200	0.02	-6	6
13	200	0.02	-6	6

Table E.6: HVDC data

Link. No.	Rec/Inv bus	Br/Bi	Trmax/Timax	Trmin/Timin	Tnr/Tni	Xcr/Xci	Alphamin/Gammamin	Nr/Ni	Bshr/Bshi
1	7	1	1.15	0.85	1.0	0.0144	5	27	3.5
1	6	1	1.15	0.85	1.0	0.0144	15	19	4.2
2	10	1	1.15	0.85	1.0	0.0144	5	27	3.5
2	11	1	1.15	0.85	1.0	0.0144	15	19	4.2

Table E.7: HVDC data contd...

Link. No.	Rec bus	Inv bus	Vdis	Idc	Pdr	Im	Rdc	Alprmin	Alprmax	cn	pn	Vbase (kV)	Vdrs(initial)
1	7	6	1.28	7.0313	9.0	1.0	0.003	10	20	0	1	500	1
2	10	11	1.28	7.0313	9.0	1.0	0.003	10	20	0	1	500	1

cn -set 1 if the dc link is on link current specification else 0.
pn -set 1 if the dc link is on rectifier-end power specification else 0.

Table E.8: Load Flow Results

Bus No.	VbO	thetaO	PGO	QGO	PLO	QLO
1	1.020000	0.000000	10.298633	-0.868422	9.000000	0.500000
2	1.000000	-1.814001	2.000000	0.571948	0.000000	0.000000
3	1.000000	-1.854604	2.000000	0.571593	0.000000	0.000000
4	1.020000	0.378500	9.000000	1.271787	0.000000	0.000000
5	1.020805	-0.042876	0.000000	0.000000	0.000000	0.000000
6	1.003236	-2.904375	0.000000	0.000000	0.000000	0.000000
7	1.010600	-5.635519	0.000000	0.000000	0.000000	0.000000
8	0.973110	-8.897476	0.000000	0.000000	12.000000	2.000000
9	1.020000	0.378516	9.000000	1.271784	0.000000	0.000000
10	1.010600	-5.635502	0.000000	0.000000	0.000000	0.000000
11	1.003259	-2.945114	0.000000	0.000000	0.000000	0.000000
12	0.973131	-8.937924	0.000000	0.000000	12.000000	2.000000
13	1.020000	-0.137122	10.200000	-0.862455	9.000000	0.500000
14	1.020802	-0.176742	0.000000	0.000000	0.000000	0.000000

Table E.9: DC Link Results

Parameter	Rectifier	Inverter
Bus no 7	6	
D.C.Voltage(pu)	1.300757	1.280000
Transformer tap Position(pu)	1.044444	1.050788
Control Angles(Deg)	11.685911	15.000000
Commutation overlap Angles(Deg)	20.558548	18.667938
Real Power flow(pu)	9.000000	8.856380
Reactive power consumption(pu)	4.034041	4.312012
Power factor	0.912526	0.899095
Current in the D.C.Link(pu)	6.919047	

Table E.10: DC Link Results

Parameter	Rectifier	Inverter
Bus no	10	11
D.C.Voltage(pu)	1.300757	1.280000
Transformer tap Position(pu)	1.044444	1.050763
Control Angles(Deg)	11.685920	15.000000
Commutation overlap Angles(Deg)	20.558541	18.667938
Real Power flow(pu)	9.000000	8.856380
Reactive power consumption(pu)	4.034042	4.312012
Power factor	0.912526	0.899095
Current in the D.C.Link(pu)	6.919047	

Appendix F

Nelson River Bipole Controller

The Nelson River Bipole controller reported in [35] uses a strategy similar to this (see Fig. F.1). The frequency response of the channels of this controller is shown in Fig. F.2.

Channel 2 of the controller is a power swing damping controller.

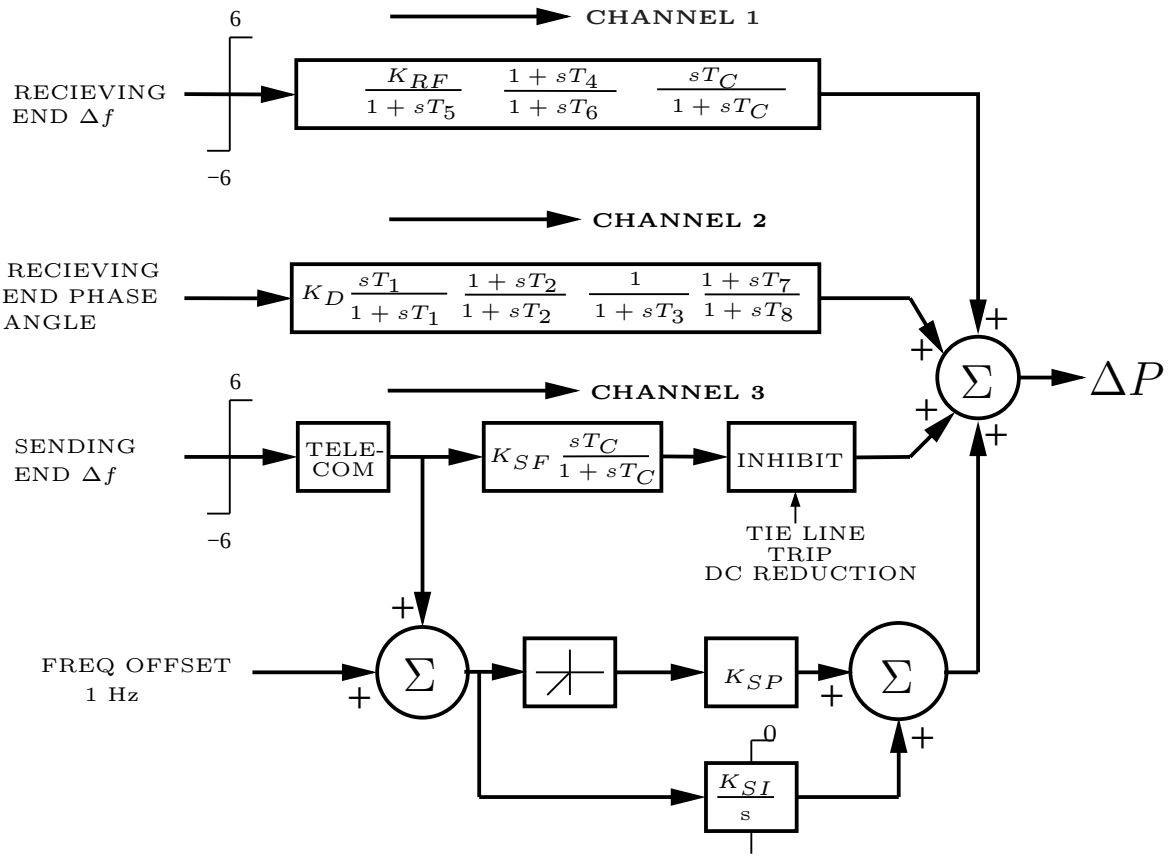

Figure F.1: Auxiliary Controller - Nelson River bipole[35]

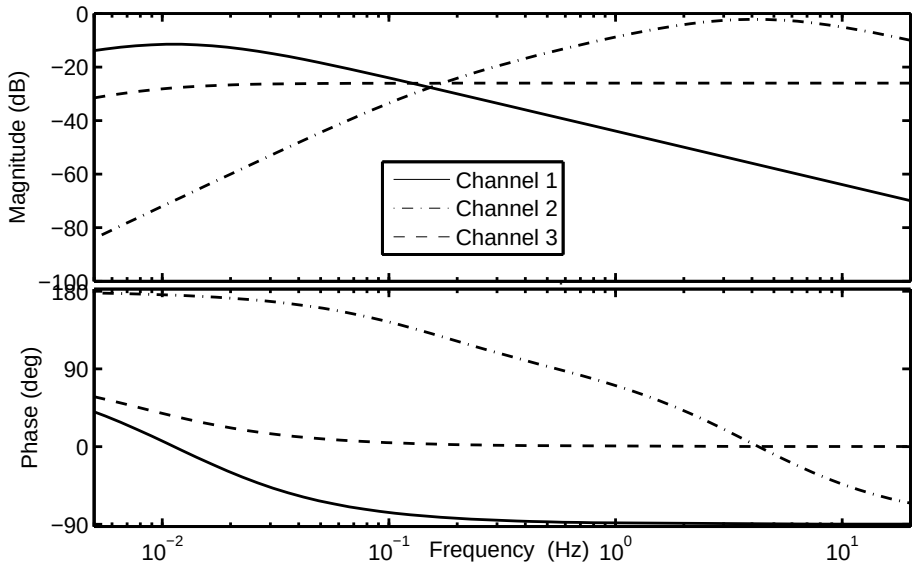

Figure F.2: Frequency Response of Transfer Functions - Nelson River Bipole Controller

Note: (a) Since the local signal (phase angle) at the receiving end of the converter is used, this channel will affect the swing modes observable at the receiving end only. (b) The controller has a large gain above 1 Hz, while the gain below 0.1 Hz is very small. This means that it will not affect slow common-mode variations. (c) The controller gives a near-90^o phase lead to the input signal in the swing mode frequency range. In other words, in this range, the power withdrawal at the receiving-end is modulated roughly in phase with the frequency. This will introduce damping[15, **?**, 58, 42].

Channel 1 (receiving-end frequency controller) and Channel 3 (sending-end frequency controller) are used to introduce transient power flow - frequency dependence, to avoid large frequency deviations in the two systems.

For this channel, the phase-shift is near zero around 0.01 Hz, where the gain is highest, indicating that the change in power withdrawal at the receiving end due to this channel is proportional to the frequency variation at that end. Hence this controller brings a power-frequency dependence for the common mode frequency at the receiving end (like a governor). Note that the gain of the controller of Channel 1 is very low in the range 0.2 - 2 Hz. Therefore, this channel allows only slow variations associated with the common-mode frequency, and does not interfere with the power-swing damping controller. The steady state gain in Channel 1 is zero due to the presence of a washout block, indicating that it does not cause a steady state change in the power flow.

The frequency response of the transfer function of Channel 3 indicates that is active for a fairly large frequency range (both slow and fast variations). Therefore, if swing mode frequencies of the sending end are observable in the measured frequency,

then this may cause a coupling with the swing modes at the receiving end.

Since greater control is desired in the under-frequency range, the sending-end controller uses additional proportional-integral action to prevent a fall beyond 1 Hz.

Appendix G

Proof of the Theorem in [59]

Theorem 8.1.5 *If A and $A+E$ are n-by-n symmetric matrices,* then

$$\lambda_k(A) + \lambda_n(E) \leq \lambda_k(A+E) \leq \lambda_k(A) + \lambda_1(E) \qquad k = 1:n$$

This follows from the minimax characterization
Example. If

$$A = \begin{bmatrix} 6.8 & 2.4 \\ 2.4 & 8.2 \end{bmatrix} \qquad \textit{and} \qquad E = \begin{bmatrix} 0.002 & 0.003 \\ 0.003 & 0.001 \end{bmatrix},$$

then $\lambda(A) = \{5, 10\}$, $\lambda(E) = \{-0.0015, 0.0045\}$, and $\lambda(A+E) = \{4.9988, 10.0042\}$ confirming that

$$5 - 0.0015 \leq 4.9988 \leq 5 + 0.0045$$
$$10 - 0.0015 \leq 10.0042 \leq 10.0045$$

Appendix H

Comparison of the eigenvalues for 3 machine detailed and analogous system

- For the analogous circuit given in the Fig.H.1 the value of the analogous parameters are given in Table H.1.
- The two HVDC links between the buses 8-9 and 4-6 are assumed to carry zero quiescent power.
- Power through the two HVDC links is modulated proportional to the frequency difference between the buses to introduce damping torque.
- The gains for such control are taken as $\mathcal{R}_1 = 0.28$ and $\mathcal{R}_2 = 0.82$ for the link 8-9 and 4-6 respectively.
- In the analogous circuit, this damping control is equivalent of introducing resistances of values $\mathcal{R}_1 = 0.28$ and $\mathcal{R}_2 = 0.82$ between the buses 8-9 and 4-6 respectively.
- In order to validate the circuit analogy method, Table H.2 shows the comparison of the eigenvalues for the detailed system and one obtained by circuit analogy. One can observe from Table H.2 that the analogous system is approximately able to capture the information about the electromechanical modes of the detailed system.
- The approximate nature of the eigenvalues of the model obtained by circuit analogy (and not exactly similar to the eigenvalues of the detailed model) is due to the fact that it is based on assumptions such as 1) synchronous machine is represented by a classical model, 2) transmission line losses are neglected, and 3) bus voltages are essentially at 1pu.

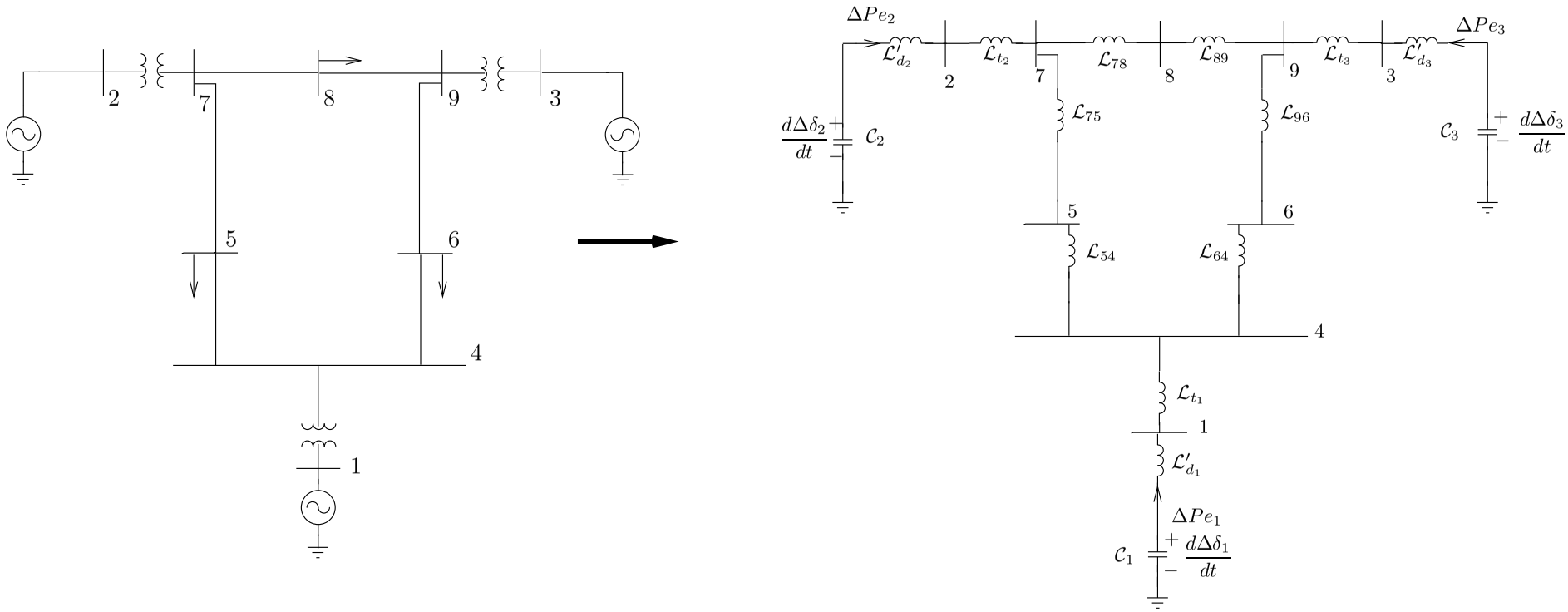

Figure H.1: Small-signal Analogous Circuit of a Three Machine System

Table H.1: Three machine analogous circuit parameters

Parameters	Value (in pu)
$\mathcal{C}_1$	0.1254
$\mathcal{C}_2$	0.0340
$\mathcal{C}_3$	0.0160
$\mathcal{L}'_{d_1}$	0.0608
$\mathcal{L}'_{d_2}$	0.1198
$\mathcal{L}'_{d_3}$	0.1813
$\mathcal{L}_{t_1}$	0.0576
$\mathcal{L}_{t_2}$	0.0625
$\mathcal{L}_{t_3}$	0.0586
$\mathcal{L}_{78}$	0.072
$\mathcal{L}_{89}$	0.1008
$\mathcal{L}_{54}$	0.085
$\mathcal{L}_{64}$	0.092
$\mathcal{L}_{75}$	0.161
$\mathcal{L}_{96}$	0.170
$\mathcal{R}_1$	0.28
$\mathcal{R}_2$	0.82

Table H.2: Comparison of eigenvalues for the detailed and analogous system with HVDC link (in damping control mode)

Original system	Analogous system
-0.3425±13.5031j	-0.3354±13.3581j
-0.1550±8.7201j	-0.1575±8.7057j